Chapter 3

Results and Discussion

Section (A)

Effect of Investigated Azo dyes on The Corrosion Behavior of Carbon Steel in 2M HCl Solution by The Mass loss Technique

3.1- Corrosion inhibition behavior

The corrosion behavior of carbon steel in aqueous environment is characterized by the extent to which it dissolves in the solution. This can be quantified using the simple relationship:

$$\Delta W = W_B - W_A \qquad (3.1)$$

where :

ΔW = loss in mass of metal in the corrosive solution.

W_B = loss in mass of metal before exposure to the corrosive solution.

W_A = loss in mass of metal after exposure to the corrosive solution.

The degree of dissolution of course, dependent on the surface area of the metal exposed and the time of exposure; hence the amount of corrosion is given with respect to area and time. The resulting quantity, corrosion rate is thus a fundamental measurement in corrosion science. Corrosion rate can be evaluated by measuring either the concentration of the dissolved metal in solution by chemical analysis or by measuring weight of a specimen before and after exposure and applying equation (3.1). The later is most common method. The

mass loss method is usually preferred because the quantity measured is directly related to the extent of corrosion and does not rely on any assumptions about reactions occurring during corrosion.

Figures (3.1 – 3.5) show the mass loss-time curves in 2M HCl solution in absence and presence of different concentrations of the selected organic compounds. Inspection of these Figures it is clear that, as the concentration of these compounds increases, the loss in mass of carbon steel samples decreases. This means that the presence of these compounds retard the corrosion of C-steel in 2M HCl or in other words, these compounds act as an inhibitors.

The linear variation of mass loss with time in uninhibited and inhibited 2M HCl indicates the absence of insoluble surface film during corrosion. In the absence of any surface film, the inhibitors are first adsorbed onto the metal surface and thereafter impede corrosion either by merely blocking the reaction sites (anodic and cathodic) or by altering the mechanism of the anodic and cathodic processes.

The percentage inhibition efficiency (%P) of the selected organic compounds were determined by using the following equation:

$$\%P = \frac{W_{free} - W_{add}}{W_{free}} X\ 100 \qquad (3.2)$$

where W_{free} and W_{add} are the loss in mass of carbon steel in the absence and presence of the selected organic compounds, respectively.

The calculated values of $\%P$ are given in Table (3.1) at 30°C. The order of the inhibition efficiencies of these compounds, decreases in the following sequence:

II > III > I > V > IV

This behavior will be discussed later .

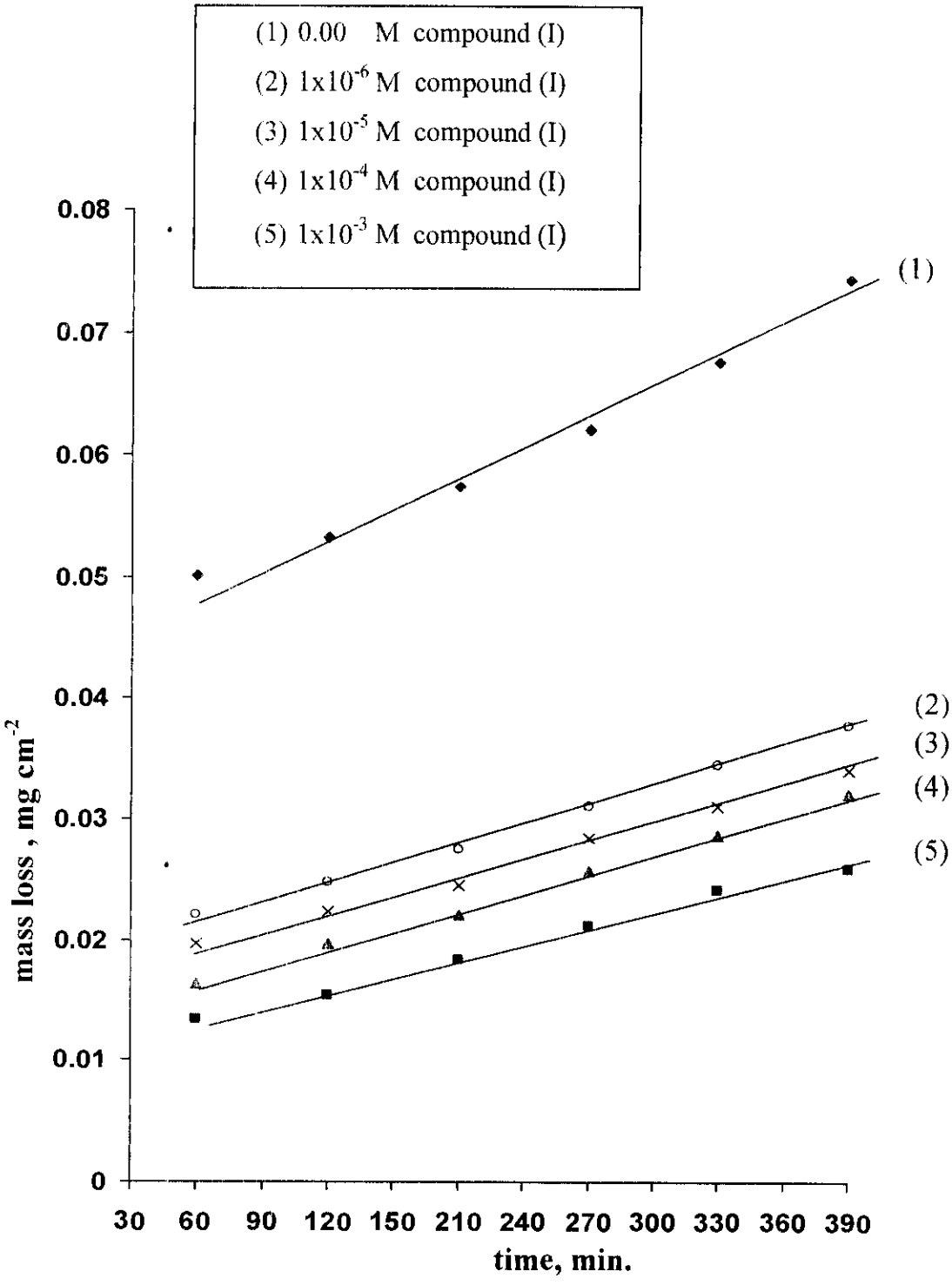

Fig.(3.1): Mass loss-time curves for the corrosion of C-steel in 2M HCl in absence and presence of different concentrations of compound (I)

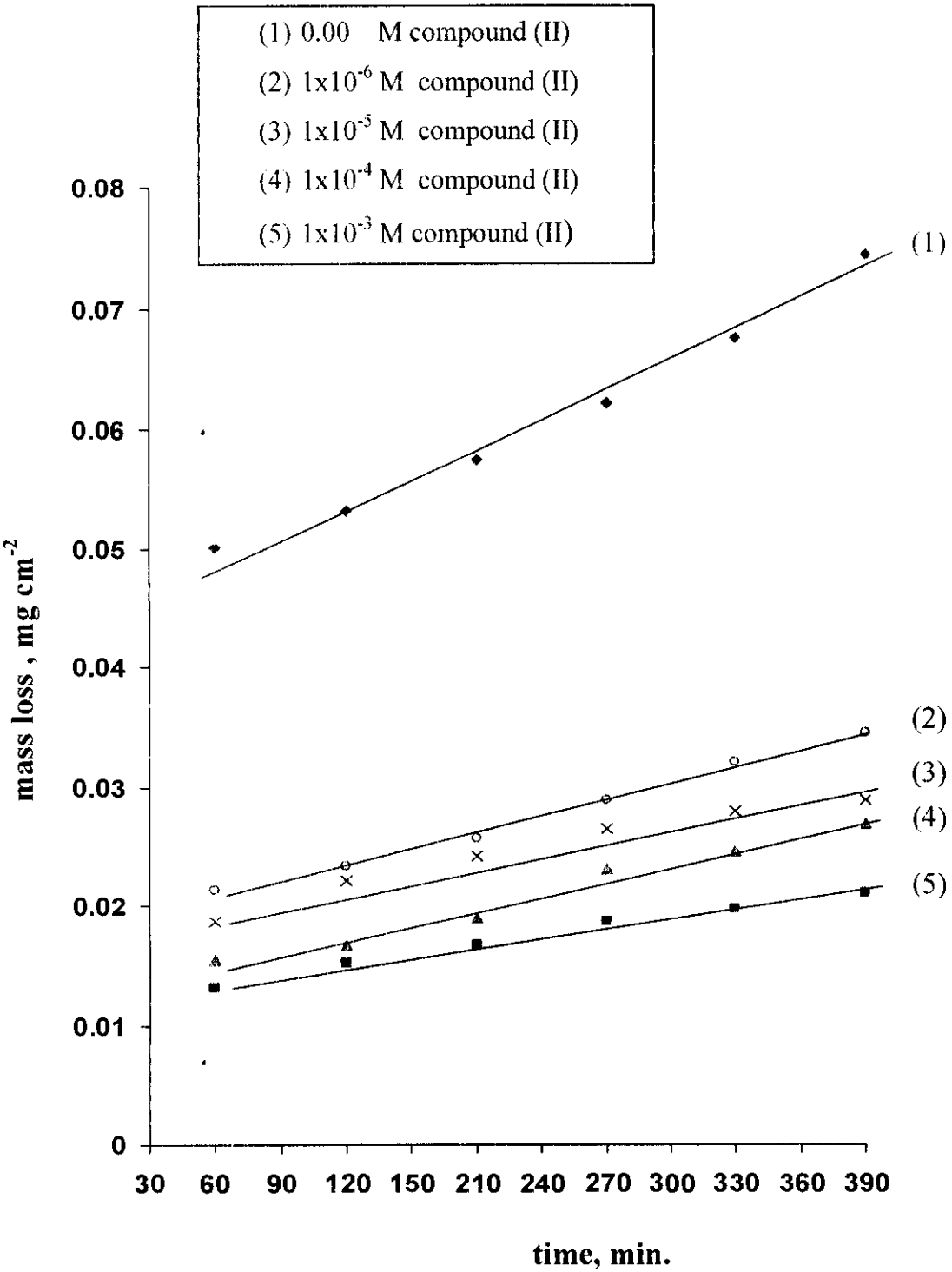

Fig.(3.2): Mass loss-time curves for the corrosion of C-steel in 2M HCl in absence and presence of different concentrations of compound (II)

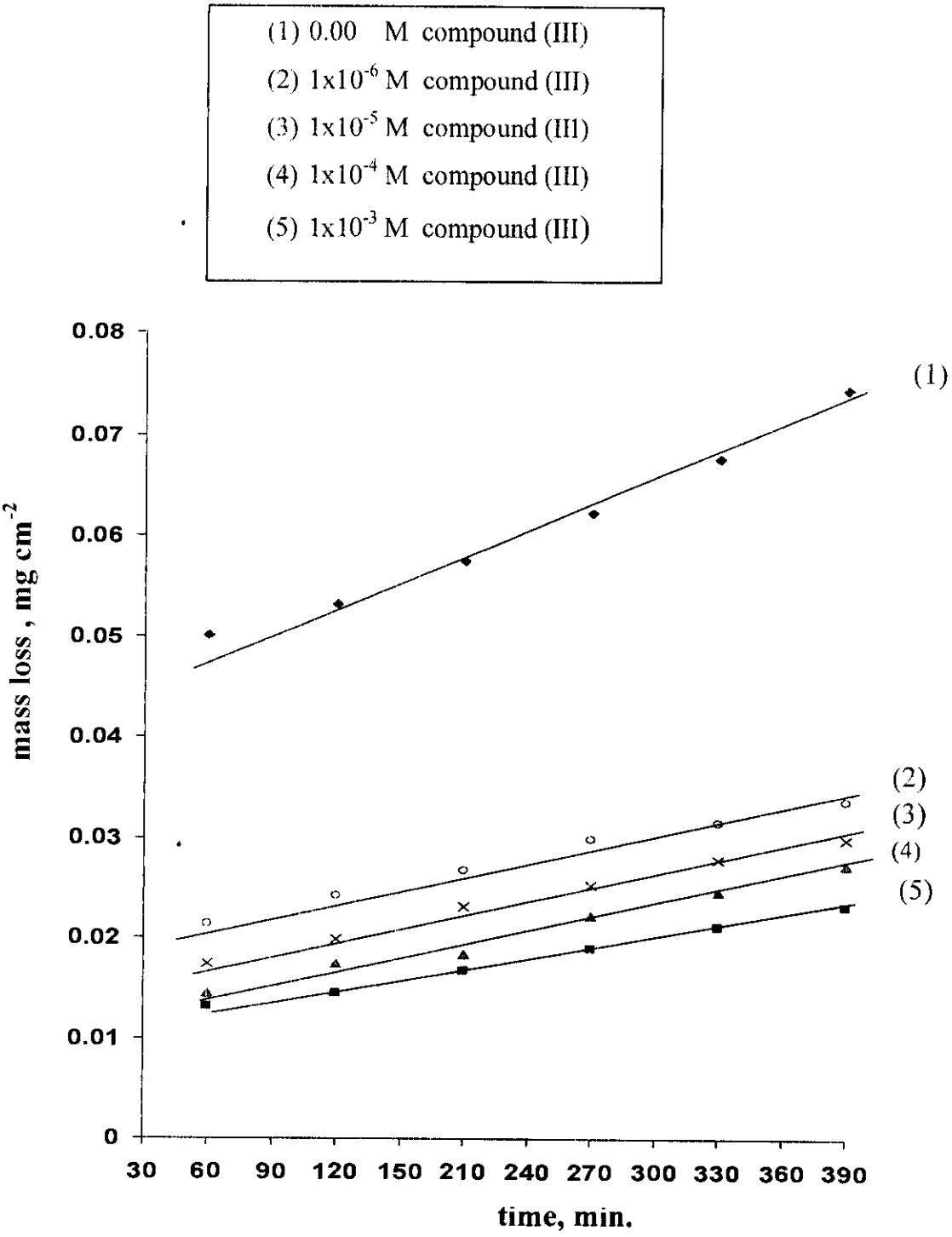

Fig.(3.3): Mass loss-time curves for the corrosion of C-steel in 2M HCl in absence and presence of different concentrations of compound (III)

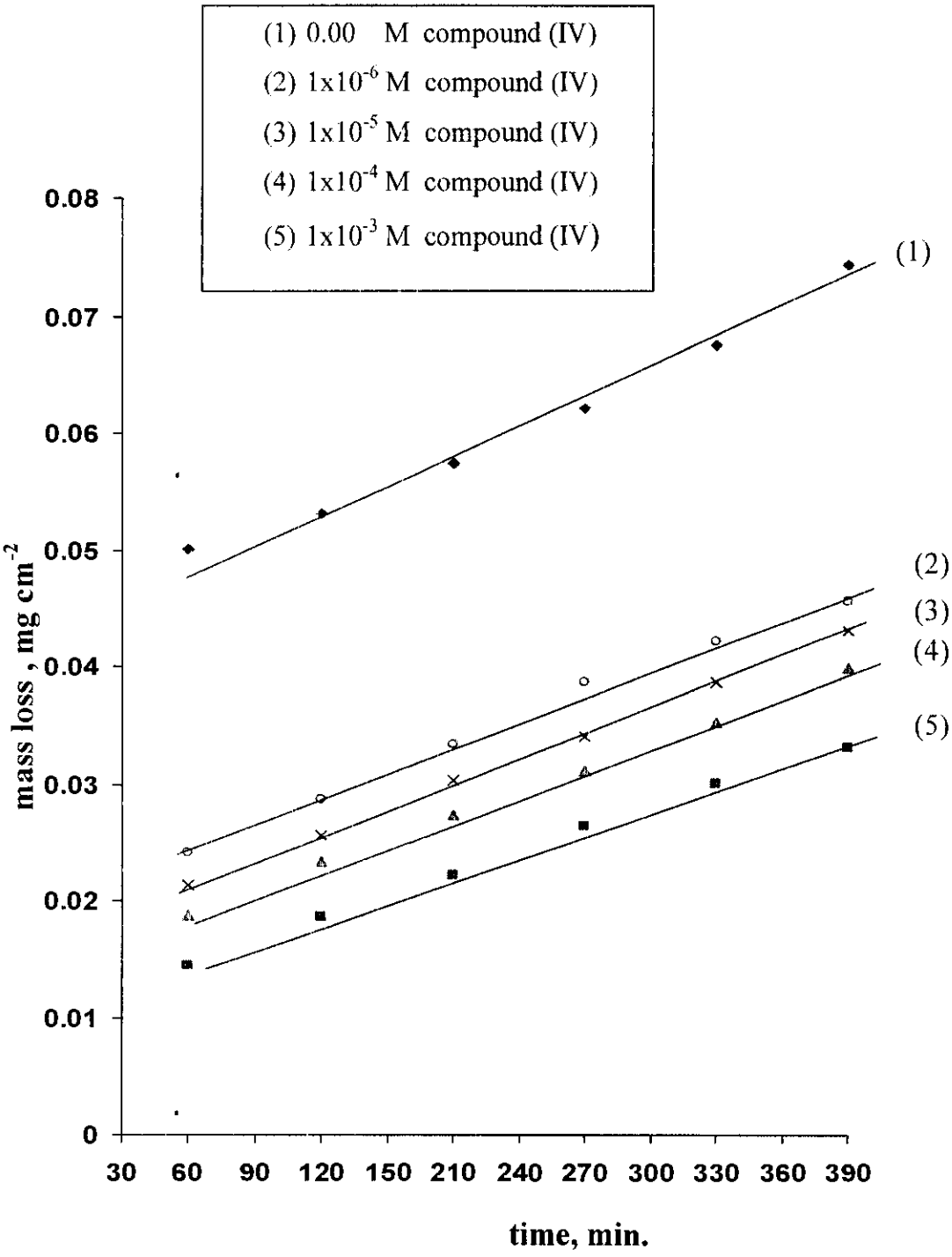

Fig.(3.4): Mass loss-time curves for the corrosion of C-steel in 2M HCl in absence and presence of different concentrations of compound (IV)

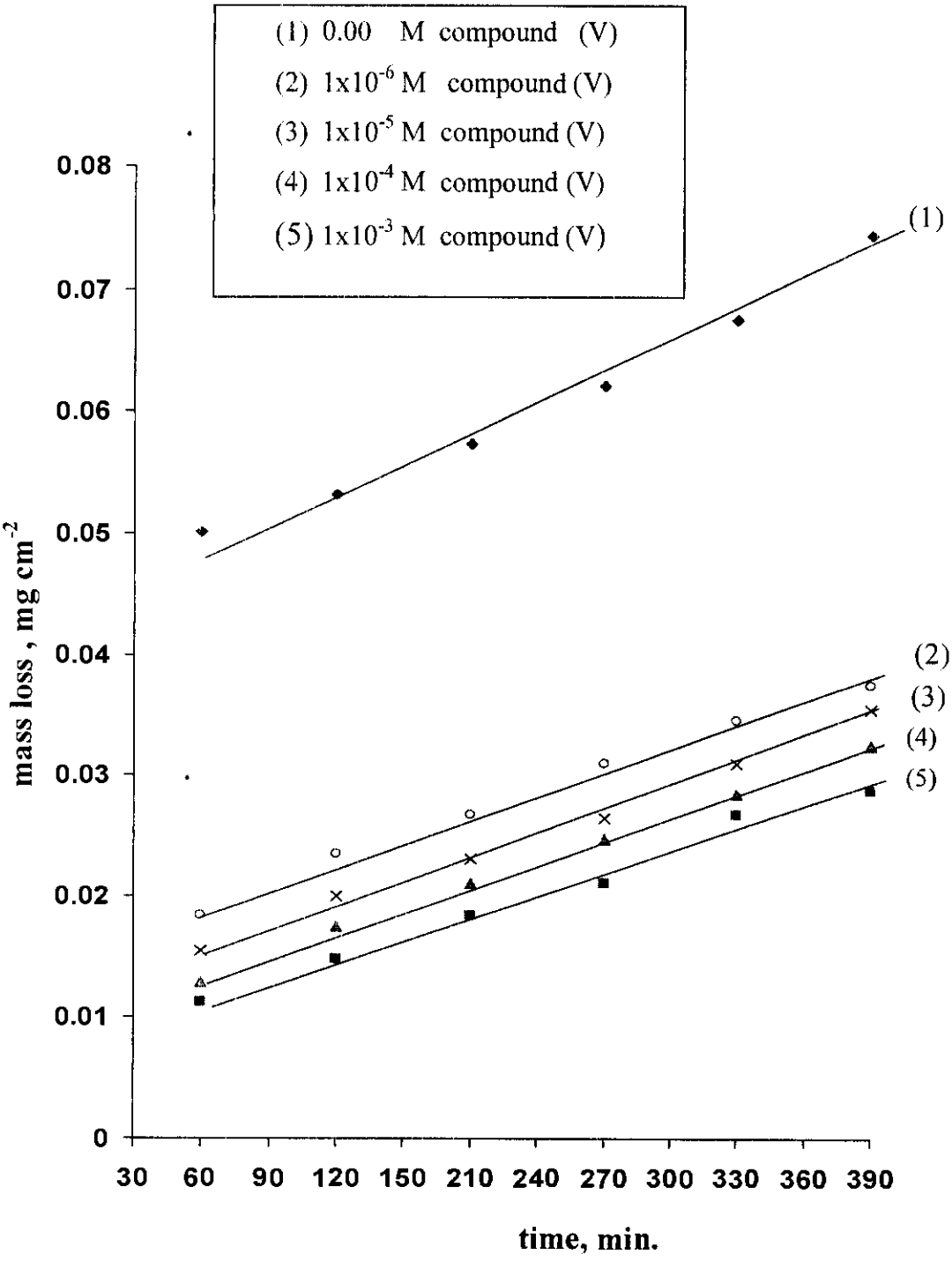

Fig.(3.5): Mass loss-time curves for the corrosion of C-steel in 2M HCl in absence and presence of different concentrations of compound (V)

Table (3.1) :

Inhibition efficiency %P of all inhibitors at different concentrations of inhibitors as determined from mass loss method at 30°C.

Inhibitors	Concentration, M	Weight loss (mg cm^{-2})	%P	θ
Compound (I)	0.00 M compound (I)	0.0744	-	-
	$1x10^{-6}$ M compound (I)	0.0349	53.09	0.5309
	$1x10^{-5}$ M compound (I)	0.0329	55.77	0.5577
	$1x10^{-4}$ M compound (I)	0.0294	60.48	0.6048
	$1x10^{-3}$ M compound (I)	0.0259	65.18	0.6518
Compound (II)	0.00 M compound (II)	0.0744	-	-
	$1x10^{-6}$ M compound (II)	0.0342	53.62	0.5362
	$1x10^{-5}$ M compound (II)	0.0288	61.29	0.6129
	$1x10^{-4}$ M compound (II)	0.0269	63.84	0.6384
	$1x10^{-3}$ M compound (II)	0.0211	71.63	0.7163
Compound (III)	0.00 M compound (III)	0.0744	-	-
	$1x10^{-6}$ M compound (III)	0.0335	54.97	0.5497
	$1x10^{-5}$ M compound (III)	0.0298	59.94	0.5994
	$1x10^{-4}$ M compound (III)	0.0272	63.44	0.6344
	$1x10^{-3}$ M compound (III)	0.0231	68.95	0.6895
Compound (IV)	0.00 M compound (IV)	0.0744	-	-
	$1x10^{-6}$ M compound (IV)	0.0433	41.80	0.4180
	$1x10^{-5}$ M compound (IV)	0.0421	43.41	0.4341
	$1x10^{-4}$ M compound (IV)	0.0398	46.50	0.4650
	$1x10^{-3}$ M compound (IV)	0.0332	55.37	0.5537
Compound (V)	0.00 M compound (V)	0.0744	-	-
	$1x10^{-6}$ M compound (V)	0.0347	53.3	0.533
	$1x10^{-5}$ M compound (V)	0.0336	54.8	0.548
	$1x10^{-4}$ M compound (V)	0.0301	59.5	0.595
	$1x10^{-3}$ M compound (V)	0.0287	61.4	0.614

3.2- Effect of temperature on corrosion process

In this part the effect of rising temperature on the corrosion rate of carbon steel in 2M HCl solution in the absence and presence of different concentrations of the azo dye compounds was studied using loss in mass measurements.

The corrosion rate R_{corr} was calculated from the following equation[70]:

$$R_{corr} = \frac{\Delta W}{S\,t} \qquad (3.3)$$

where :

Δ W is the loss in mass of metal in the corrosive solution.

S is the surface area (cm^2).

t is the time (min).

As shown from the figures (3.7- 3.26) and Table (3.2), that the corrosion rate increases and hence inhibition efficiency decreases as the temperature increases. This indicates that the rising of temperature decreases the inhibition process and the best inhibition efficiency is obtained at 30°C.

The apparent activation energy (E_a) of the corrosion of carbon steel in 2M HCl solution in the absence and presence of the selected azo dye compounds at different temperatures, were calculated form the Arrhenius equation [71-73]:

$$R_{corr} = A \exp^{(-Ea/RT)} \qquad (3.4)$$

and the logarithmic form

$$\log R_{corr} = \log A - \frac{Ea}{2.303\,RT} \qquad (3.5)$$

where A is the frequency factor, R is the universal gas constant and T is the absolute temperature. Arrhenius plot of logarithmic values of corrosion rate log

R_{corr} against the reciprocal of absolute temperatures ($\frac{1}{T}$) is shown graphically in Figures (3.27 -3.31), the values of activation energy (E_a*) were calculated form the slopes of these straight lines and are given in Table (3.3).

Inspection of Table (3.3), it is clear that the values of E_a* increasing by increasing the inhibitors concentration. This was attributed to an appreciable decrease in the adsorption process of the inhibitor on the metal surface with increase of temperature and corresponding increase in the reaction rate because of the greater area of the steel surface that is exposed to HCl solution.

The extents of the increase in the values of activation energy is proportional to the inhibition efficiency of the inhibitor. This indicate that the energy barrier of the corrosion reaction increases in the presence of these additives. This means that by the addition of azo dye compounds in the corrosive media, the corrosion reaction will be further pushed to the surface sites that are characterized by higher values of activation energies (E_a*). This means that, carbon steel corrosion occurs at the uncovered part of the surface. Thus adsorption of azo dyes was assumed to occur on the higher energy sites[74]. The presence of azo dye compounds which result in the blocking of the active sites, must be associated with an increase in the activation energy (E_a*) of carbon steel in the inhibited sites.

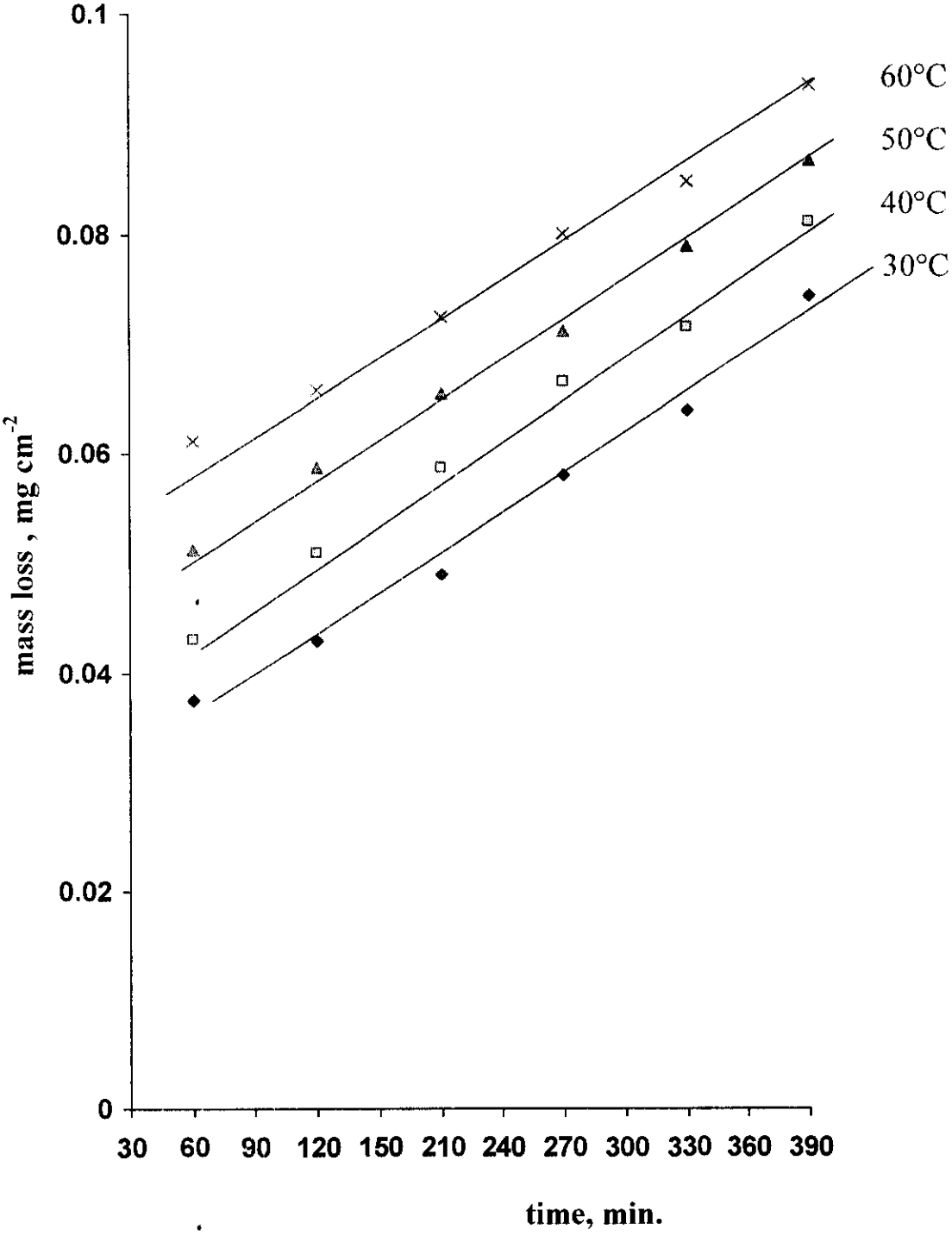

Fig.(3.6): Mass loss - time curves for the corrosion of C-steel in 2M HCl at different temperatures

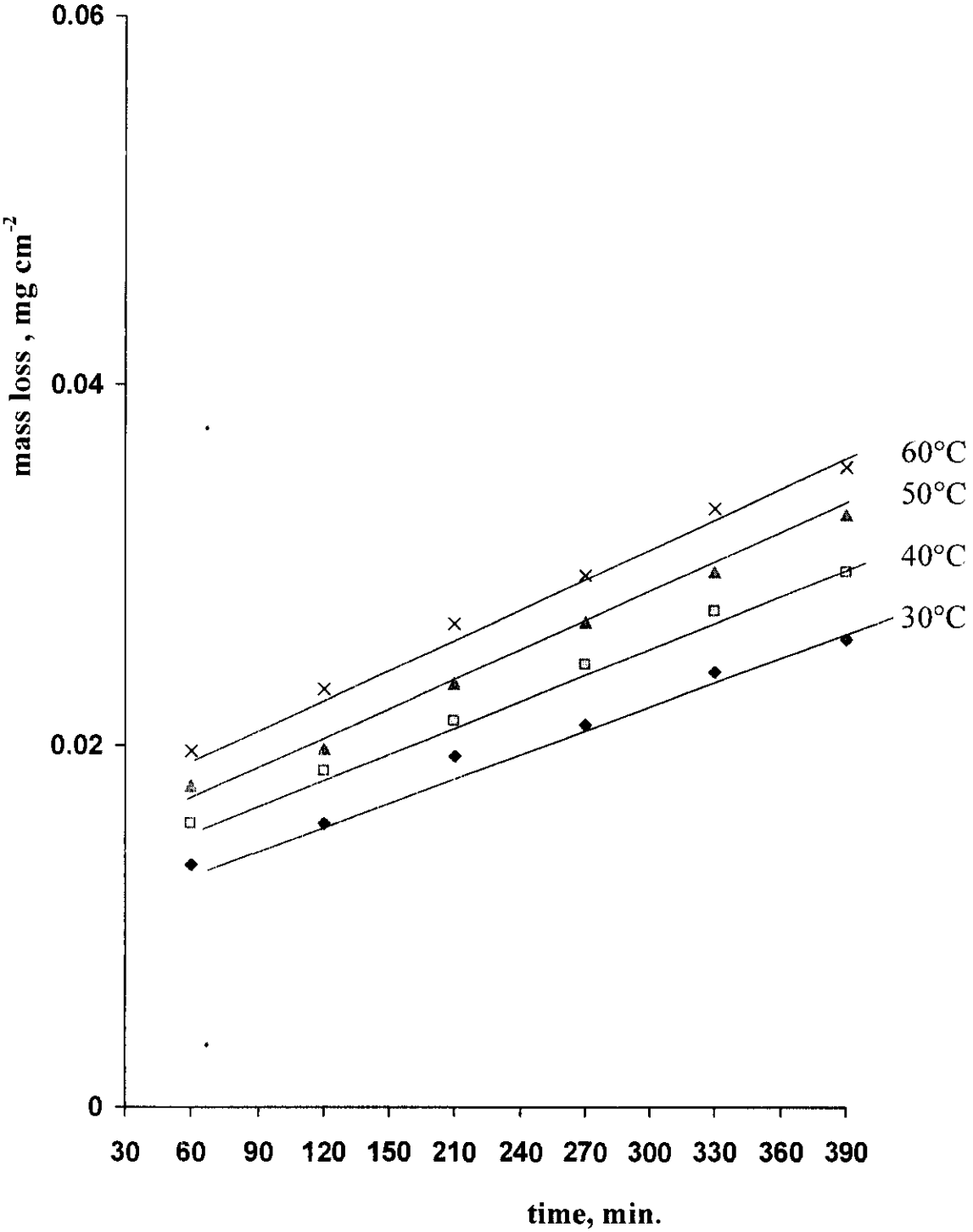

Fig.(3.7): Mass loss-time curves for the corrosion of C-steel in 2M HCl containing 10^{-3}M of compound (I) at different temperatures

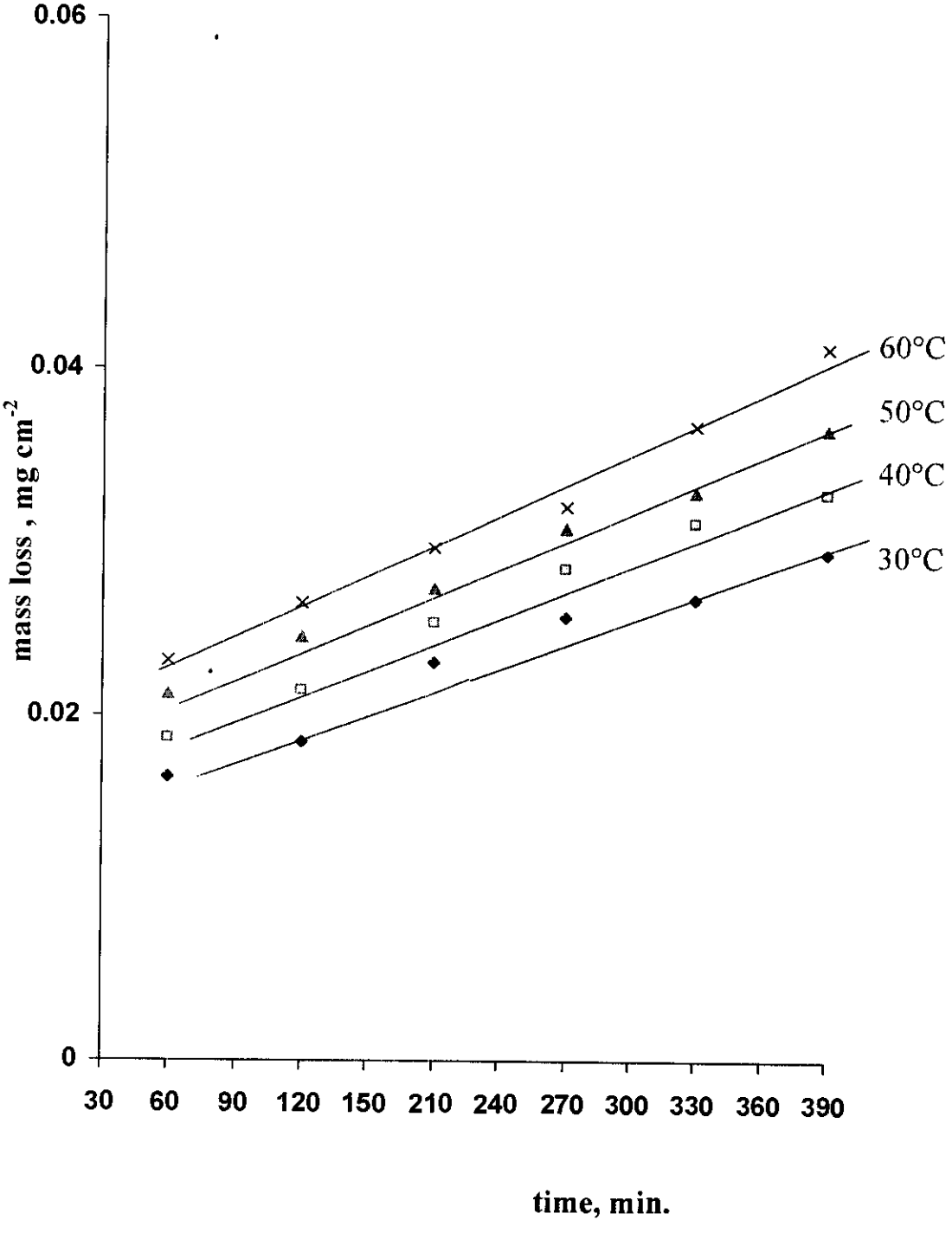

Fig.(3.8): .Mass loss-time curves for the corrosion of C-steel in 2M HCl containing 10^{-4}M of compound (I) at different temperatures

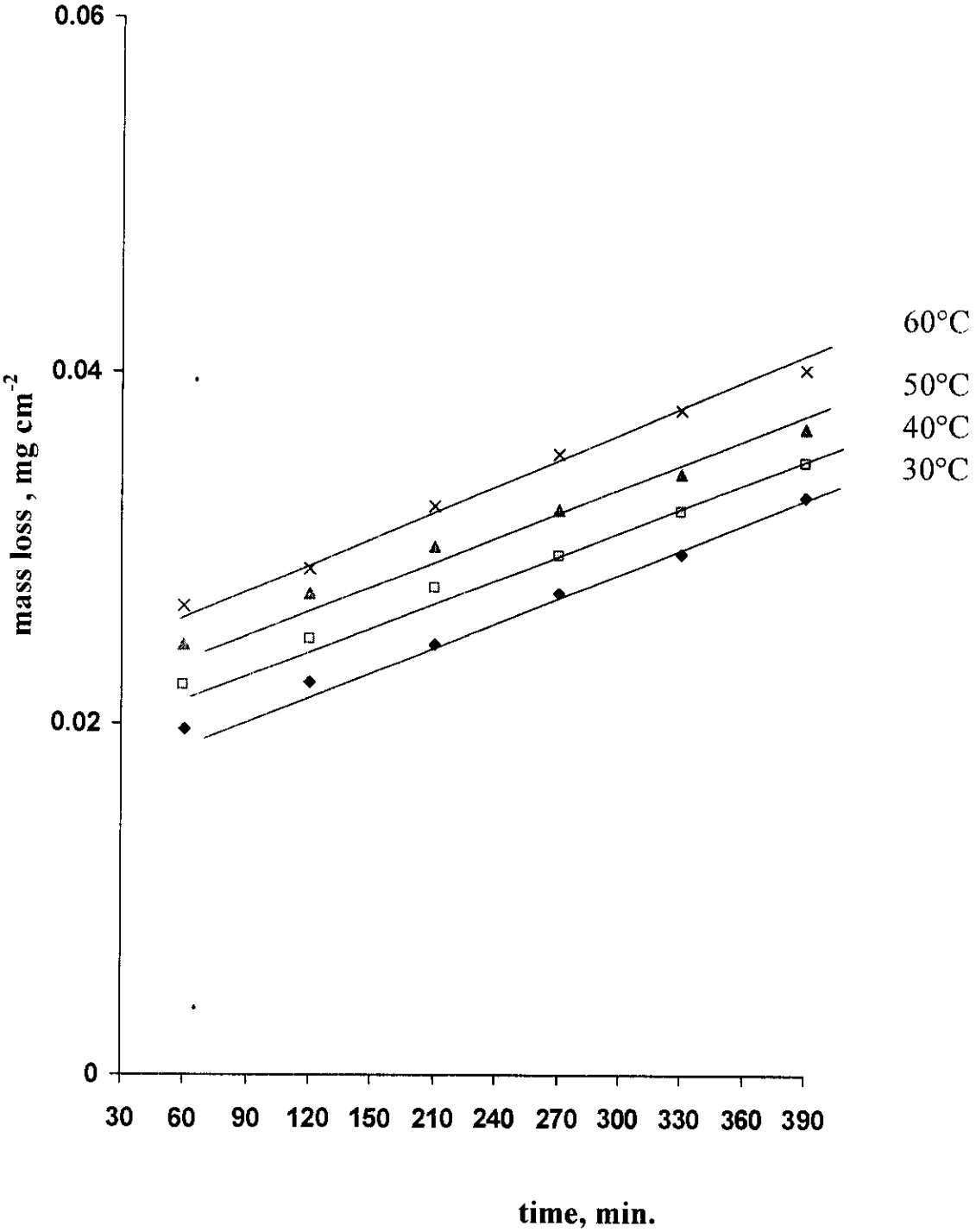

Fig.(3.9): Mass loss-time curves for the corrosion of C-steel in 2M HCl containing 10^{-5}M of compound (I) at different temperatures

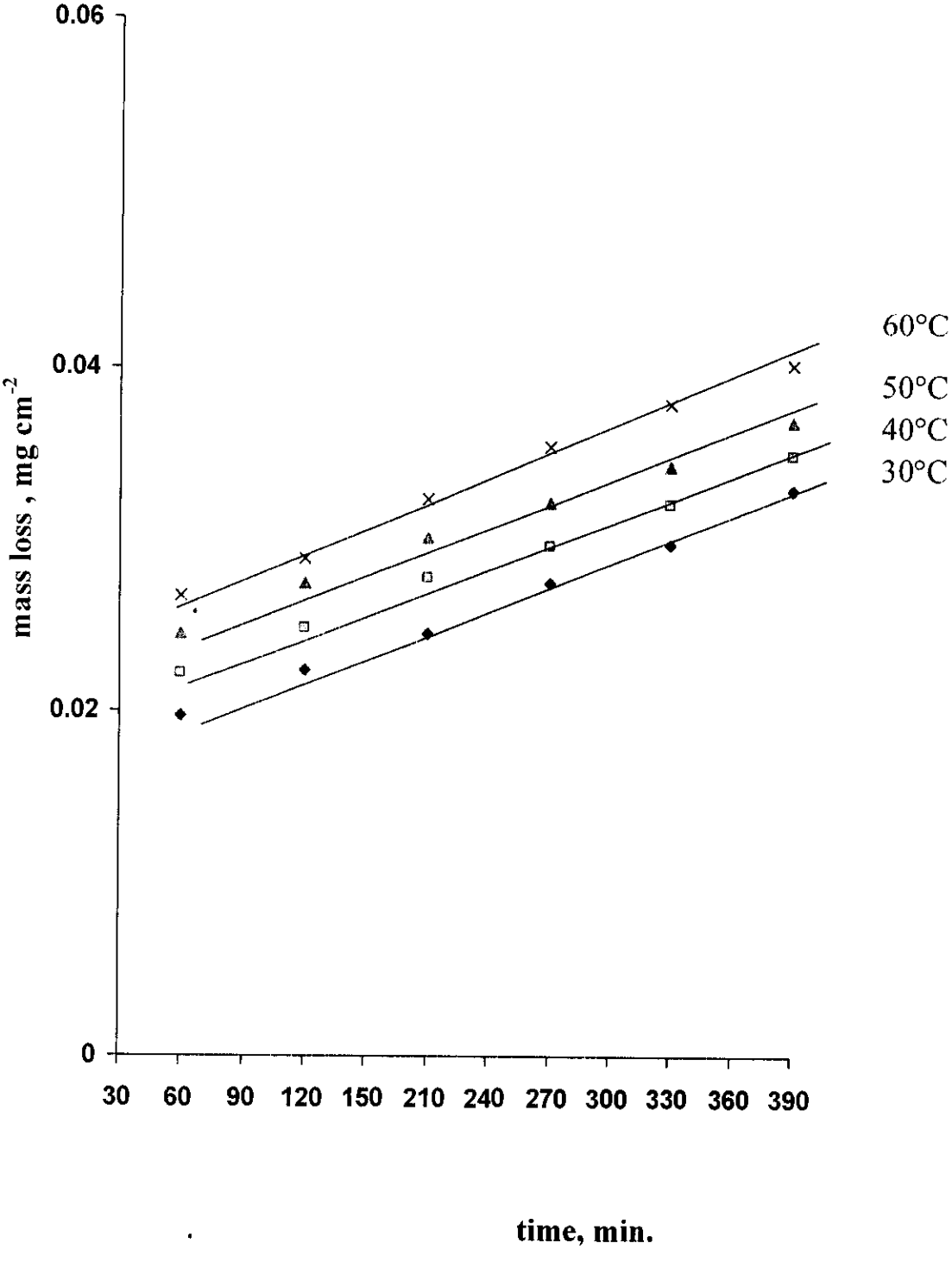

Fig.(3.10): Mass loss-time curves for the corrosion of C-steel in 2M HCl containing 10^{-6}M of compound (I) at different temperatures

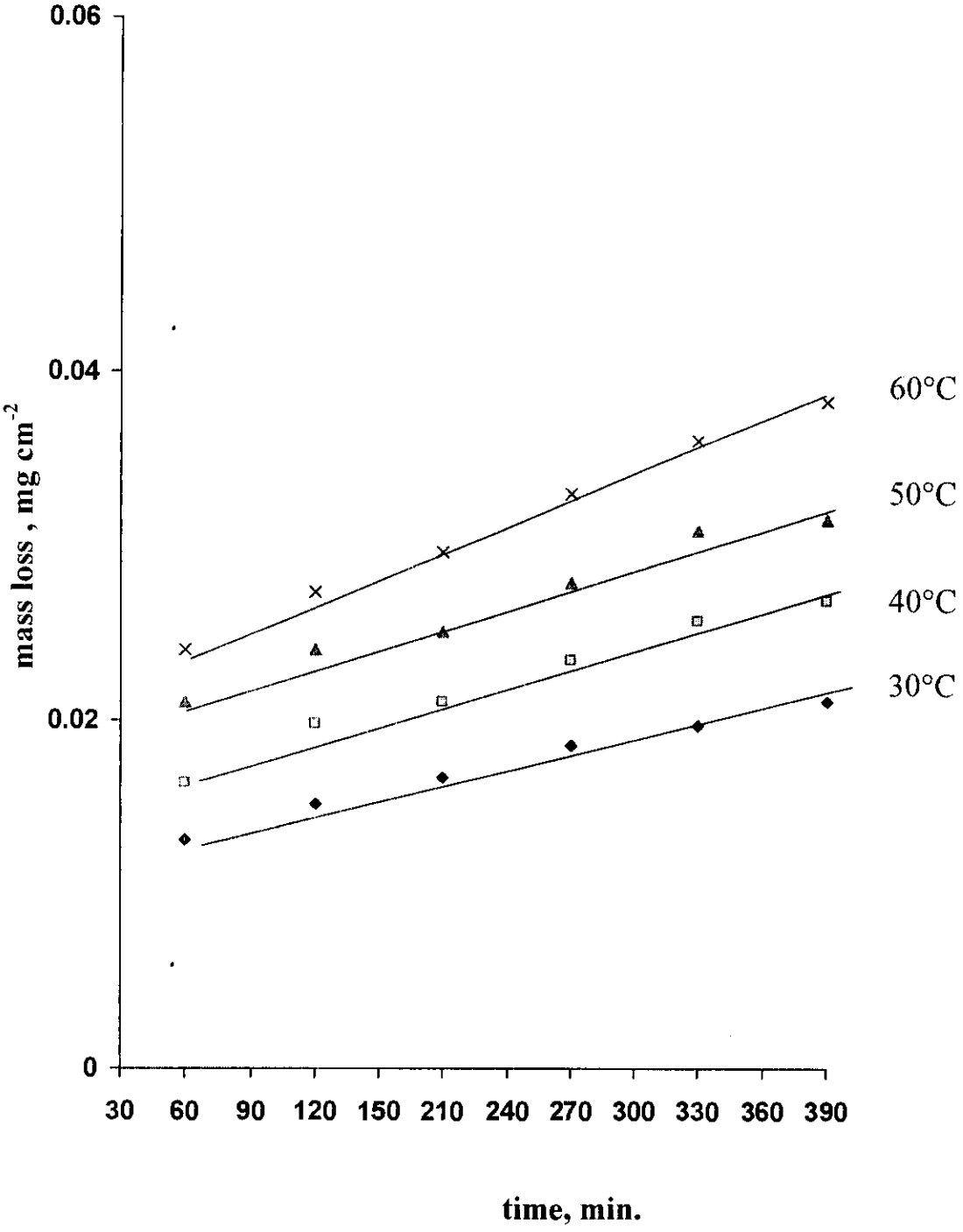

Fig.(3.11): Mass loss-time curves for the corrosion of C-steel in 2M HCl containing 10^{-3}M of compound (II) at different temperatures

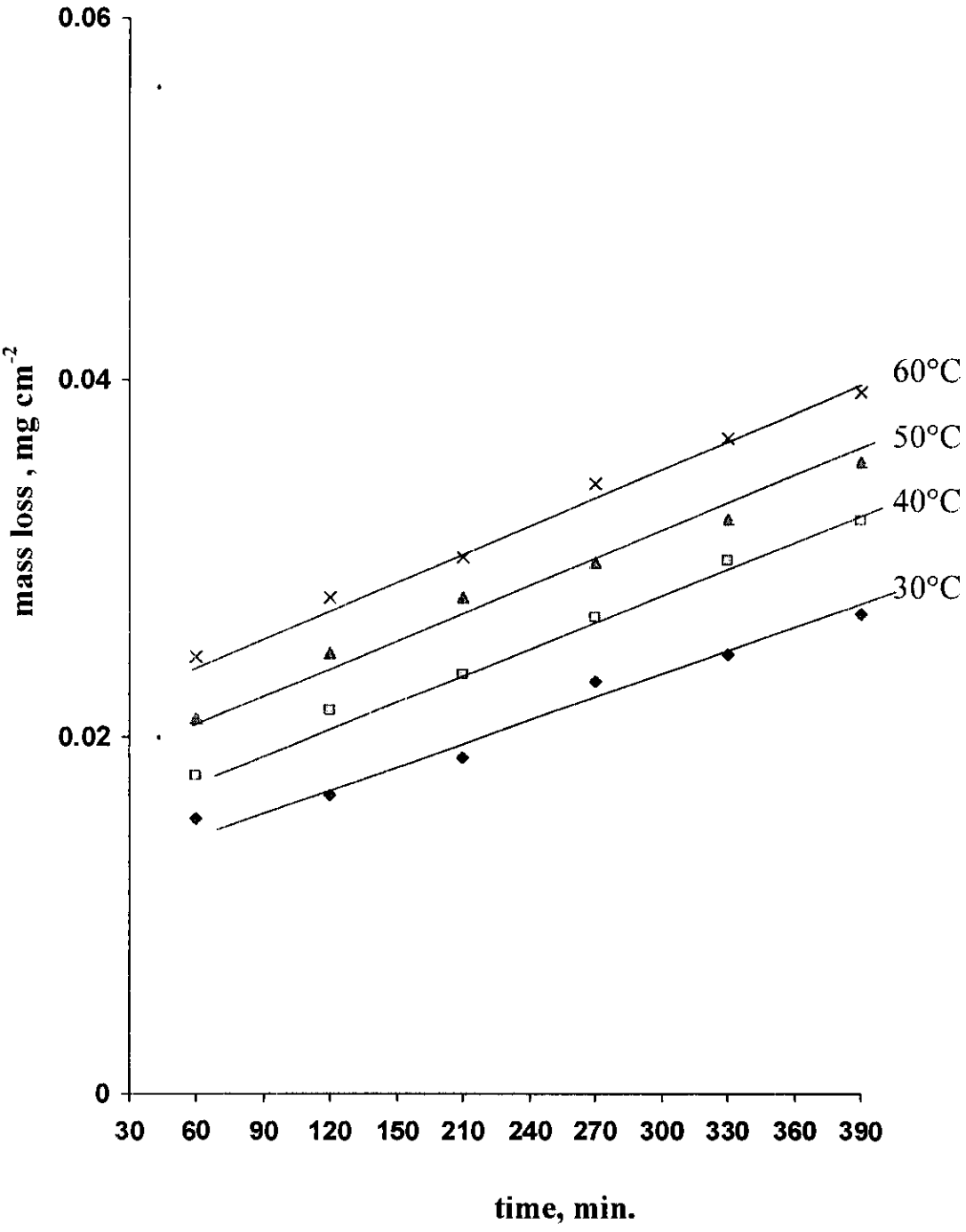

Fig.(3.12): Mass loss-time curves for the corrosion of C-steel in 2M HCl containing 10^{-4} M of compound (II) at different temperatures

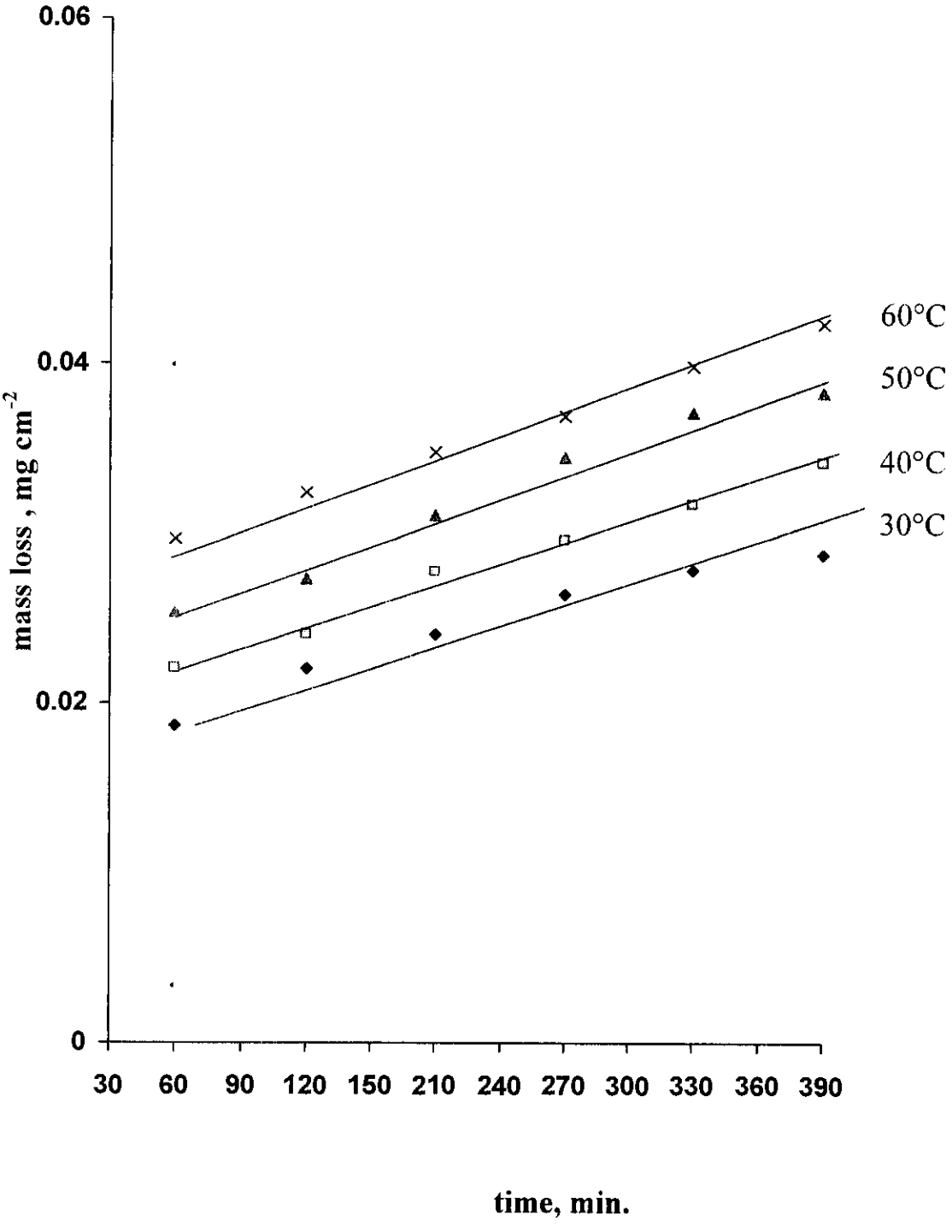

Fig.(3.13): Mass loss-time curves for the corrosion of C-steel in 2M HCl containing 10^{-5}M of compound (II) at different temperatures

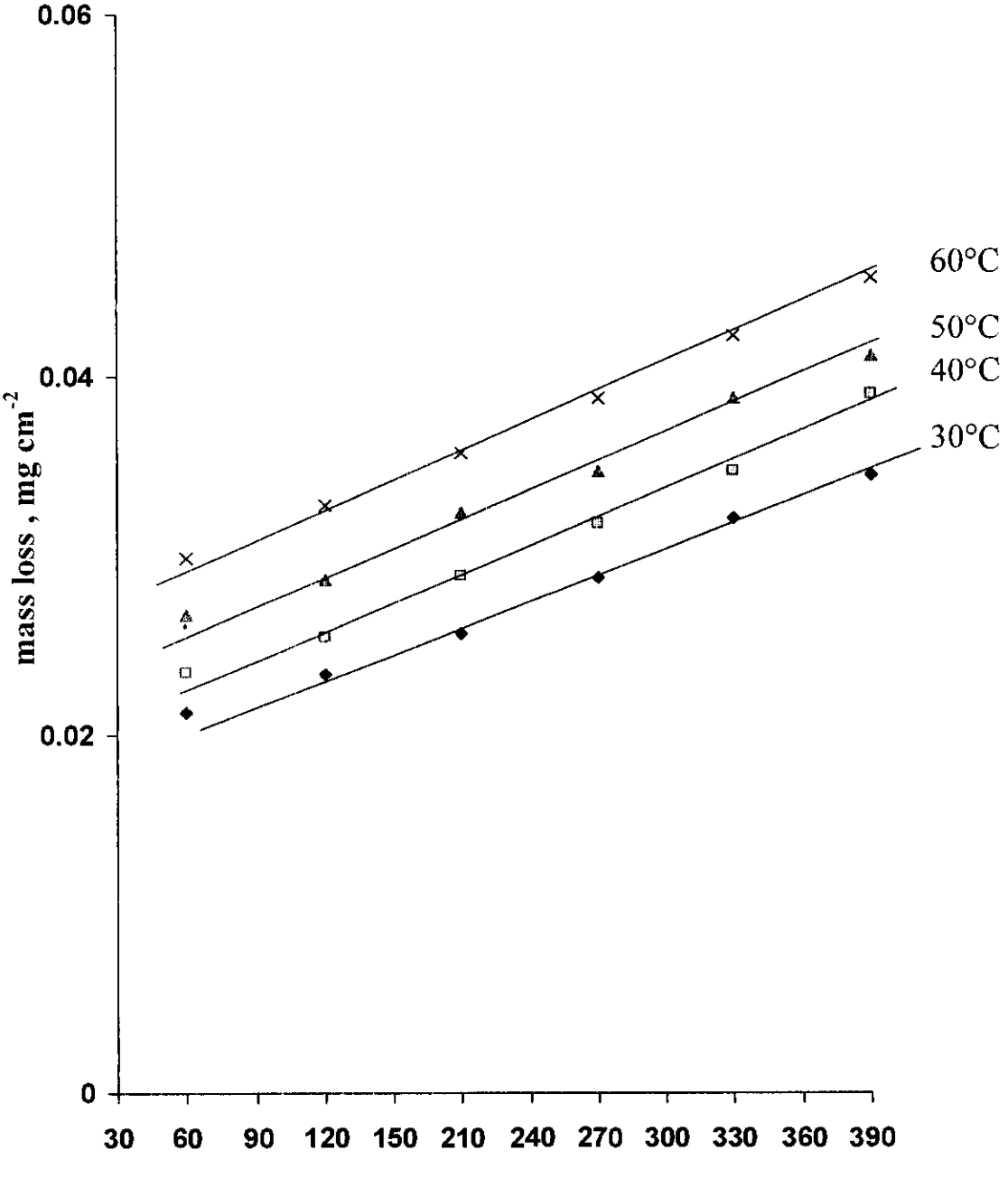

Fig.(3.14): Mass loss-time curves for the corrosion of C-steel in 2M HCl containing 10^{-6} M of compound (II) at different temperatures

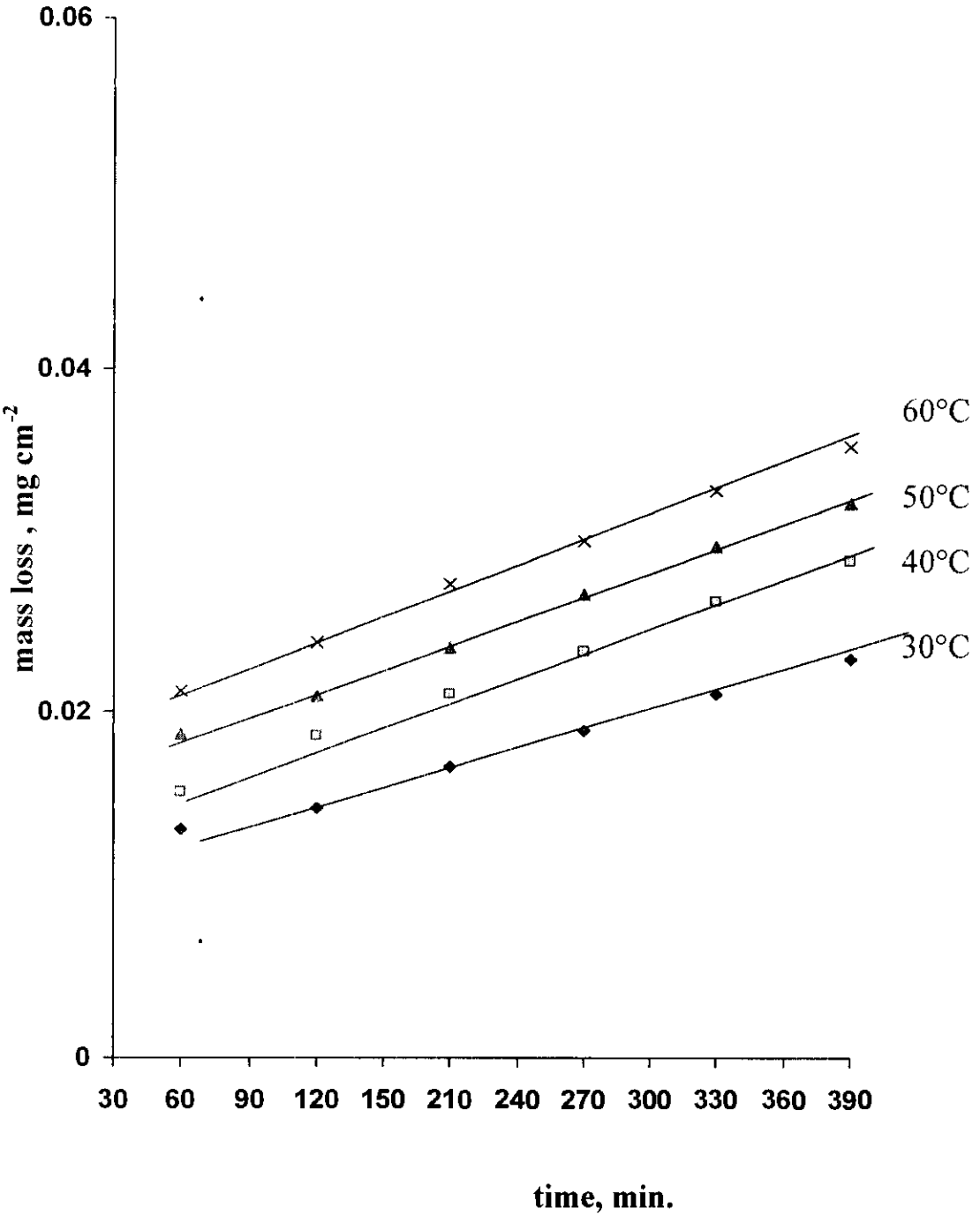

Fig.(3.15): Mass loss-time curves for the corrosion of C-steel in 2M HCl containing 10^{-3}M of compound (III) at different temperatures

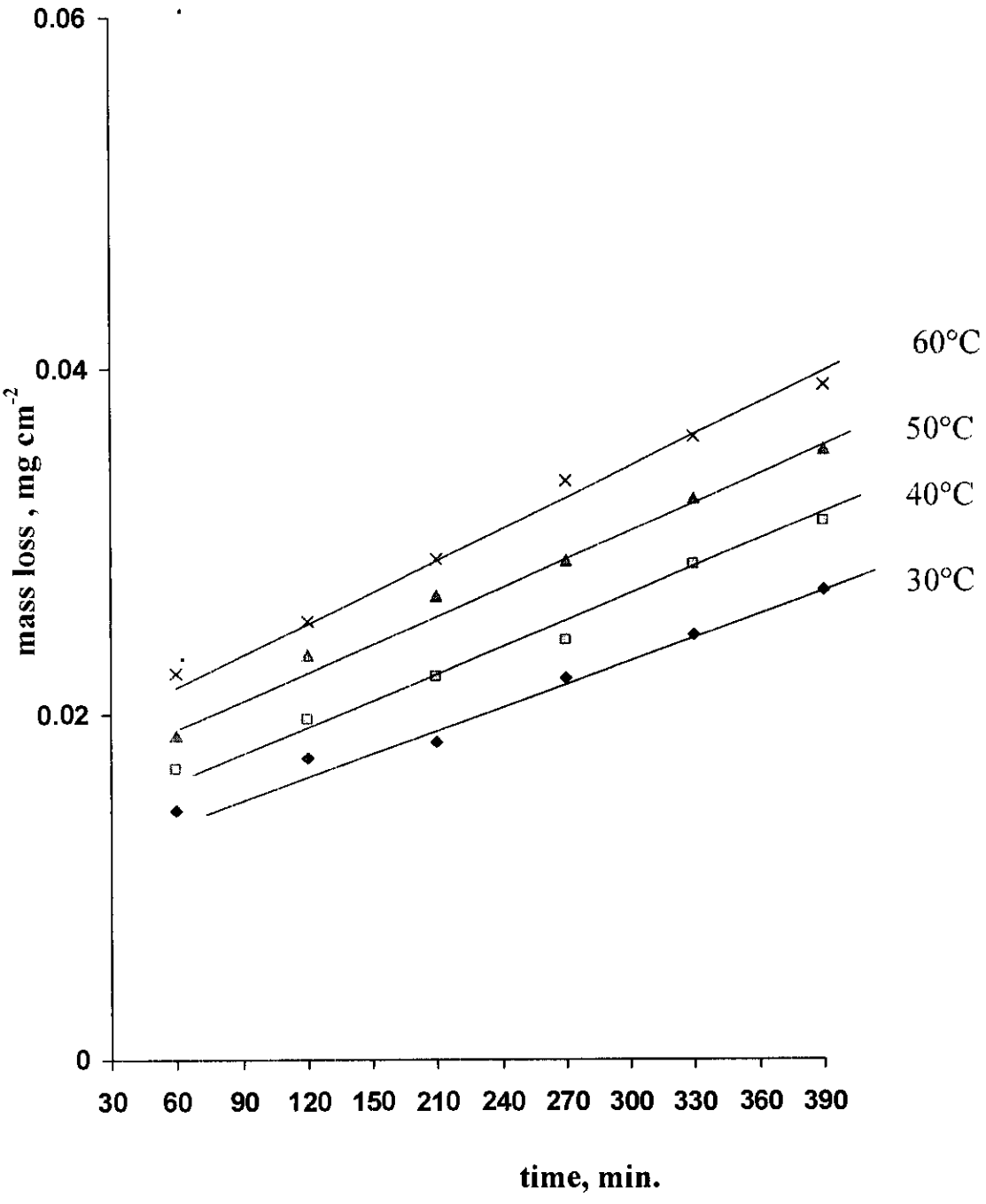

Fig.(3.16): Mass loss-time curves for the corrosion of C-steel in 2M HCl containing 10^{-4}M of compound (III) at different temperatures

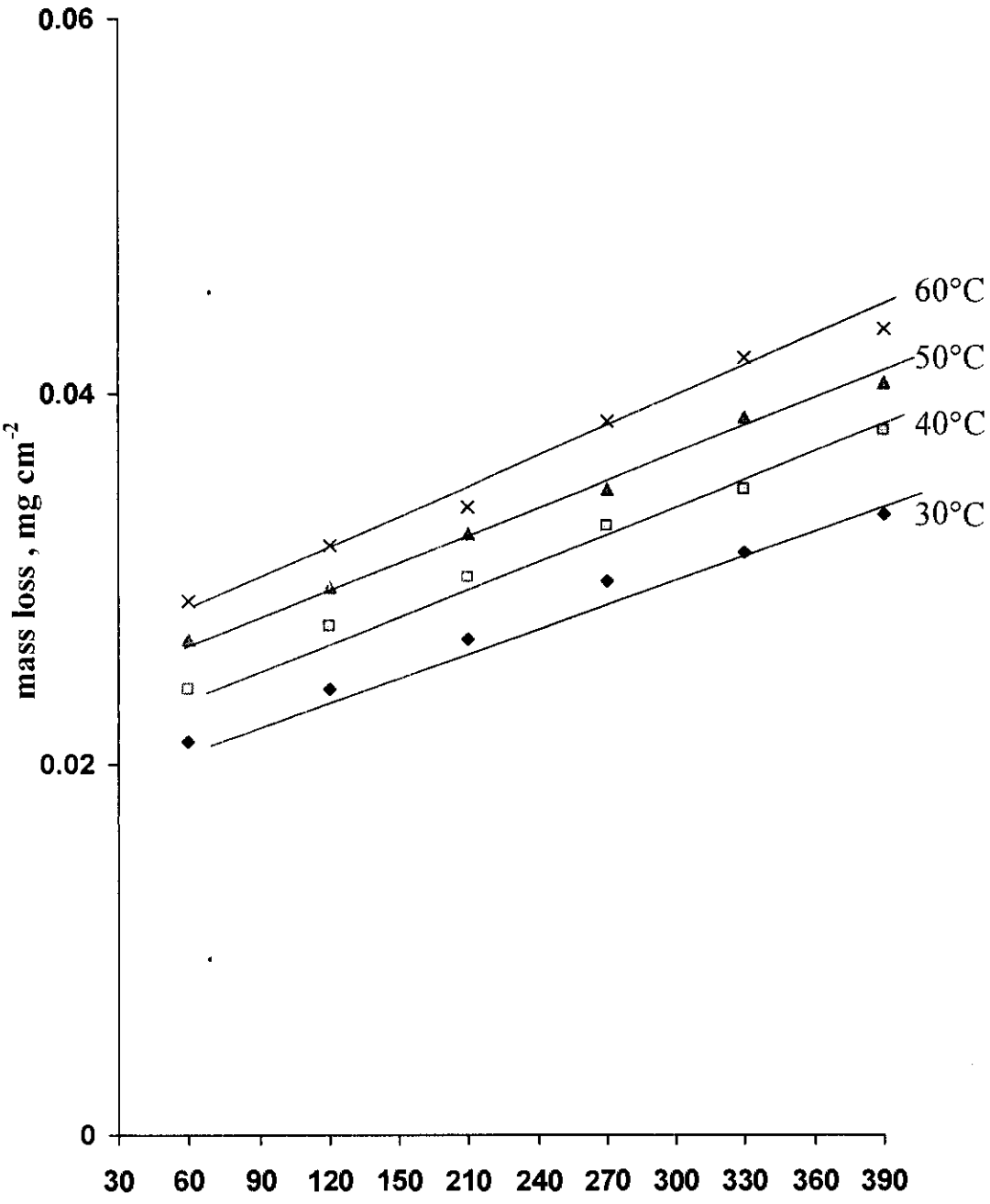

Fig.(3.17): Mass loss-time curves for the corrosion of C-steel in 2M HCl containing 10^{-5}M of compound (III) at different temperatures

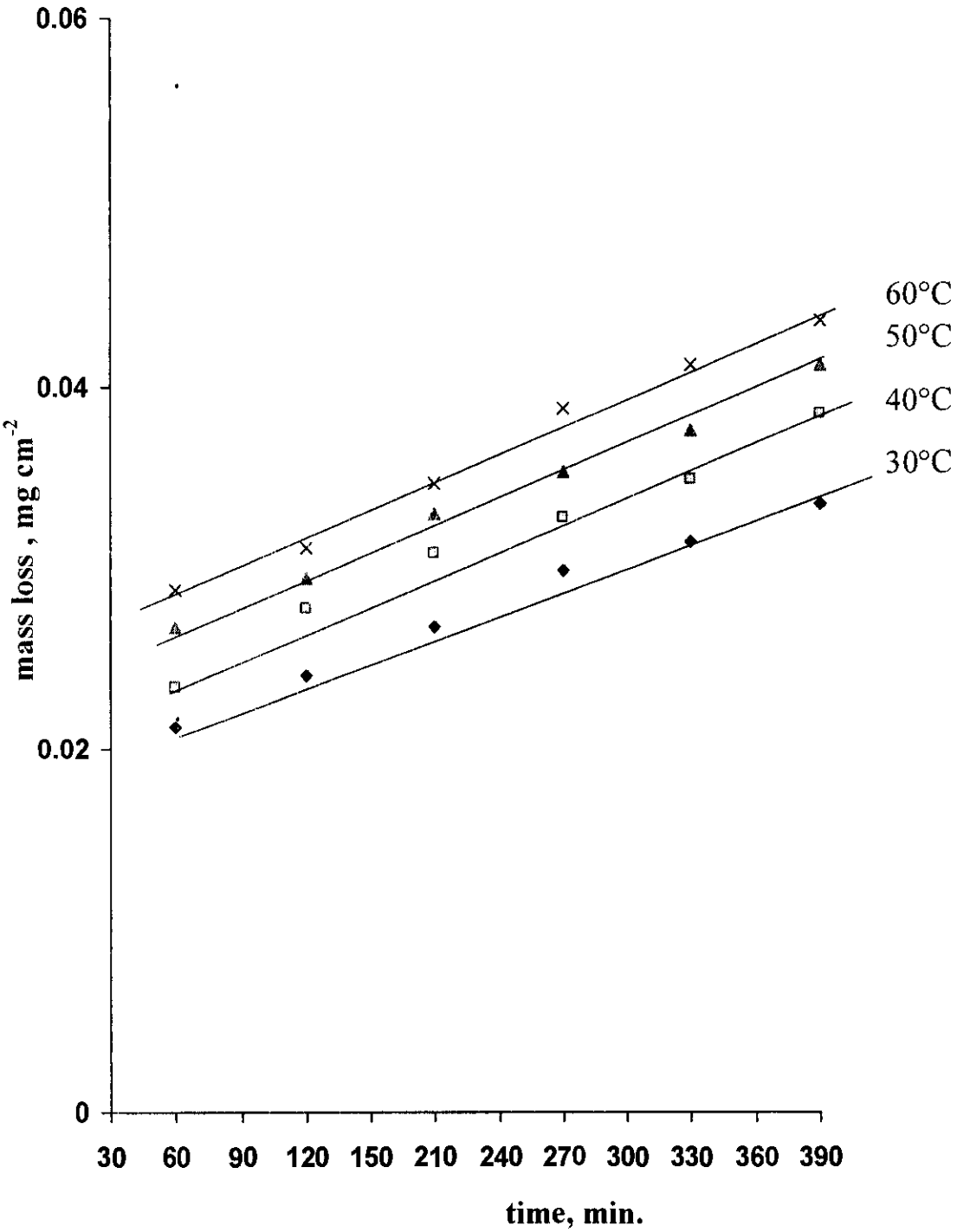

Fig.(3.18): Mass loss-time curves for the corrosion of C-steel in 2M HCl containing 10^{-6} M of compound (III) at different temperatures

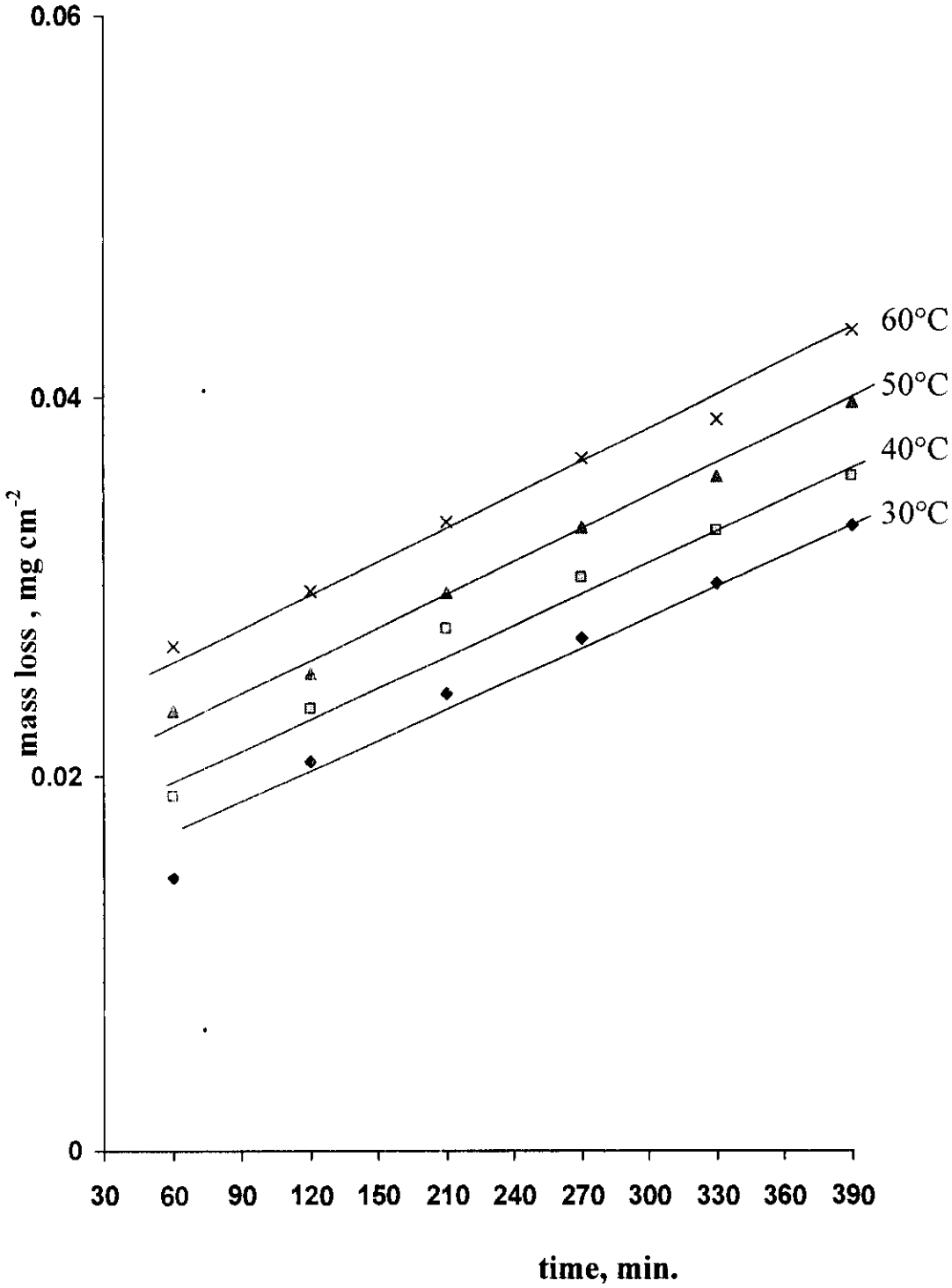

Fig.(3.19): Mass loss-time curves for the corrosion of C-steel in 2M HCl containing 10^{-3} M of compound (IV) at different temperatures

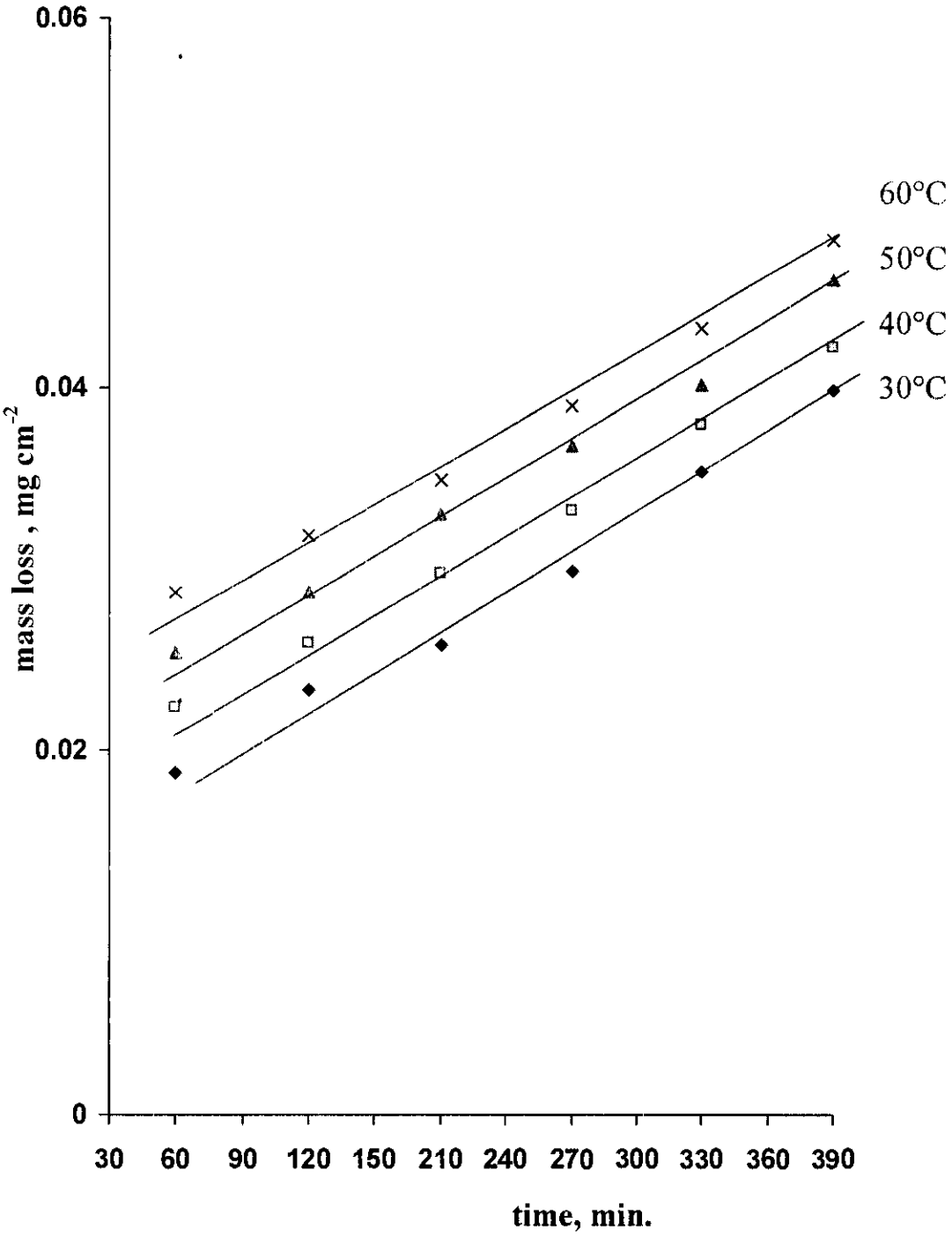

Fig.(3.20):. Mass loss-time curves for the corrosion of C-steel in 2M HCl containing 10^{-4} M of compound (IV) at different temperature

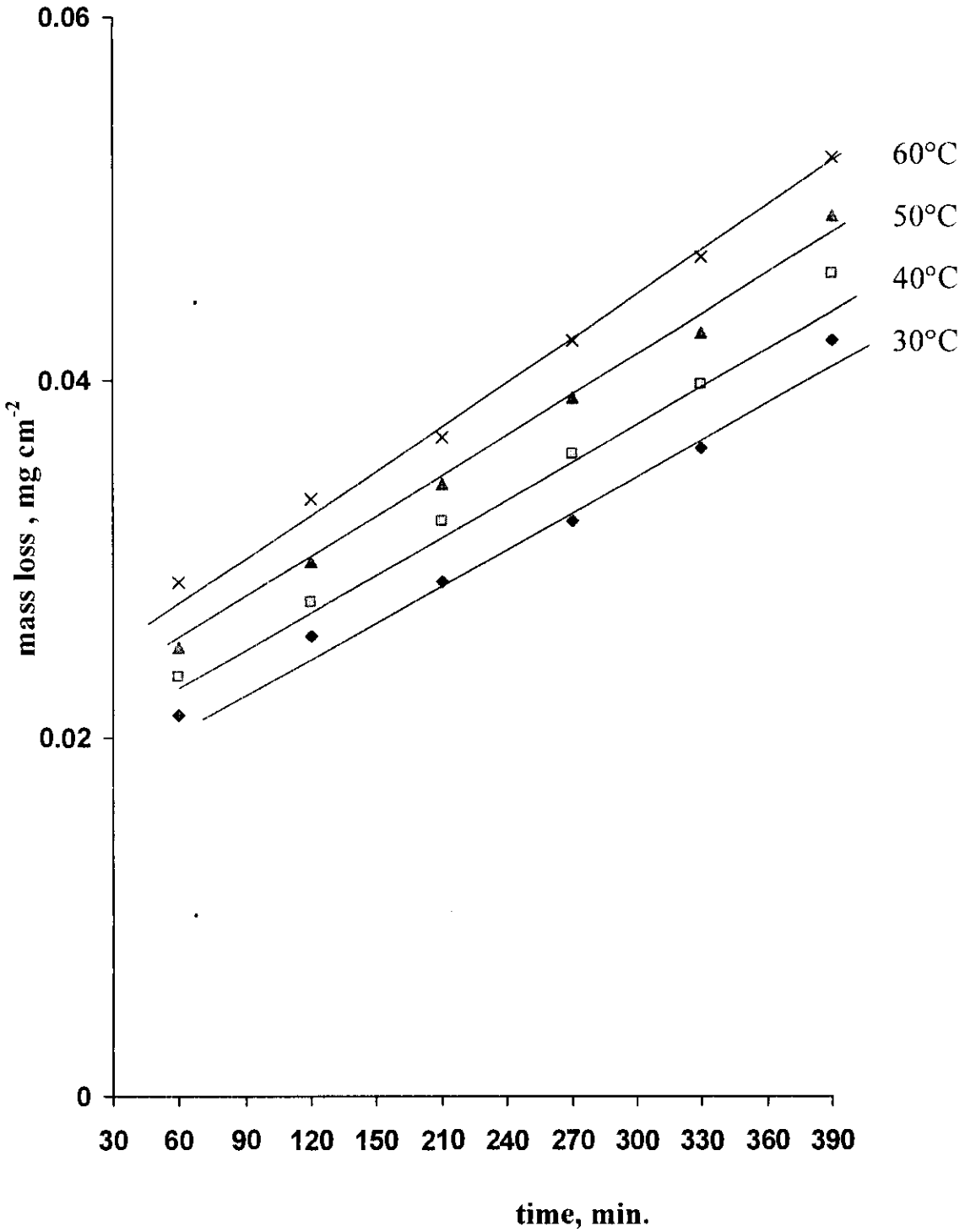

Fig.(3.21): Mass loss-time curves for the corrosion of C-steel in 2M HCl containing 10^{-5} M of compound (IV) at different temperatures

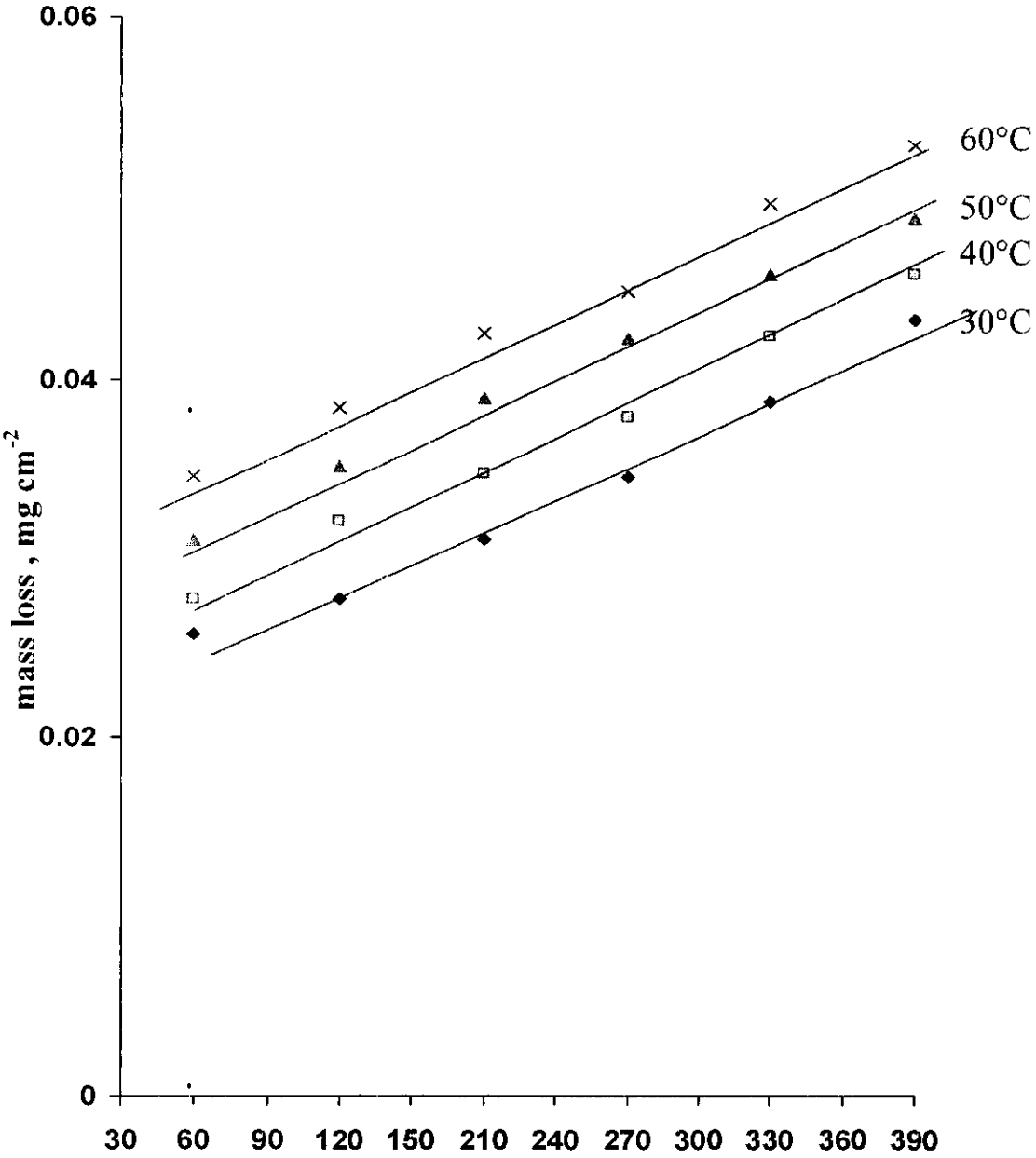

Fig.(3.22): Mass loss-time curves for the corrosion of C-steel in 2M HCl containing 10^{-6} M of compound (IV) at different temperatures

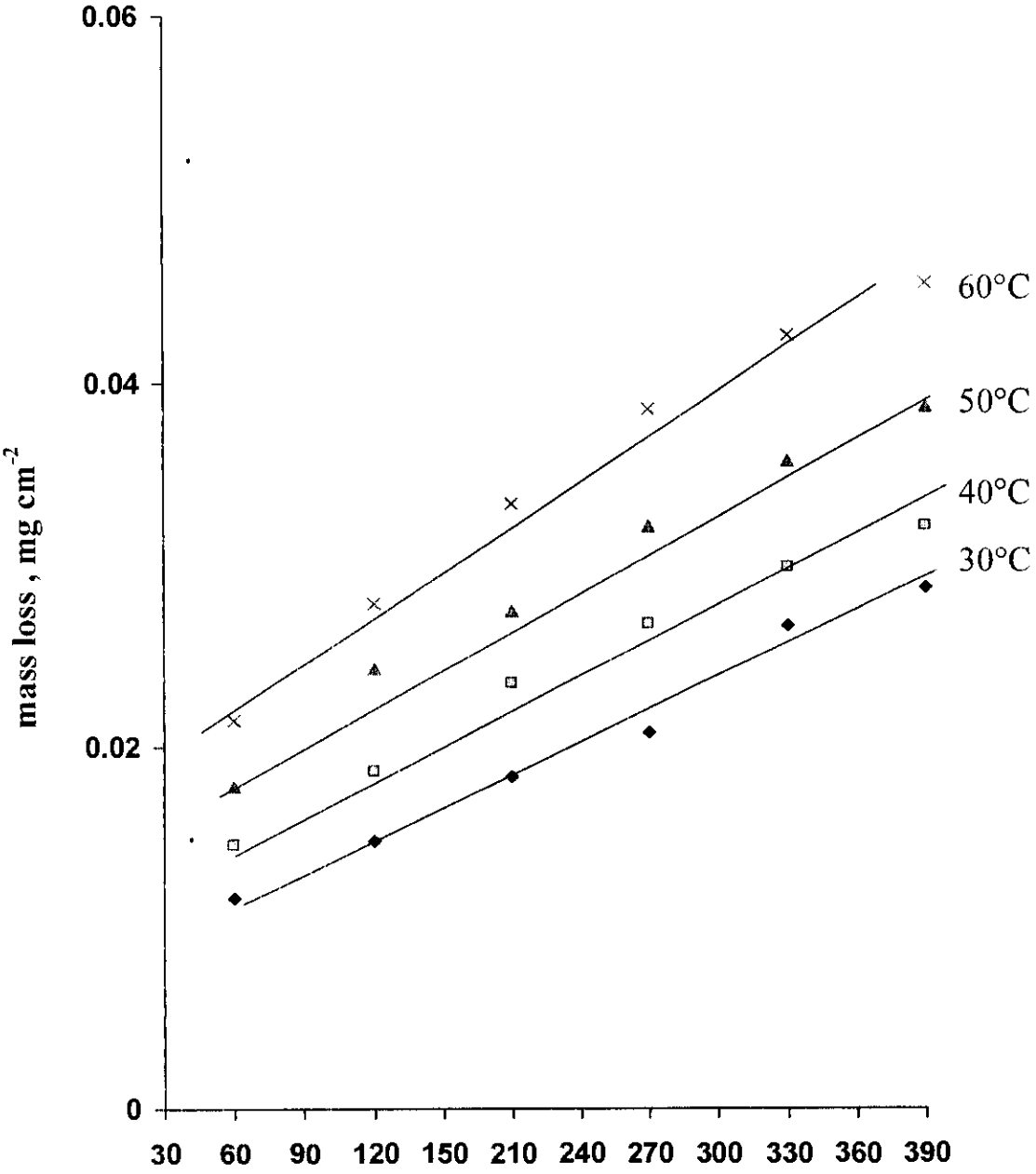

Fig.(3.23): Mass loss-time curves for the corrosion of C-steel in 2M HCl containing 10^{-3}M of compound (V) at different temperatures

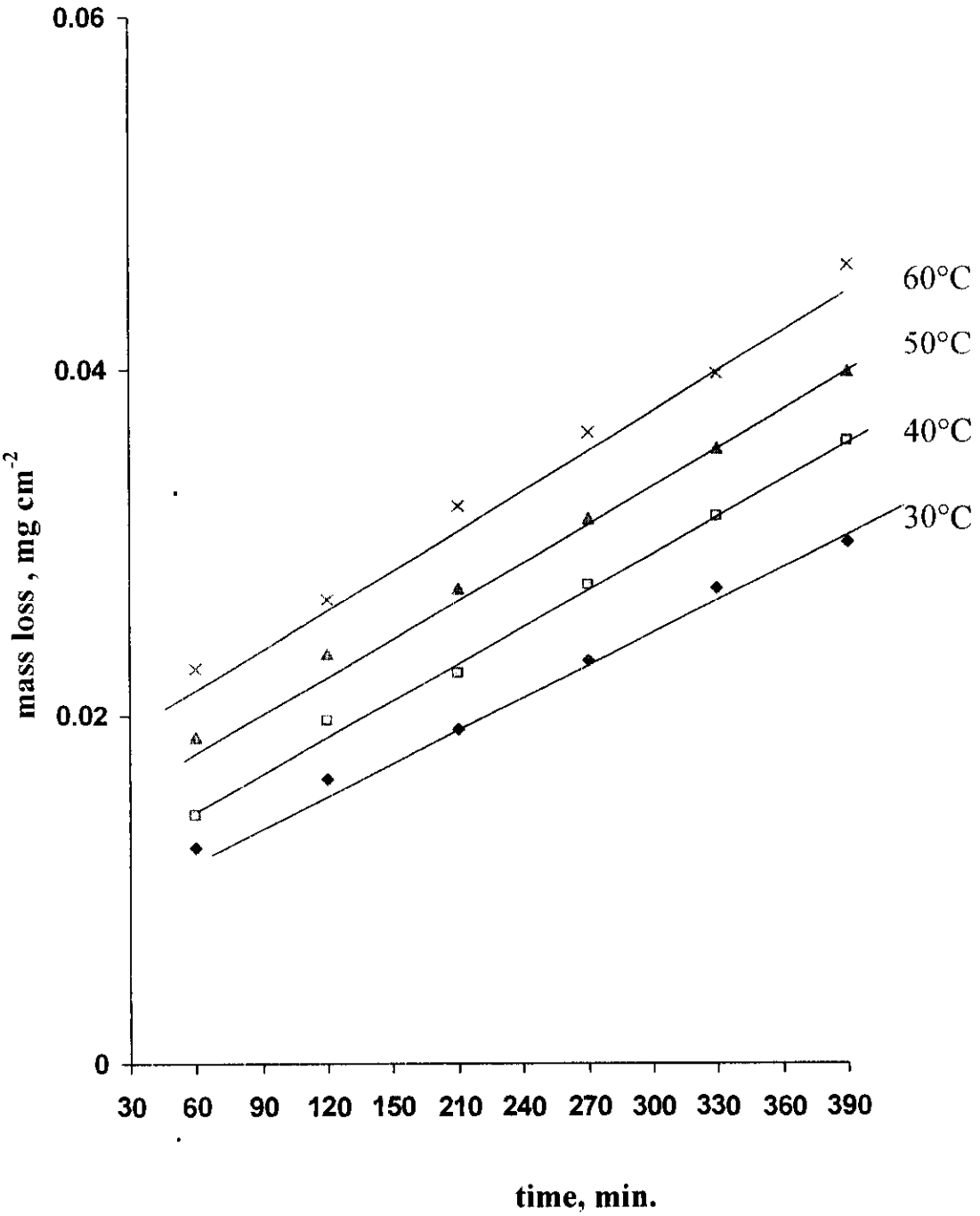

Fig.(3.24): Mass loss-time curves for the corrosion of C-steel in 2M HCl containing 10^{-4}M of compound (V) at different temperatures

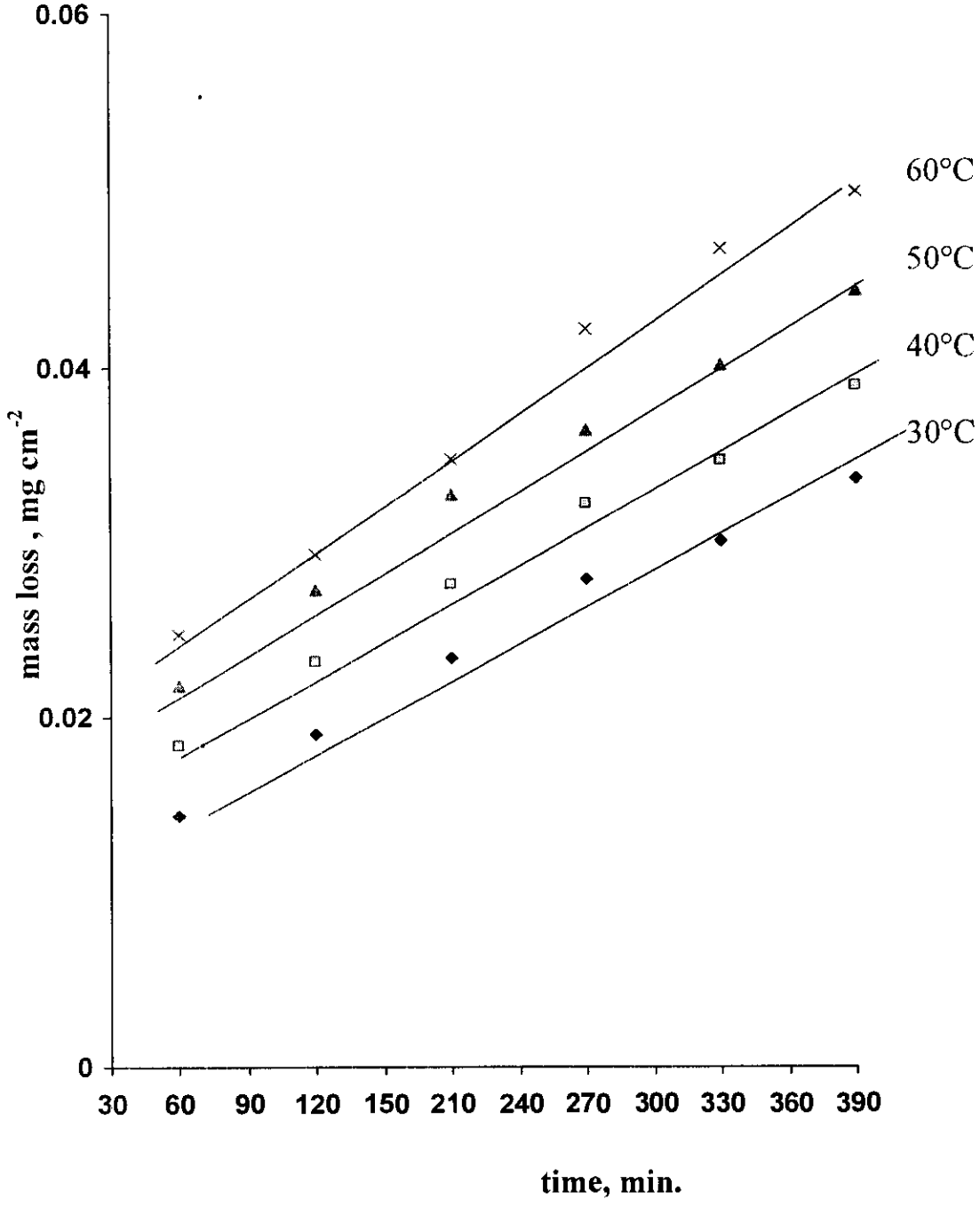

Fig.(3.25): Mass loss-time curves for the corrosion of C-steel in 2M HCl containing 10^{-5}M of compound (V) at different temperatures

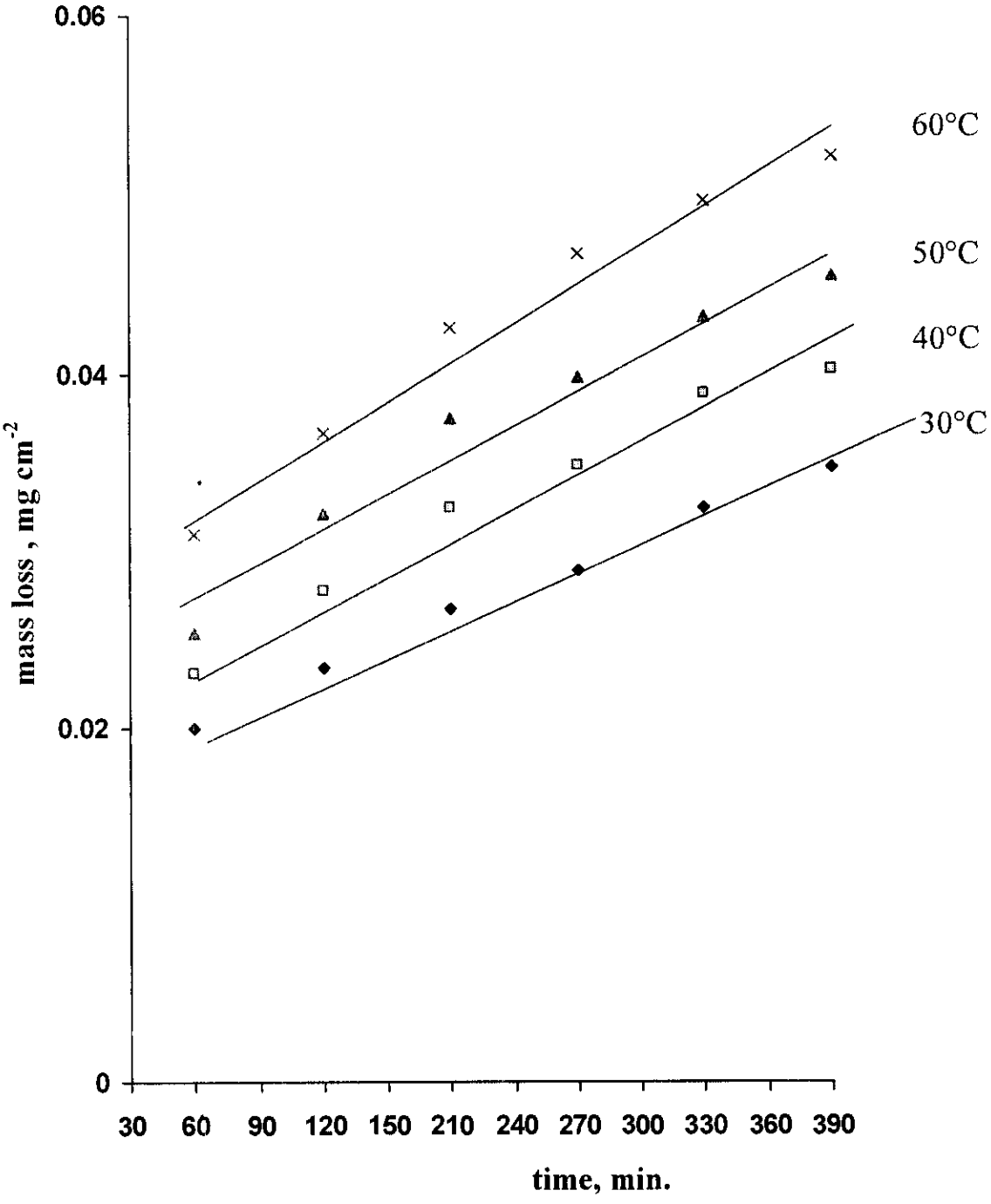

Fig.(3.26): Mass loss-time curves for the corrosion of C-steel in 2M HCl containing 10^{-6} M of compound (V) at different temperatures

Table (3.2): The effect of temperature on the corrosion parameters of C-steel in 2M HCl containing different concentrations of inhibitor

Conc.	Temp. °C	Free 2M HCl	Compound (I)			Compound (II)			Compound (III)			Compound (IV)			Compound (V)		
		Wt. loss	Wt. loss	IE	θ	Wt. loss	IE	θ	Wt. loss	IE	θ	Wt. loss	IE	θ	Wt. loss	IE	θ
10^{-3}			-	-	-	-	-	-	-	-	-	-	-	-	-	-	-
	30 °C	0.0744	0.0254	65.18	0.6518	0.0211	71.63	0.7163	0.0231	68.95	0.6895	0.0332	55.37	0.5537	0.0287	61.4	0.614
	40 °C	0.081	0.0296	63.45	0.6345	0.0268	66.91	0.6691	0.0288	64.44	0.6444	0.0358	53.82	0.5382	0.0321	60.37	0.6037
	50 °C	0.0865	0.0326	62.08	0.6208	0.0315	63.58	0.6358	0.0321	62.89	0.6289	0.0397	52.36	0.5236	0.0387	55.26	0.5526
	60 °C	0.0934	0.0354	60.59	0.5059	0.0382	59.10	0.5910	0.0354	62.09	0.6209	0.0435	46.28	0.4628	0.0454	51.39	0.5139
10^{-4}			-	-	-	-	-	-	-	-	-	-	-	-	-	-	-
	30 °C	0.0744	0.0294	60.48	0.6048	0.0269	63.48	0.6384	0.0272	63.44	0.6344	0.0398	46.50	0.4650	0.0301	59.5	0.595
	40 °C	0.081	0.0328	59.50	0.5950	0.0321	60.37	0.6037	0.0311	61.60	0.6160	0.0441	45.55	0.4555	0.0358	55.80	0.5580
	50 °C	0.0865	0.0365	57.80	0.5780	0.0354	59.07	0.5907	0.0352	59.30	0.5930	0.0475	45.05	0.4505	0.0398	53.98	0.5398
	60 °C	0.0934	0.0411	55.99	0.5599	0.0393	57.92	0.5792	0.0389	58.35	0.5835	0.0538	42.39	0.4239	0.0459	50.85	0.5085
10^{-5}			-	-	-	-	-	-	-	-	-	-	-	-	-	-	-
	30 °C	0.0744	0.0329	55.77	0.5577	0.0288	61.29	0.6129	0.0298	59.94	0.5994	0.0421	43.41	0.4341	0.0336	54.8	0.548
	40 °C	0.081	0.0348	49.50	0.4950	0.0342	57.77	0.5777	0.0379	53.20	0.5320	0.0465	42.59	0.4259	0.0389	51.97	0.5197
	50 °C	0.0865	0.0368	47.86	0.4786	0.0382	55.83	0.5583	0.0412	52.36	0.5236	0.0499	40.92	0.4092	0.0443	48.78	0.4878
	60 °C	0.0934	0.0401	46.35	0.4635	0.0422	52.78	0.5278	0.0465	50.12	0.5012	0.0539	38.54	0.3854	0.0498	46.68	0.4668
10^{-6}			-	-	-	-	-	-	-	-	-	-	-	-	-	-	-
	30 °C	0.0744	0.0349	53.09	0.5309	0.0345	53.62	0.5362	0.0335	54.97	0.5497	0.0433	41.80	0.4180	0.0347	53.3	0.533
	40 °C	0.081	0.0384	49.50	0.4950	0.0389	51.97	0.5197	0.0384	52.59	0.5259	0.0498	38.51	0.3851	0.0402	50.37	0.5037
	50 °C	0.0865	0.0411	47.86	0.4786	0.0411	49.47	0.4947	0.0411	50.05	0.5005	0.0551	36.30	0.3630	0.0454	47.51	0.4751
	60 °C	0.0934	0.0448	46.35	0.4635	0.0454	48.17	0.4817	0.0435	49.89	0.948	0.0594	34.26	0.3426	0.0521	44.21	0.4421

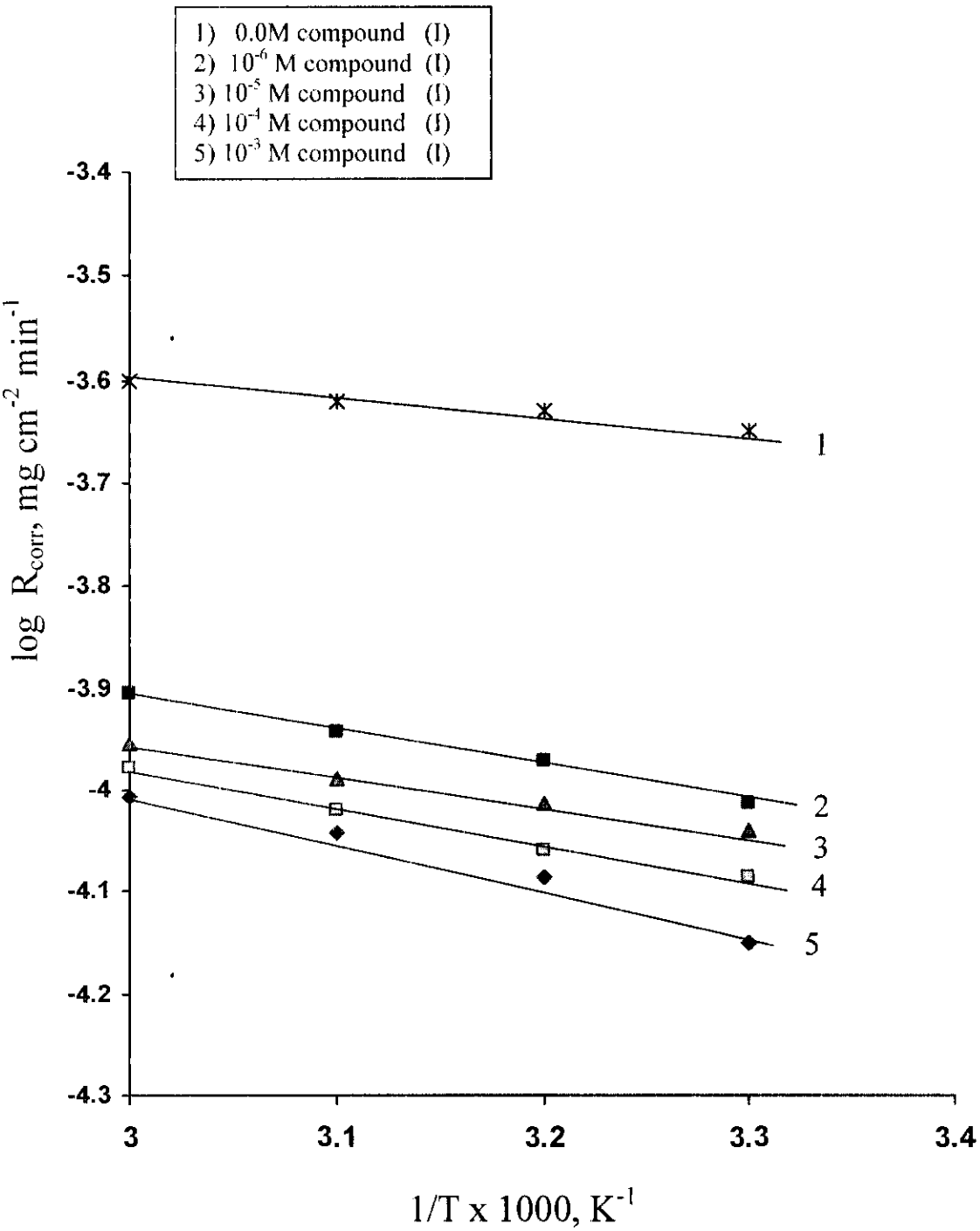

Fig. (3.27): log corrosion rate vs. 1/T for corrosion of carbon steel in 2M HCl containing different concentrations of compound (I).

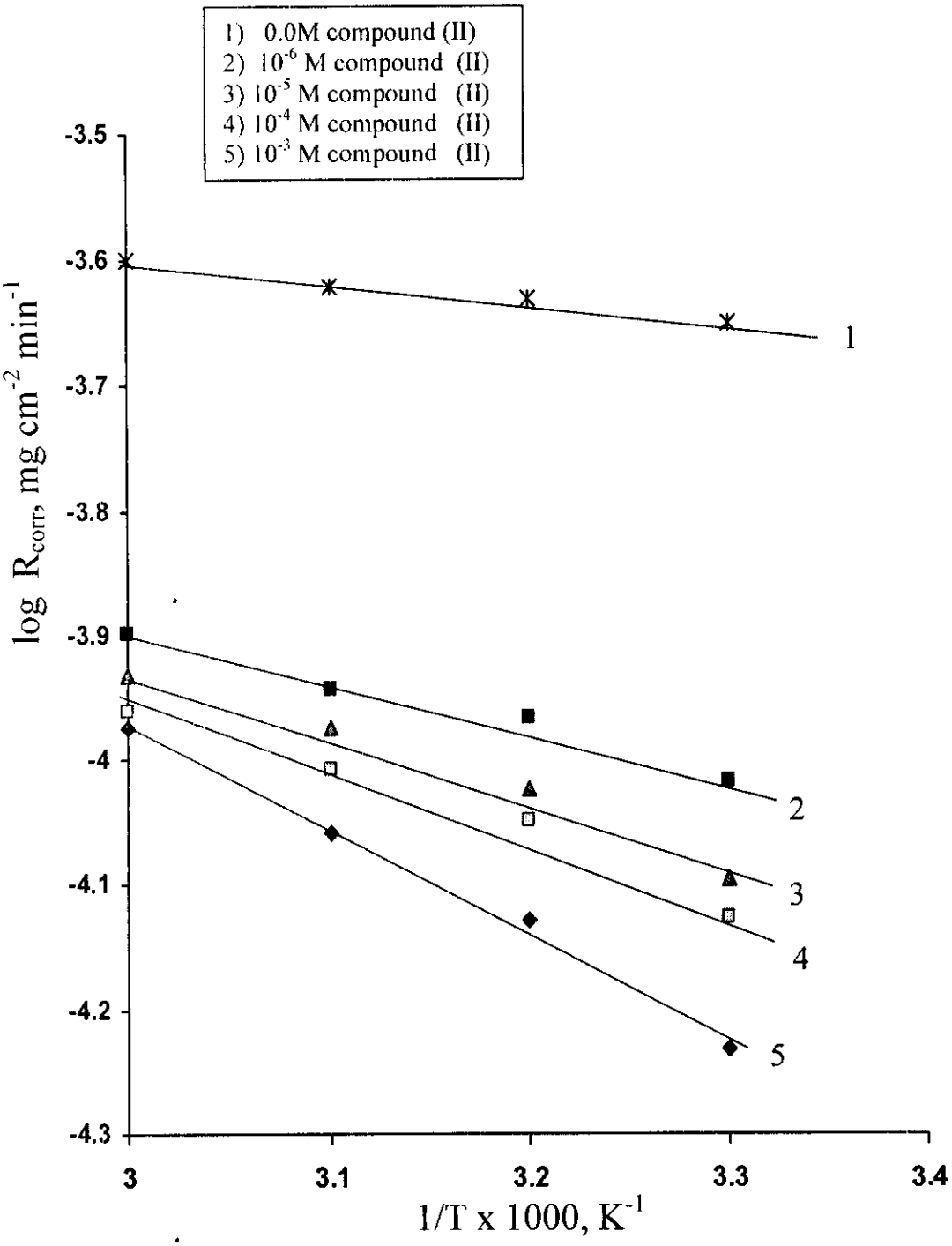

Fig. (3.28): log corrosion rate vs. 1/T for corrosion of carbon steel in 2M HCl containing different concentrations of compound (II).

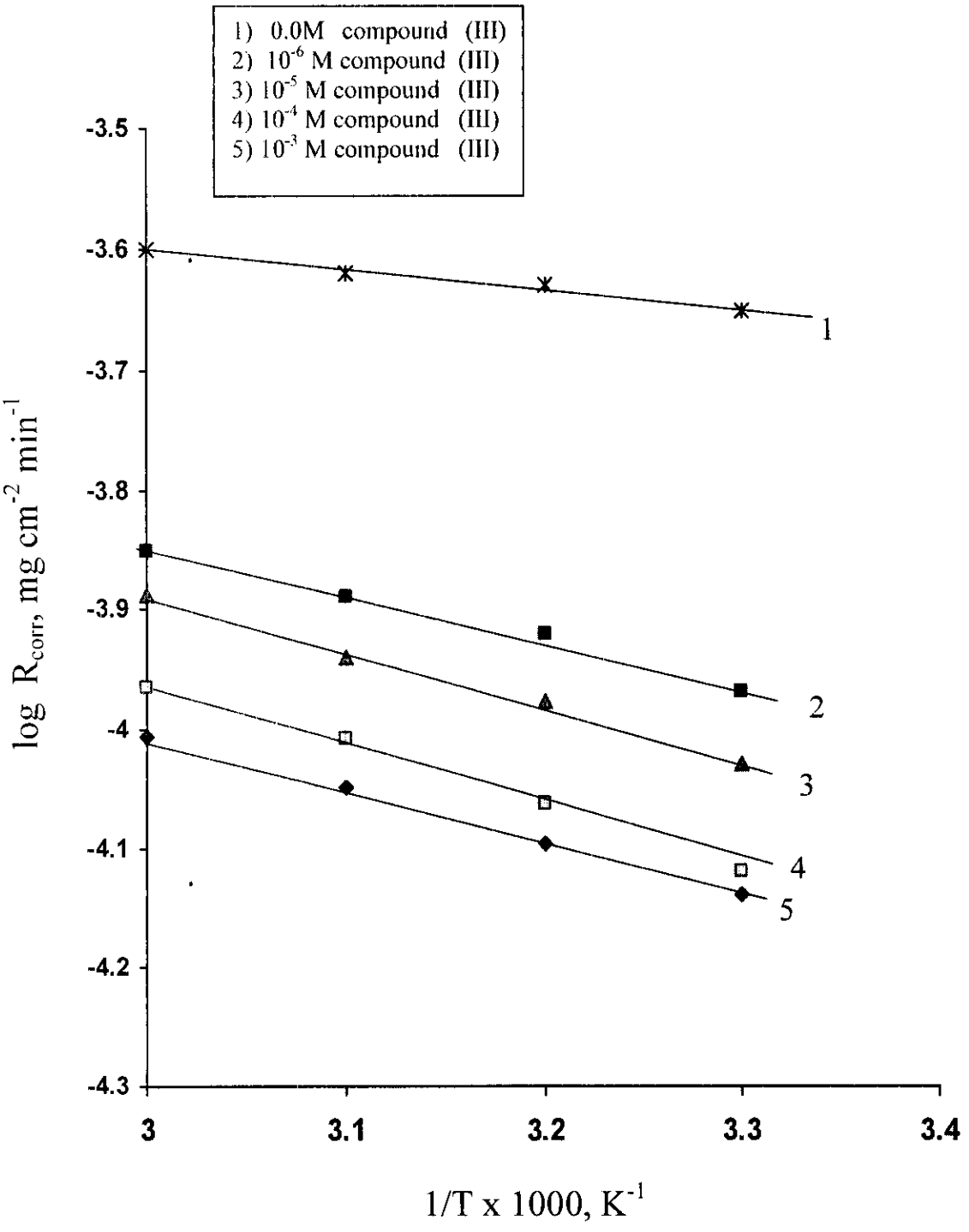

Fig. (3.29): log corrosion rate vs. 1/T for corrosion of carbon steel in 2M HCl containing different concentrations of compound (III).

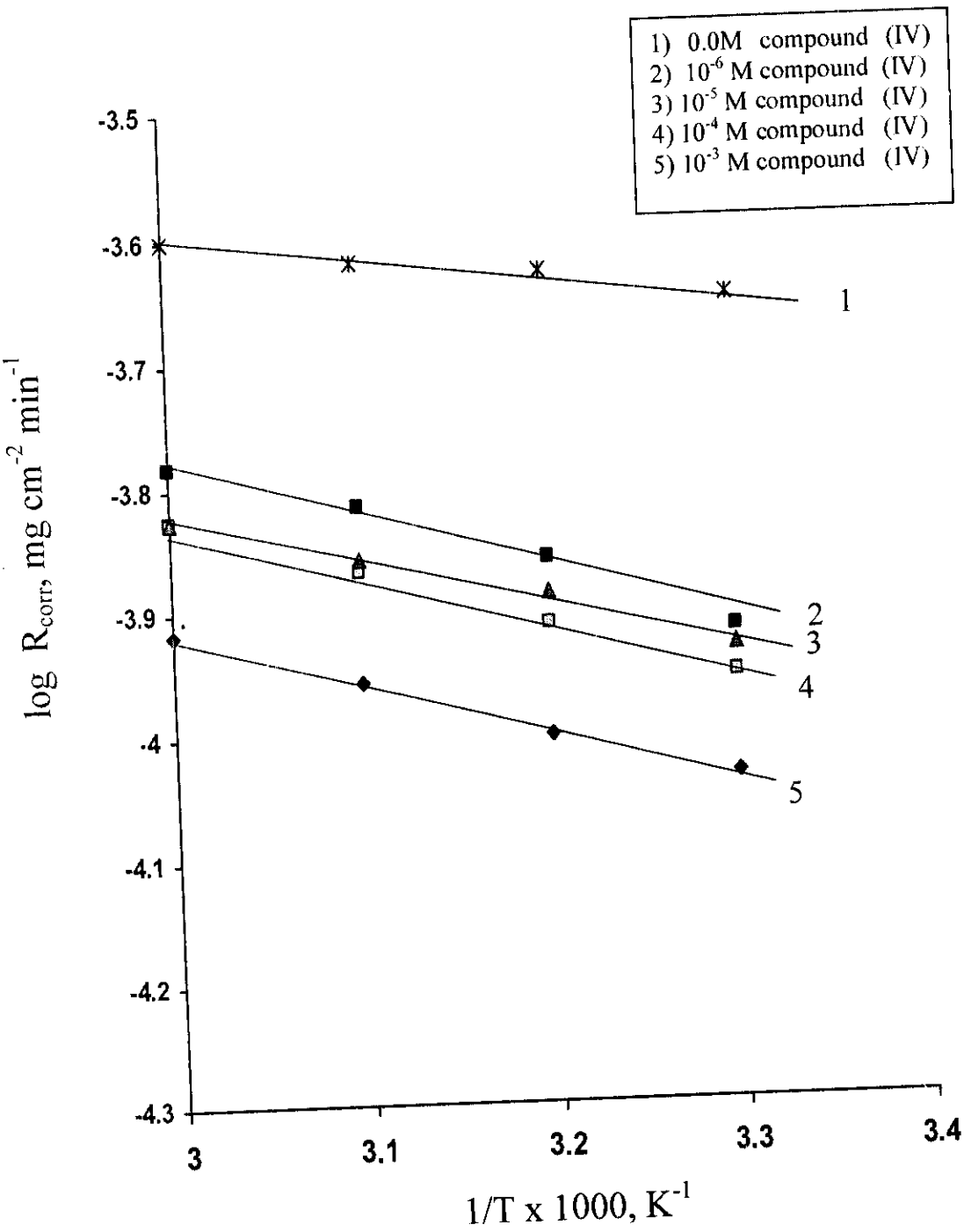

Fig. (3.30): log corrosion rate vs. 1/T for corrosion of carbon steel in 2M HCl containing different concentrations of compound (IV).

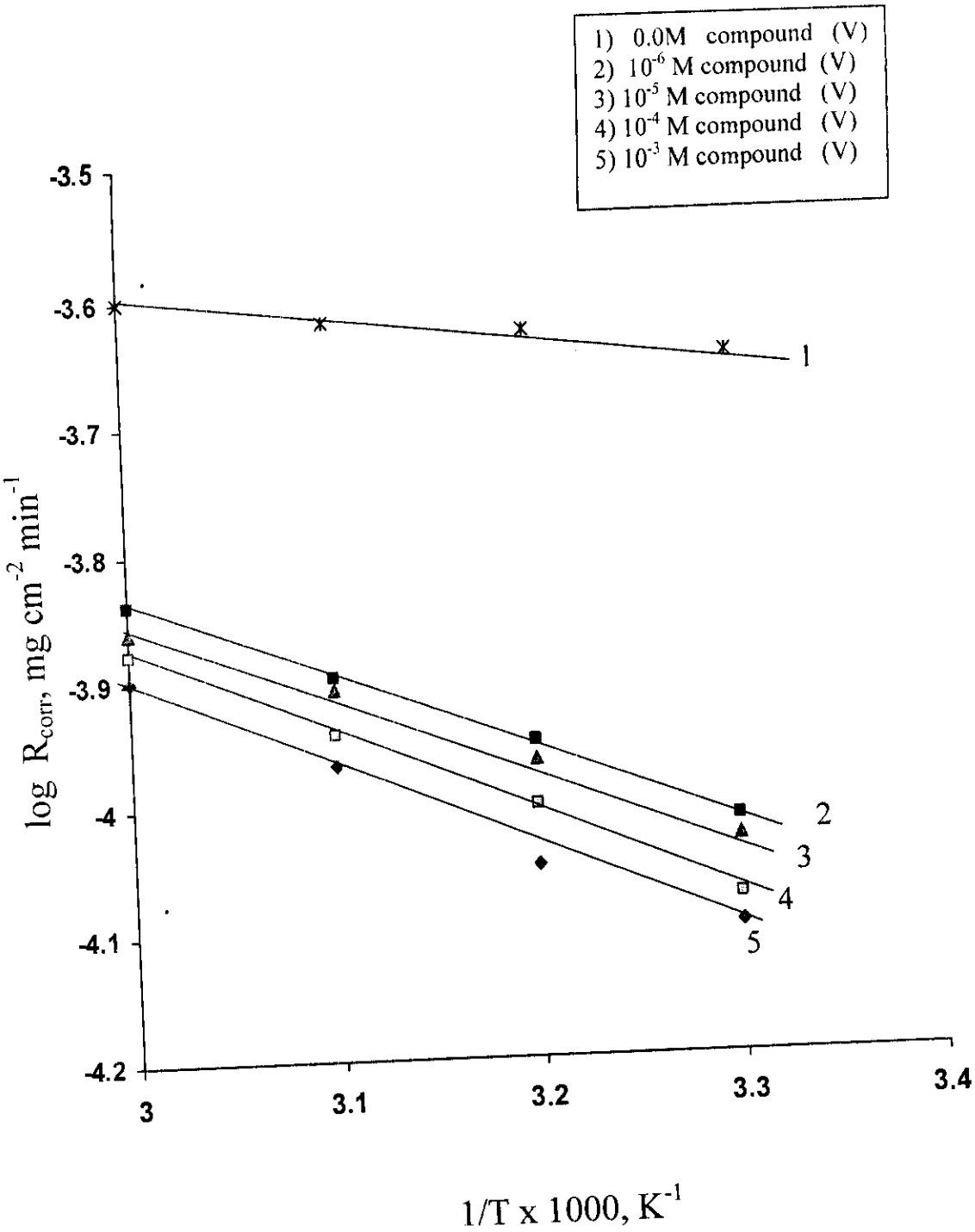

Fig. (3.31): log corrosion rate vs. 1/T for corrosion of carbon steel in 2M HCl containing different concentrations of compound (V).

3.3- Adsorption isotherms

Adsorption of organic inhibitors on the metal surface represents the most important action of these compounds. The extent and mode of adsorption depend on definite physico-chemical properties of the organic molecules such as functional group, aromaticity and π-orbital character of the donating electrons, steric effects, electron density of the donor atom and the electronic structure of the molecules[75-78]. The adsorption extent also depends on the metal surface and the electrolyte.

The adsorption of an organic compound on the surface of a metal is regarded as a substitutional adsorption process between the organic compound in the aqueous phase (Org_{aq}) and the water molecule adsorbed on the electrode surface $(H_2O)_{ad}$.

$$Org_{aq} + XH_2O_{(ads)} \Leftrightarrow Org_{ad} + X\,H_2O_{(aq)} \qquad (3.6)$$

where X is the size ratio, that is the number of water molecules replaced by one inhibitor molecule[79]. When the equilibrium of the process described in equation (3.5) is reached, it is possible to obtain different expressions for the adsorption isotherm plots and thus, the degree of surface coverage θ can be plotted as a function of the concentration of organic inhibitors.

The degree of surface coverage (θ) was calculated using the following equation:

$$\theta = 1 - \frac{W_{add}}{W_{free}} \qquad (3.7)$$

where W_{free} and W_{add} are the loss in mass in the absence and presence of the additive compounds, respectively. The value of θ have been inserted into Tables (3.1 -3.2). The degree of surface coverage θ was found to increase with increasing the concentration of additive, and decreases with raising temperature from 30°C

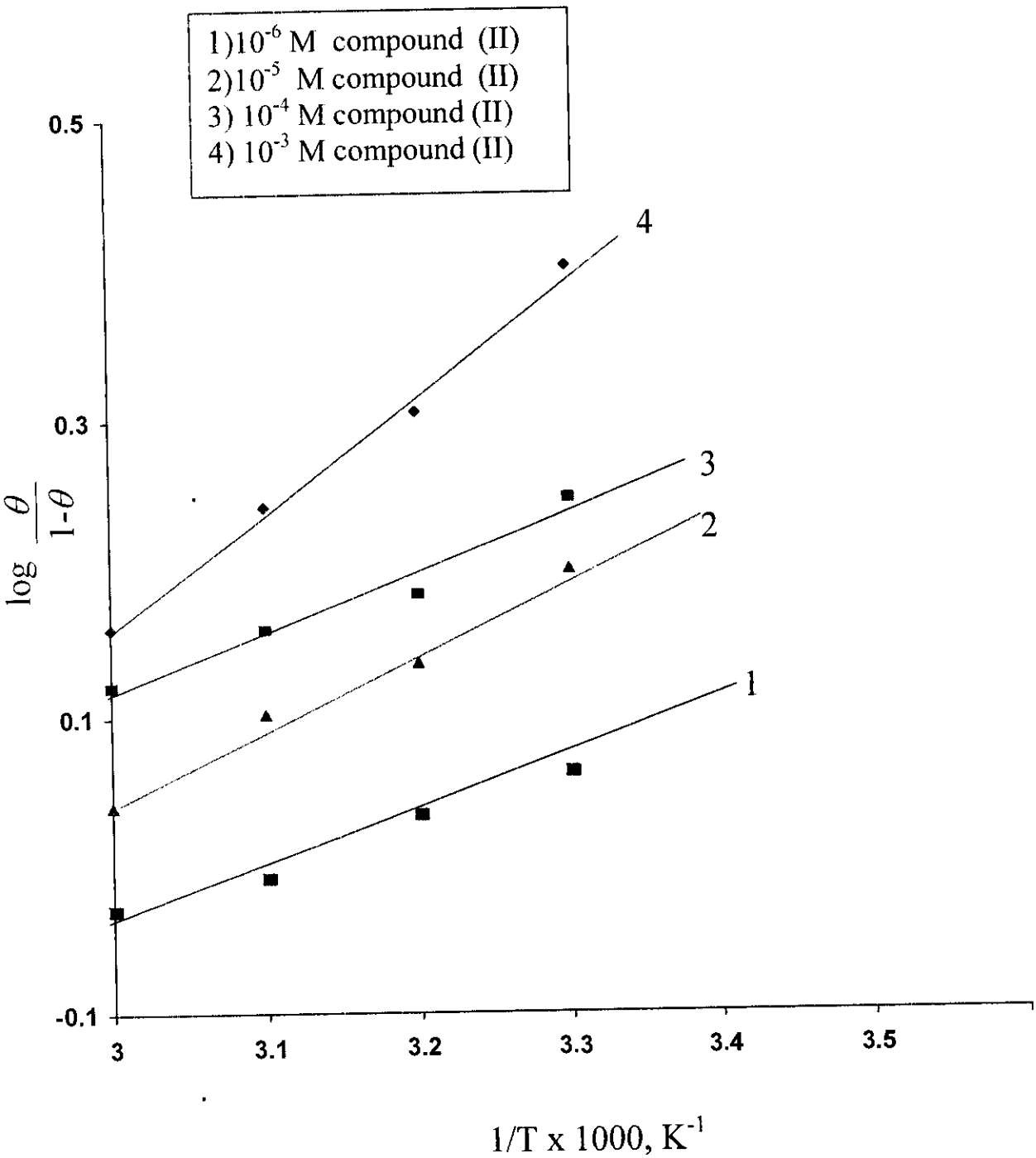

Fig. (3.33): Plots of log $\frac{\theta}{1-\theta}$ vs. 1/T for corrosion of carbon steel in 2M HCl containing different concentrations of compound (II).

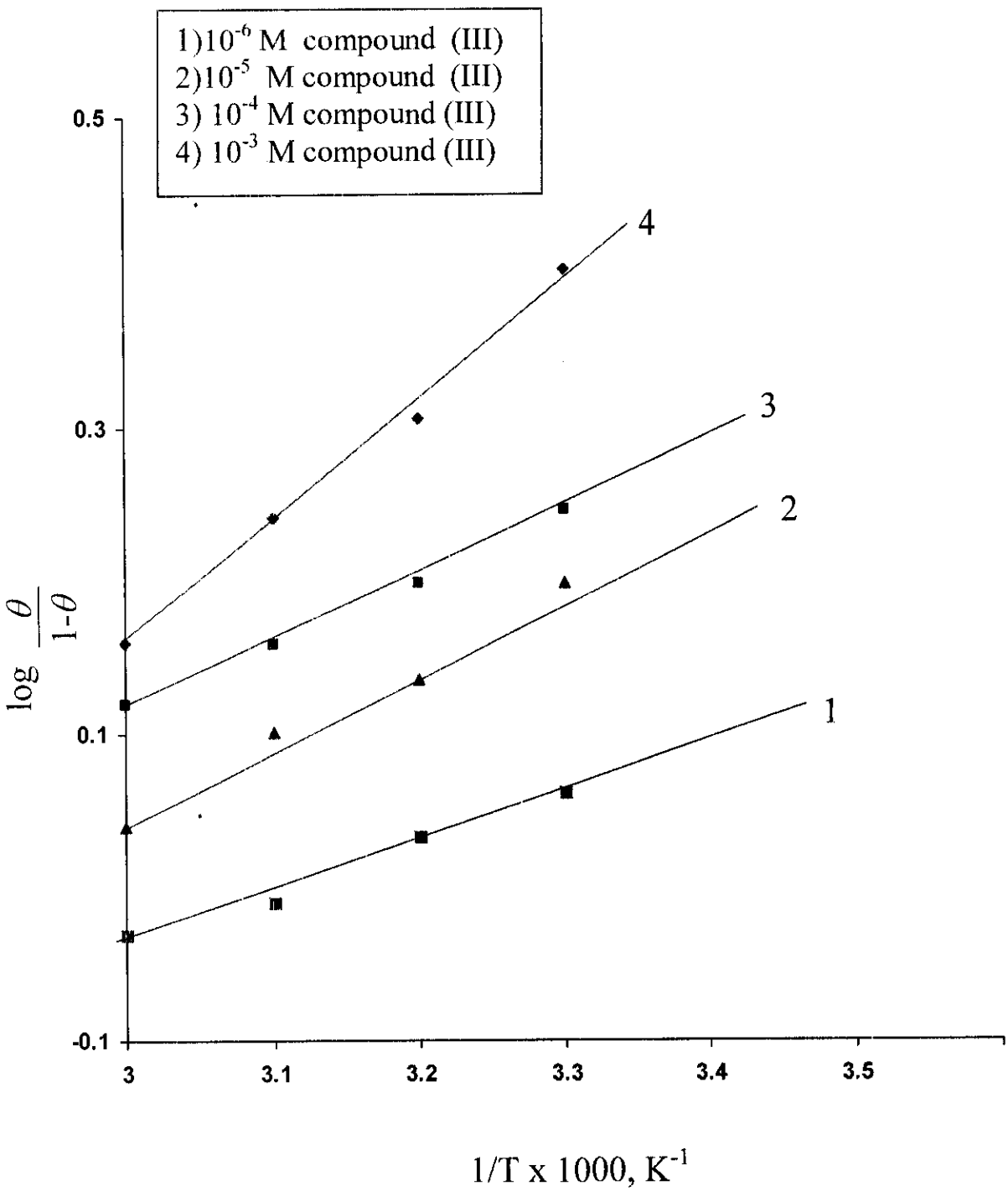

Fig. (3.34): Plots of log $\frac{\theta}{1-\theta}$ vs. 1/T for corrosion of carbon steel in 2M HCl containing different concentrations of compound (III).

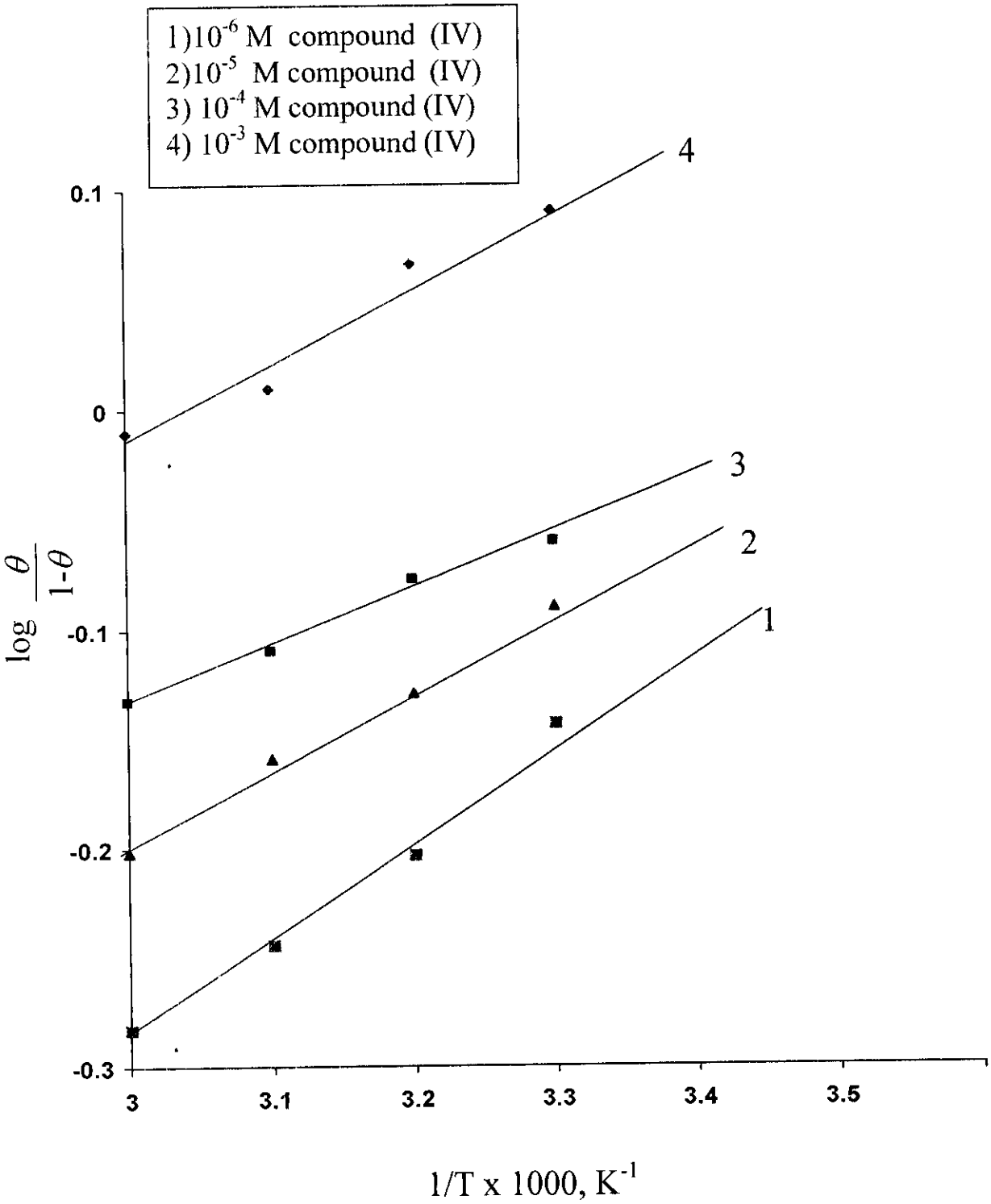

Fig. (3.35): Plots of log $\frac{\theta}{1-\theta}$ vs. 1/T for corrosion of carbon steel in 2M HCl containing different concentrations of compound (IV).

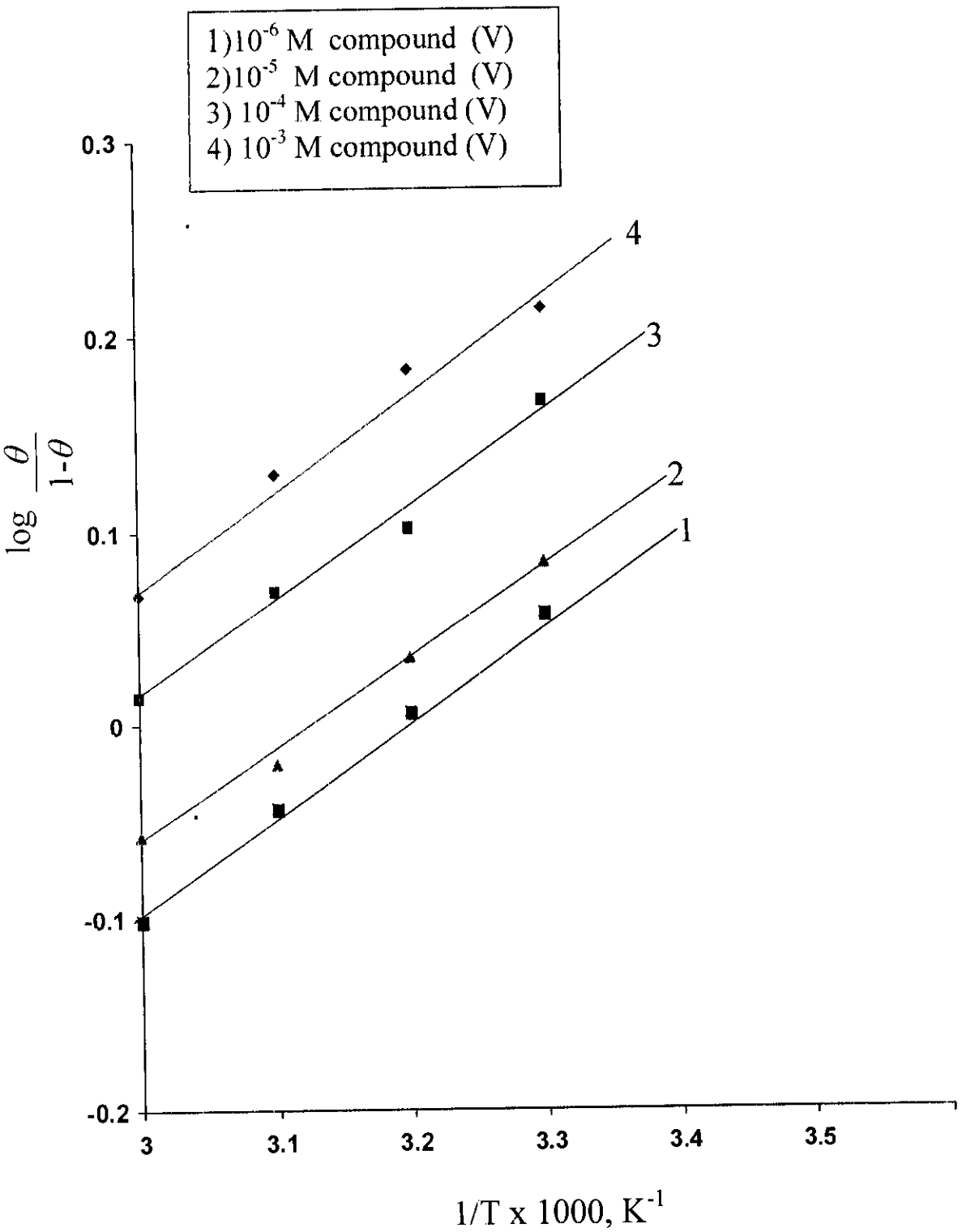

Fig. (3.36): Plots of log $\frac{\theta}{1-\theta}$ vs. 1/T for corrosion of carbon steel in 2M HCl containing different concentrations of compound (V).

3.4 - Thermodynamic parameters

The Langmuir adsorption isotherm may be formulated as :

$$\frac{C}{\theta} = \frac{1}{K} + C \qquad (3.10)$$

where K is the equilibrium constant for adsorption process. The plot of log $\frac{C}{\theta}$ versus log C was found to be linear for each additives. Figures (3.37-3.41). The equilibrium constant (K) for adsorption desorption process for each compounds for organic additive, on the steel surface can be calculated from the reciprocal of the antilogarithm of the intercept. The K values are listed in Table (3.3)

The thermodynamic parameters for adsorption process: free energy $(\Delta G)_{ads}$ and entropy $(\Delta S)_{ads}$ of the investigated compounds can be calculated from the thermodynamic relations.

$$K = \exp\left(\frac{-\Delta G_{ads}}{RT}\right) \qquad (3.11)$$

$$\Delta G_{ads} = \Delta H_{ads} - T\,\Delta S_{ads} \qquad (3.12)$$

The calculated values of ΔG_{ads} and ΔS_{ads} over the temperature rang from 30°C to 60°C are recorded in Tables (3.3- 3.7). The negative values of ΔG_{ads} indicate the spontaneous adsorption of the additives on the C-steel surface and its values also, indicate that the inhibition process become less favorable as the temperature is increased from 30°C -60°C. This conclusion is in agreement with the values of %P. It is decreased as the temperature is raised (Table 3.2). This result proves that the best inhibition efficiency occurs at 30°C. This is agree with what expected, since the adsorption is an exothermic process and is always accompanied by decrease of entropy change. ΔS is decreased with decreasing temperature. This low values of ΔS support the higher absorbability of azo dye compounds on the surface of carbon steel.

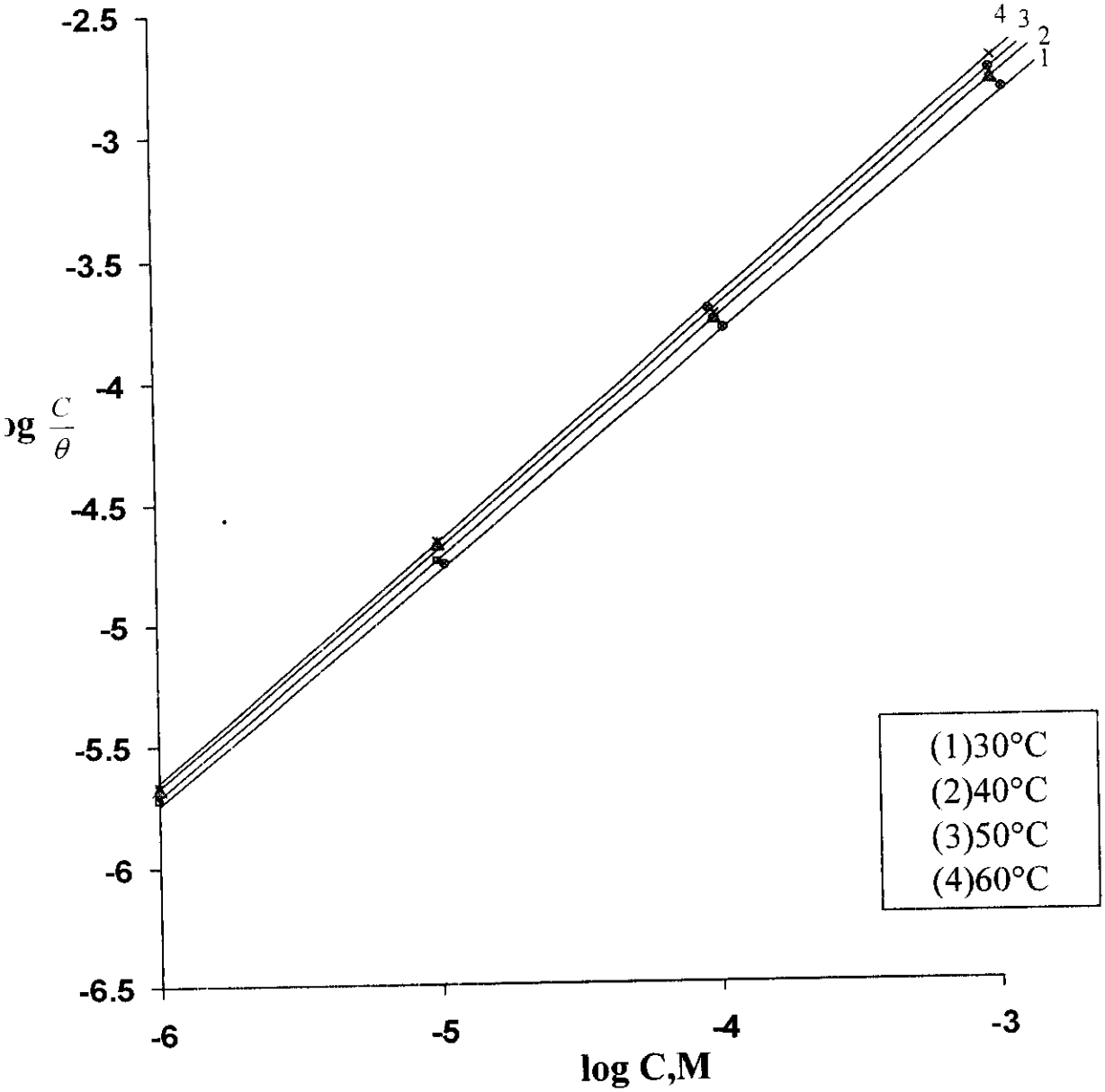

Fig.(3.37) Langmuir adsorption isotherm plotted as log (C/θ) vs log C for corrosion of C-steel in 2M HCl containing different concentrations of compound (I) at different temperatures.

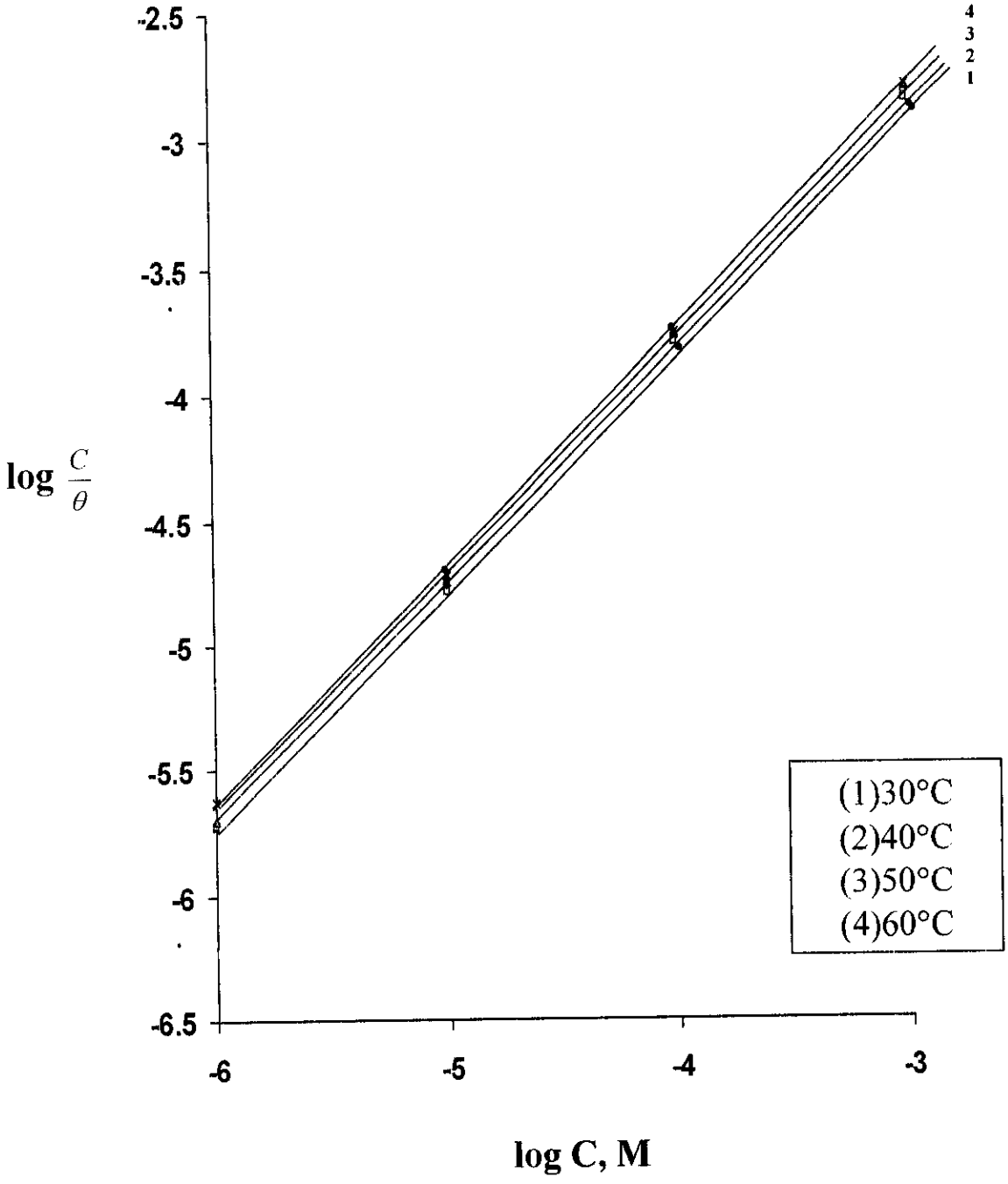

Fig.(3.38) Langmuir adsorption isotherm plotted as log (C/θ) vs log C for corrosion of C-steel in 2M HCl containing different concentrations of compound (II) at different temperatures.

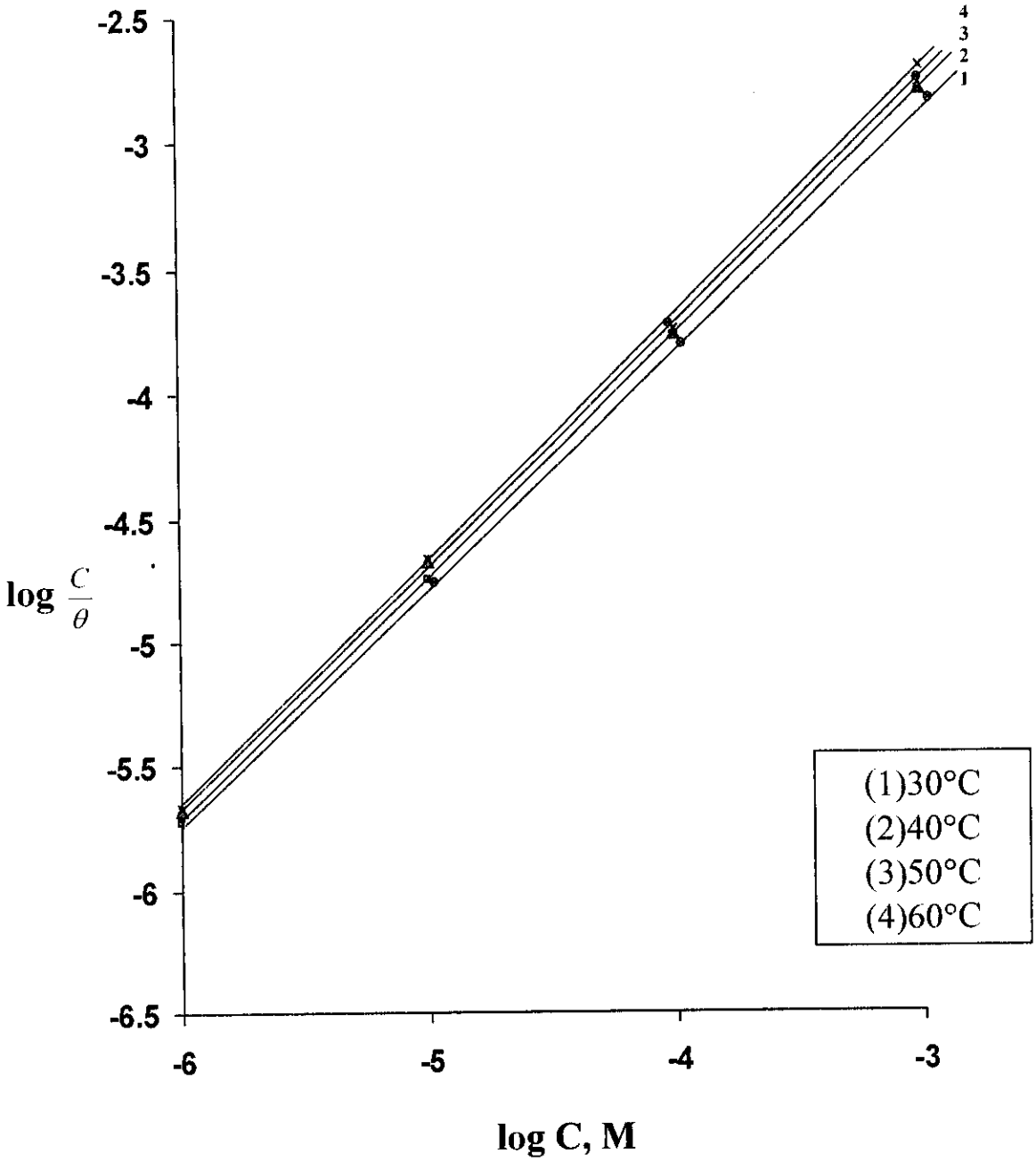

Fig.(3.39) Langmuir adsorption isotherm plotted as log (C/θ) vs log C for corrosion of C-steel in 2M HCl containing different concentrations of compound (III) at different temperatures.

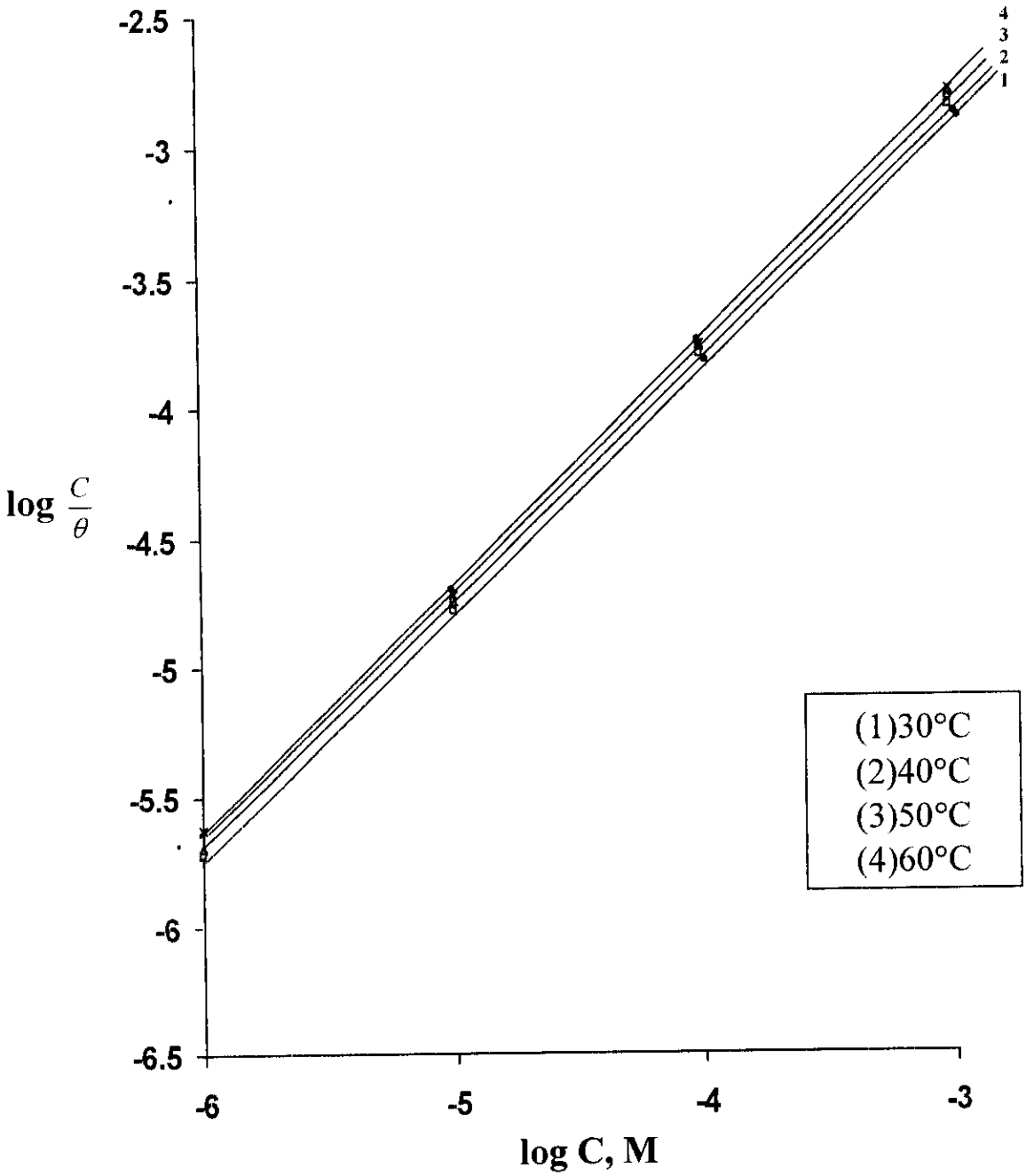

Fig.(3.40) Langmuir adsorption isotherm plotted as log (C/θ) vs log C for corrosion of C-steel in 2M HCl containing different concentrations of compound (IV) at different temperatures.

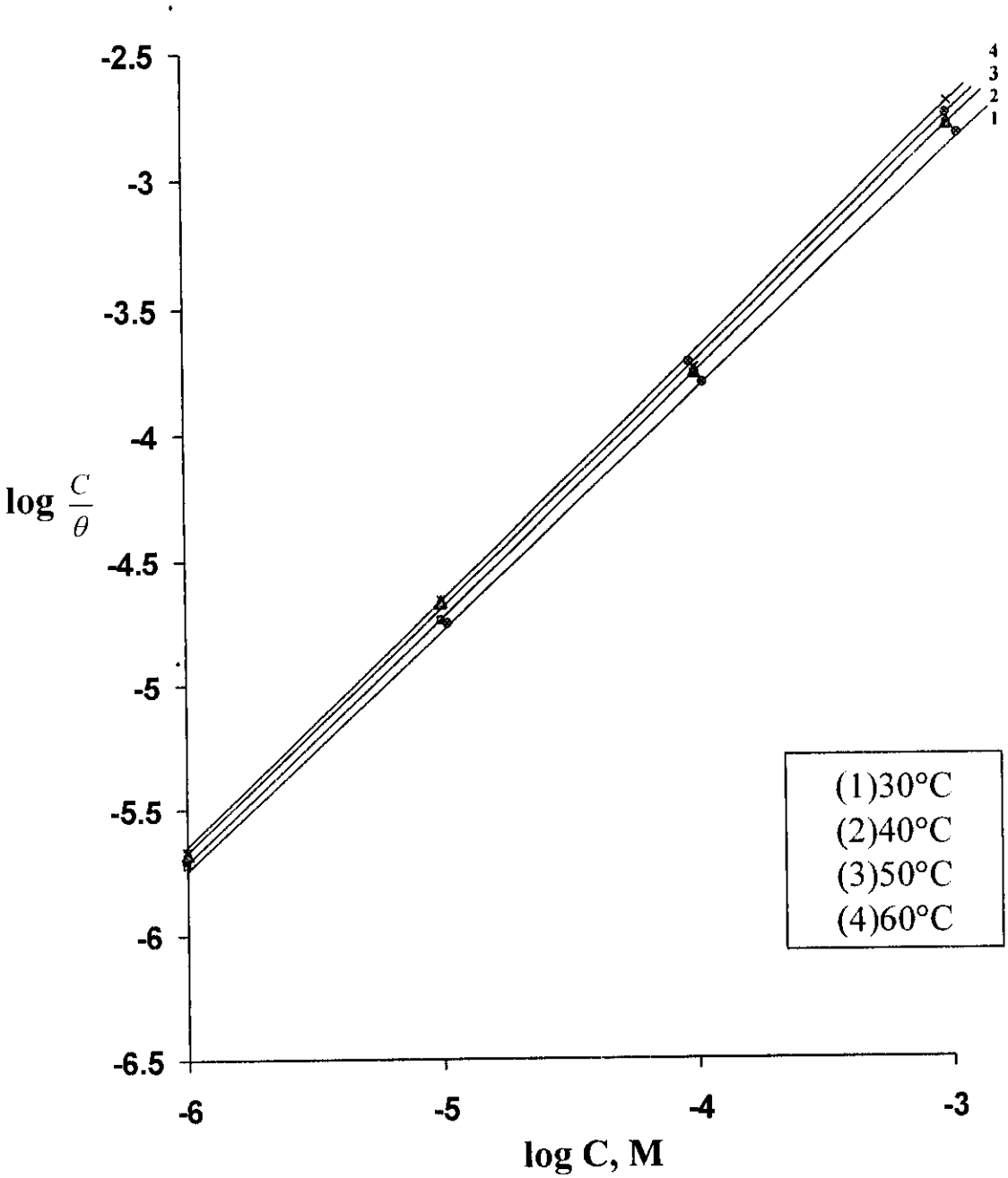

Fig.(3.41) Langmuir adsorption isotherm plotted as log (C/θ) vs log C for corrosion of C-steel in 2M HCl containing different concentrations of compound (V) at different temperatures.

Table (3.3) : Activation parameters for the dissolution of C-steel in 2M HCl in the absence and presence of different concentrations of inhibitor (I)

concentration M	Temperature (°C)	K	Activation parameters			
			$E_a°$ (KJ mol^{-1})	$-\Delta H°$ (KJ mol^{-1})	$-\Delta G°$ (KJ mol^{-1})	$\Delta S°$ (J mol^{-1} k^{-1})
10^{-6}	30	$1.88x10^{-6}$	9.54	9.50	36.40	84.5
	40	$2.05x10^{-6}$			37.82	86.3
	50	$2.09x10^{-6}$			39.08	87.6
	60	$2.15x10^{-6}$			40.37	88.8
10^{-5}	30	$1.79x10^{-5}$	10.43	9.88	30.47	67.95
	40	$2.02x10^{-5}$			31.79	70.00
	50	$2.09x10^{-5}$			32.90	71.26
	60	$2.15x10^{-5}$			33.99	72.40
10^{-4}	30	$1.65x10^{-4}$	11.77	10.27	24.48	46.89
	40	$1.68x10^{-4}$			25.32	48.08
	50	$1.73x10^{-4}$			26.21	49.34
	60	$1.78x10^{-4}$			26.29	48.10
10^{-3}	30	$1.54x10^{-3}$	12.44	10.78	18.50	25.47
	40	$1.58x10^{-3}$			19.17	26.80
	50	$1.61x10^{-3}$			19.83	28.01
	60	$1.78x10^{-3}$			21.01	30.72

Table (3.4) : Activation parameters for the dissolution of C-steel in 2M HCl in the absence and presence of different concentrations of inhibitor (II)

concentration M	Temperature (°C)	K	Activation parameters			
			$E_a°$ (KJ mol^{-1})	$-\Delta H°$ (KJ mol^{-1})	$-\Delta G°$ (KJ mol^{-1})	$\Delta S°$ (J mol^{-1} k^{-1})
10^{-6}	30	$1.80x10^{-6}$	10.85	9.88	36.29	79.6
	40	$1.92x10^{-6}$			37.65	81.5
	50	$2.02x10^{-6}$			38.99	83.1
	60	$2.05x10^{-6}$			40.24	84.4
10^{-5}	30	$1.63x10^{-5}$	11.68	10.91	30.12	63.39
	40	$1.73x10^{-5}$			30.30	61.72
	50	$1.79x10^{-5}$			32.49	66.81
	60	$1.89x10^{-5}$			33.65	68.28
10^{-4}	30	$1.56x10^{-4}$	12.87	11.49	24.33	42.37
	40	$1.65x10^{-4}$			25.28	44.05
	50	$1.69x10^{-4}$			26.15	45.38
	60	$1.72x10^{-4}$			27.02	46.63
10^{-3}	30	$1.39x10^{-3}$	13.97	12.12	18.23	20.16
	40	$1.49x10^{-3}$			19.01	22.01
	50	$1.58x10^{-3}$			19.78	23.71
	60	$1.69x10^{-3}$			20.58	25.40

Table (3.5) : Activation parameters for the dissolution of C-steel in 2M HCl in the absence and presence of different concentrations of inhibitor (III)

concentration M	Temperature (°C)	K	Activation parameters			
			$E_a°$ (KJ mol^{-1})	$-\Delta H°$ (KJ mol^{-1})	$-\Delta G°$ (KJ mol^{-1})	$\Delta S°$ (J mol^{-1} k^{-1})
10^{-6}	30	1.81×10^{-6}	10.60	9.66	36.30	82.8
	40	1.90×10^{-6}			37.62	84.3
	50	1.99×10^{-6}			38.95	85.8
	60	2.07×10^{-6}			40.27	87.2
10^{-5}	30	1.63×10^{-5}	11.88	10.00	30.23	66.76
	40	1.87×10^{-5}			31.59	68.97
	50	1.91×10^{-5}			32.66	70.15
	60	1.99×10^{-5}			33.78	71.41
10^{-4}	30	1.56×10^{-4}	12.66	10.33	24.33	46.20
	40	1.62×10^{-4}			25.23	47.60
	50	1.68×10^{-4}			26.14	48.94
	60	1.71×10^{-4}			26.99	50.30
10^{-3}	30	1.45×10^{-3}	12.82	11.21	18.34	23.53
	40	1.55×10^{-3}			19.11	25.23
	50	1.59×10^{-3}			19.80	26.59
	60	1.61×10^{-3}			20.44	27.71

Table (3.6) : Activation parameters for the dissolution of C-steel in 2M HCl in the absence and presence of different concentrations of inhibitor (IV)

concentration M	Temperature (°C)	K	Activation parameters			
			$E_a°$ (KJ mol^{-1})	$-\Delta H°$ (KJ mol^{-1})	$-\Delta G°$ (KJ mol^{-1})	$\Delta S°$ (J mol^{-1} k^{-1})
10^{-6}	30	2.39×10^{-6}	9.12	8.44	37.00	90.5
	40	2.63×10^{-6}			38.47	92.3
	50	2.76×10^{-6}			39.83	93.7
	60	2.92×10^{-6}			41.22	95.1
10^{-5}	30	2.30×10^{-5}	10.25	8.95	31.11	73.13
	40	2.34×10^{-5}			33.21	77.50
	50	2.44×10^{-5}			33.32	75.44
	60	2.59×10^{-5}			34.51	76.75
10^{-4}	30	2.18×10^{-4}	11.50	9.20	25.16	52.67
	40	2.19×10^{-4}			26.01	53.70
	50	2.22×10^{-4}			26.88	54.73
	60	2.36×10^{-4}			27.88	56.09
10^{-3}	30	1.87×10^{-3}	12.07	9.55	18.98	31.12
	40	1.80×10^{-3}			19.50	31.78
	50	1.91×10^{-3}			20.29	33.25
	60	2.21×10^{-3}			21.33	35.37

Table (3.7) : Activation parameters for the dissolution of C-steel in 2M HCl in the absence and presence of different concentrations of inhibitor (V)

concentration M	Temperature (°C)	K	Activation parameters			
			$E_a°$ (KJ mol^{-1})	$-\Delta H°$ (KJ mol^{-1})	$-\Delta G°$ (KJ mol^{-1})	$\Delta S°$ (J mol^{-1} k^{-1})
10^{-6}	30	1.87×10^{-6}	9.30	8.75	36.38	88.3
	40	1.98×10^{-6}			37.73	89.7
	50	2.10×10^{-6}			39.09	91.3
	60	2.26×10^{-6}			40.50	92.7
10^{-5}	30	1.82×10^{-5}	10.30	9.02	30.52	70.95
	40	1.92×10^{-5}			31.67	72.36
	50	2.05×10^{-5}			32.85	72.94
	60	2.14×10^{-5}			33.98	74.95
10^{-4}	30	1.68×10^{-4}	11.78	9.33	24.51	50.99
	40	1.79×10^{-4}			25.49	51.62
	50	1.85×10^{-4}			26.39	52.81
	60	1.96×10^{-4}			27.37	54.17
10^{-3}	30	1.62×10^{-3}	12.25	9.60	18.63	29.80
	40	1.65×10^{-3}			19.29	30.95
	50	1.81×10^{-3}			20.14	32.63
	60	1.94×10^{-3}			20.97	34.14

Section (B)

Kinetics of The Corrosion Inhibition of Carbon Steel in Hydrochloric Acid Solutions Using Galvanostatic Polarization Technique

Section (B)

Kinetics of The Corrosion Inhibition of Carbon Steel in Hydrochloric Acid Solutions Using Galvanostatic Polarization Technique

3.5 Galvanostatic polarization

The technique of anodic and cathodic polarization of metals are frequently used to study the phenomena of metal corrosion and passivation. It yields useful information on the electrode behavior, action of inhibitive and aggressive anions and the effect of the environmental conditions. In this technique , an external applied electric current is used and can be varied as will, the experiment can be performed in relatively short time. When a Tafel equation is applicable for both anodic and cathodic polarization, the point of intersection of the two Tafel lines corresponding to the stationary conditions of corrosion. The function of a substance as an inhibitor or stimulator may thus be due to its effect on polarization curves, and consequent displacement of the point of intersection.

The corrosion kinetics of carbon steel was studied extensively [82-87] from the examination of kinetics of hydrogen evolution reaction (h.e.r.). The effect of some organic compounds on the corrosion reaction kinetic were further examined.

The effect of increasing concentration of azo dyes compounds on the anodic and cathodic polarization curves of carbon steel was examined in 2M HCl solution and are represented in Figures (3.42 -3.46) for compounds I, II, III, IV and V, respectively.

Inspection of the curves of Figures (3.42 -3.46) one can observe at first, a transition region in which the potential increases (anodic polarization) or decreases

(cathodic polarization)slowly with current density following this region there is a rapid linear build up of potential with current density (Tafel region).

Transition region[88], which starts from the free corrosion potential and extends to the beginning of the Tafel region is characterized by the simultaneous occurrence of cathodic hydrogen evolution and anodic dissolution of metal. The former leads to coverage of a fraction θ_H of the electrodes surface by adsorbed OH^- groups $Fe(OH)_{ads}$. Having no common intermediate, these two reactions compete and, hence, give rise to mixed kinetics. McCaffery[89] considered that at the corrosion potential almost the whole electrode surface is covered by $(FeH)_{ads.}$ consequently, the coverage fraction θ_H, close to 1 at cathodic potentials, and decreases when anodic polarization is increased.

Further inspection of the curves of Figures (3.42 -3.46) reveals that the presence of increasing concentration of azo dye compounds cause a decrease in the rate of anodic dissolution reaction i.e. shifting the anodic current- potential curves in the anodic direction. This may be ascribed to a parallel adsorption of the organic molecules over the corroding surface.

From the cathodic polarization curves illustrated in Figs. (3.42-3.46), its clear that the increase of the additives concentration shifts the current-potential curves towards less cathodic potentials. Azo dye compounds like other adsorption inhibitors, are known to undergo specific adsorption i.e. they adsorb in the inner part of the double layer. In doing so the adsorbed species replace some of the H_3O^+ ion i.e. the additives blocks part of the surface and hence decrease the rate of hydrogen evolution reaction and consequently the rate of the overall corrosion reaction is produced.

The values of corrosion current density (I_{corr}) was determined by the intersection of the extrapolated of cathodic and anodic Tafel lines (linear part) with the stationary corrosion potential (E_{corr}).

The percentage inhibition efficiency (%*P*) imparted by the added inhibitor, which is defined as the percentage of the relative decrease in corrosion rate brought about by the presence of a certain concentration of the inhibitor is given by:

$$\%P = \left[1 - \frac{I_{add}}{I_{free}}\right] 100 \qquad (3.13)$$

where I_{free} and I_{add} are the corrosion current densities in the absence and presence of the inhibitors, respectively.

Tables (3.8-3.12) show the effect of increasing concentrations of azo dye compounds on the corrosion parameters such as: cathodic Tafel slop b_c, anodic Tafel slop b_a, corrosion potential E_{corr}, corrosion current density I_{corr}, percentage inhibition efficiency (%P) and surface coverage θ.

From these Tables, it is clear that the corrosion potentials (E_{corr}) is shifted to more positive values and Tafel lines are shifted to more positive and negative potential for anodic and cathodic process, respectively, relative to the blank curve. This means that this compounds influence both anodic and cathodic process. However, the data suggested that these compounds act mainly as mixed type inhibitors. The values of anodic and cathodic Tafel slopes (b_a & b_c) are approximately constant which suggest the simple blocking of the available surface area of the metal by the inhibitors molecules. In other words, the adsorbed inhibitor molecule decreases the surface area available for the both metal dissolution and hydrogen evolution reaction without affecting the reaction mechanism[90]. The reaction between the metal covered with inhibitor molecule may take place by diffusion of H^+ and Cl^- ions through the pores of the protective layer on the metal surface.

From these Figures (3.42-3.46) and Tables (3.8-3.12) it is cleat that the increase of additive concentrations decrease the corrosion current density (I_{corr}), and hence increase the inhibition efficiency of these compounds.

At one and the same inhibitor concentration the degree of inhibition efficiency decreases according to the following sequence :

$$II > III > I > V > IV$$

The values of inhibition efficiencies were evaluated using the galvanostatic polarization and mass loss measurements show an agreement and conformity of the experimental results. However, there are small differences in the values obtained from the two techniques. These difference may be due to the short time taken by the electrochemical measurements.

3.6 Adsorption isotherms

The resulted inhibitive action of azo dye compounds due to adsorption of its compounds on the C-steel surface making a barrier for charge and mass transfer between the metal and corrosive environment. As the concentration of azo dye compounds increases, the fraction of C-steel surface covered by adsorbed molecules (θ) increases resulting in higher inhibition efficiency.

The degree of surface coverage (θ) was calculated using the following equation :

$$\theta = 1 - \frac{I_{add}}{I_{free}} \qquad (3.14)$$

where I_{free} and I_{add} are the corrosion current densities in the absence and presence of the additive compounds, respectively. The value of θ are reported in Tables (3.6-3.12). The degree of surface coverage θ was found to increase with increasing the concentration of additives.

Attempts were made to fit θ values to various isotherms e.g. (Frumkin, Temkin, Freundlich and Langmuir). The best fit was obtained with Langmuir isotherm according to the following equation.

$$\frac{\theta}{1-\theta} = KC \qquad (3.15)$$

and rearranging it gives:

$$\frac{C}{\theta} = \frac{1}{K} + C \qquad (3.16)$$

where (C) is the concentration of additive is the equilibrium constant of adsorption.

The plot of $\log \frac{C}{\theta}$ against log C gives a straight lines of intercept $\log \frac{1}{K}$. The plots are shown for azo dye additives in Figure (3.47). the resulted straight lines from the above relation have almost the unit slopes. This indicates that, the adsorption of azo dye compounds on the carbon steel surface follows Langmuir adsorption isotherm and consequently, there is no interaction between the molecules adsorbed at the steel surface.

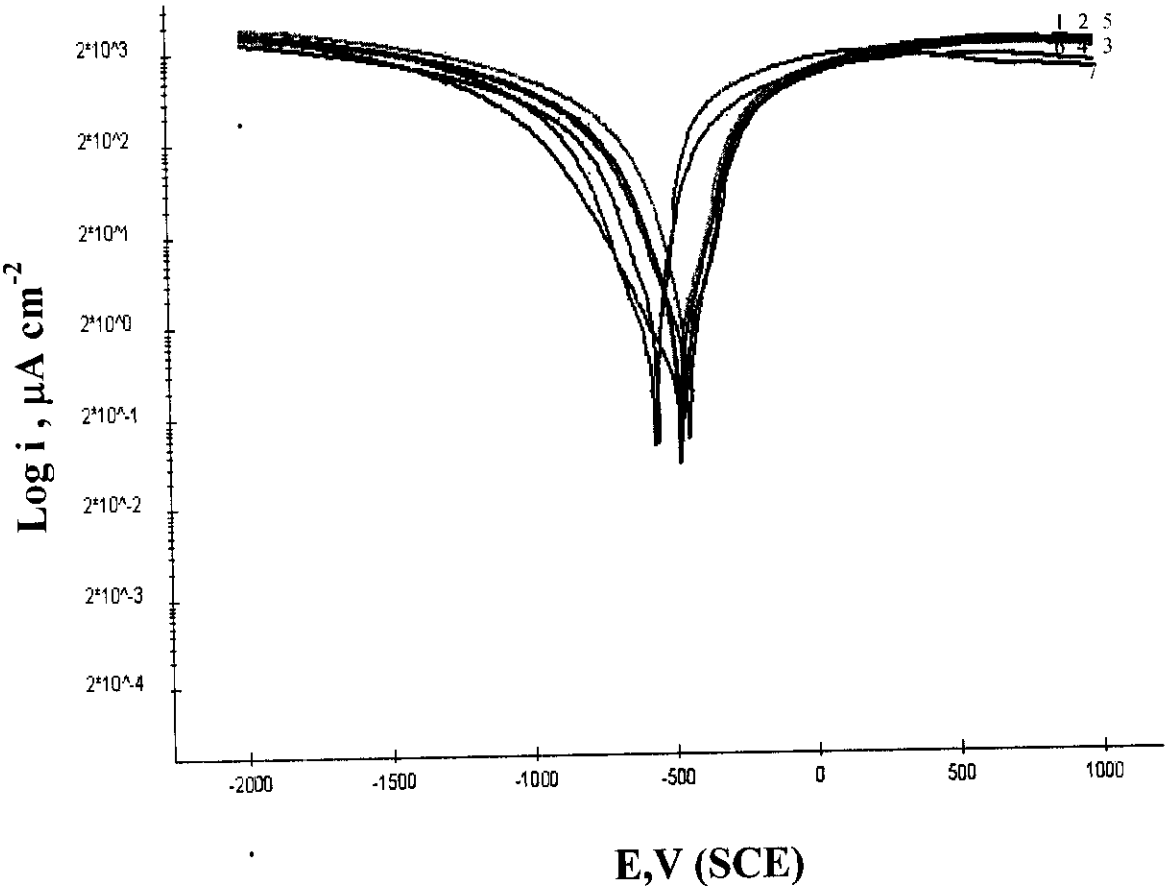

Fig.(3.42): Galvanostatic polarization curves for the dissolution of carbon steel in 2M HCl in absence and presence of different concentrations of compound (I) at 30°C. (1) 2 M HCl; (2) 2M HCl +1x10^{-6} M compound I (3) 2M HCl +1x10^{-5} M; (4) 2M HCl +5x10^{-5} M; (5) 2M HCl +1x10^{-4} M ;(6) 2M HCl +5x10^{-4} M;(7) 2M HCl +1x10^{-3} M

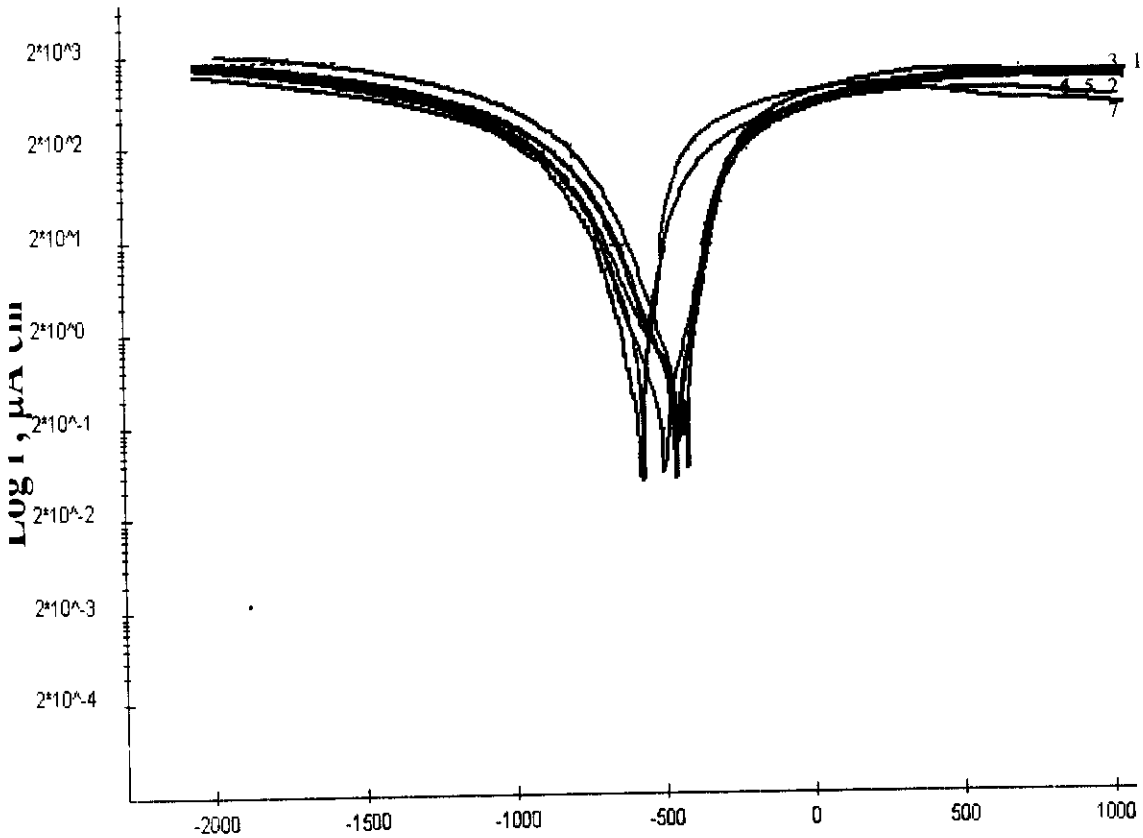

Fig.(3.43): Galvanostatic polarization curves for the dissolution of carbon steel in 2M HCl in absence and presence of different concentrations of compound (II) at 30°C. (1) 2 M HCl; (2) 2M HCl +1x10^{-6} M compound II (3) 2M HCl +1x10^{-5} M; (4) 2M HCl +5x10^{-5} M; (5) 2M HCl +1x10^{-4} M ;(6) 2M HCl +5x10^{-4} M;(7) 2M HCl +1x10^{-3} M

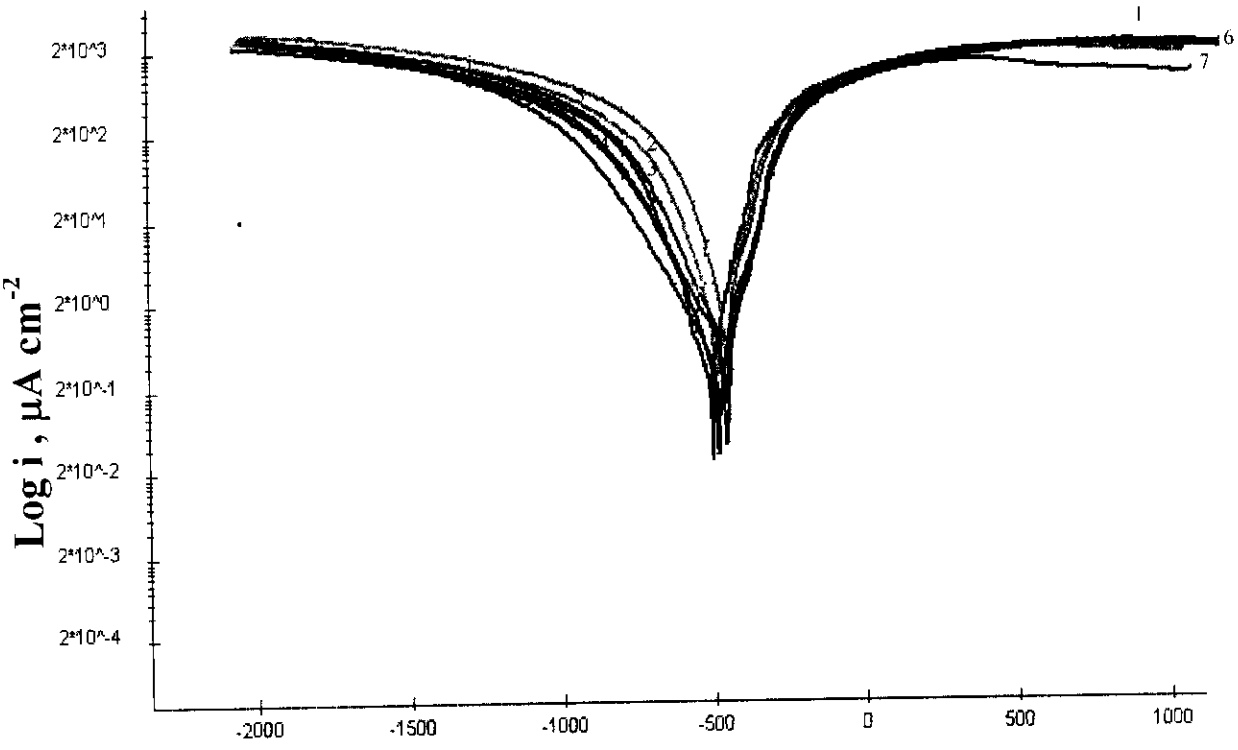

Fig.(3.44): Galvanostatic polarization curves for the dissolution of carbon steel in 2M HCl in absence and presence of different concentrations of compound (III) at 30°C. (1) 2 M HCl; (2) 2M HCl +1x10^{-6} M compound III (3) 2M HCl +1x10^{-5} M; (4) 2M HCl +5x10^{-5} M; (5) 2M HCl +1x10^{-4} M ;(6) 2M HCl +5x10^{-4} M;(7) 2M HCl +1x10^{-3} M

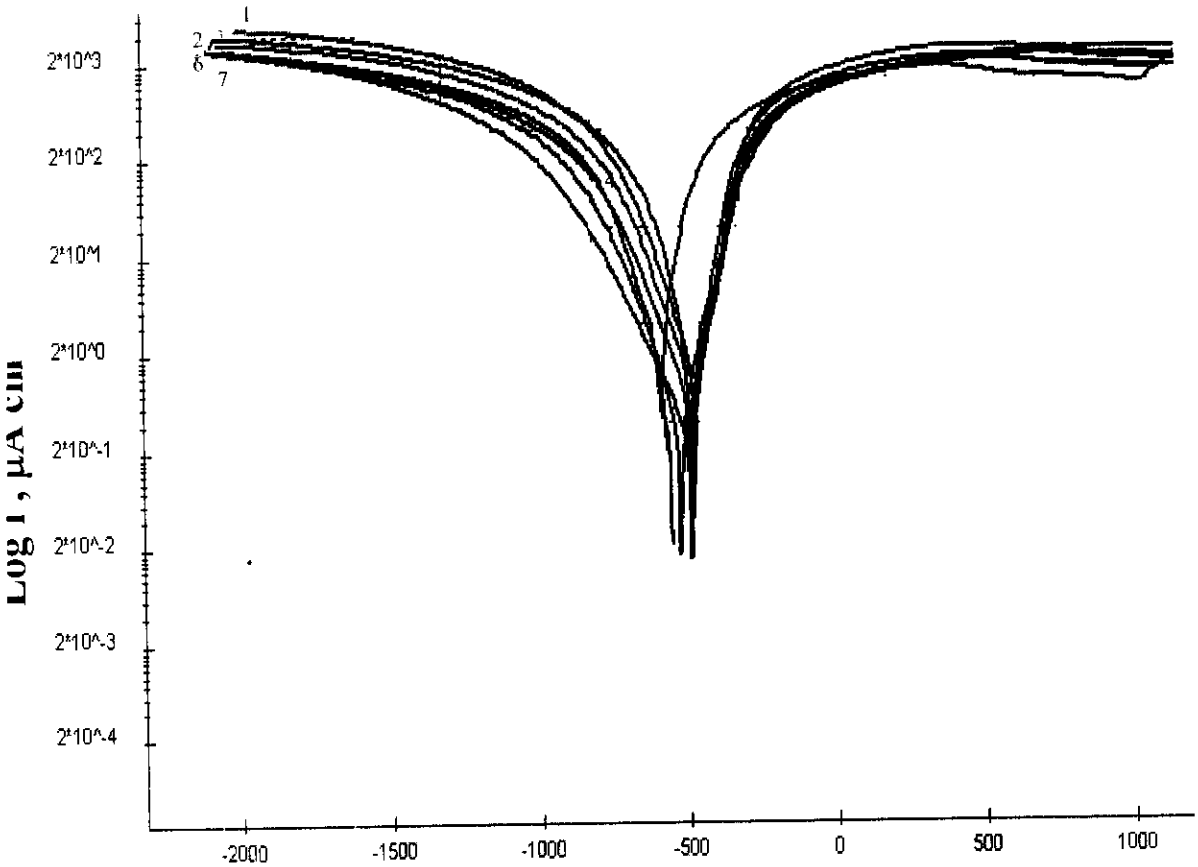

Fig.(3.45): Galvanostatic polarization curves for the dissolution of carbon steel in 2M HCl in absence and presence of different concentrations of compound (IV) at 30°C. (1) 2 M HCl; (2) 2M HCl +1x10^{-6} M compound IV (3) 2M HCl +1x10^{-5} M; (4) 2M HCl +5x10^{-5} M; (5) 2M HCl +1x10^{-4} M ;(6) 2M HCl +5x10^{-4} M;(7) 2M HCl +1x10^{-3} M

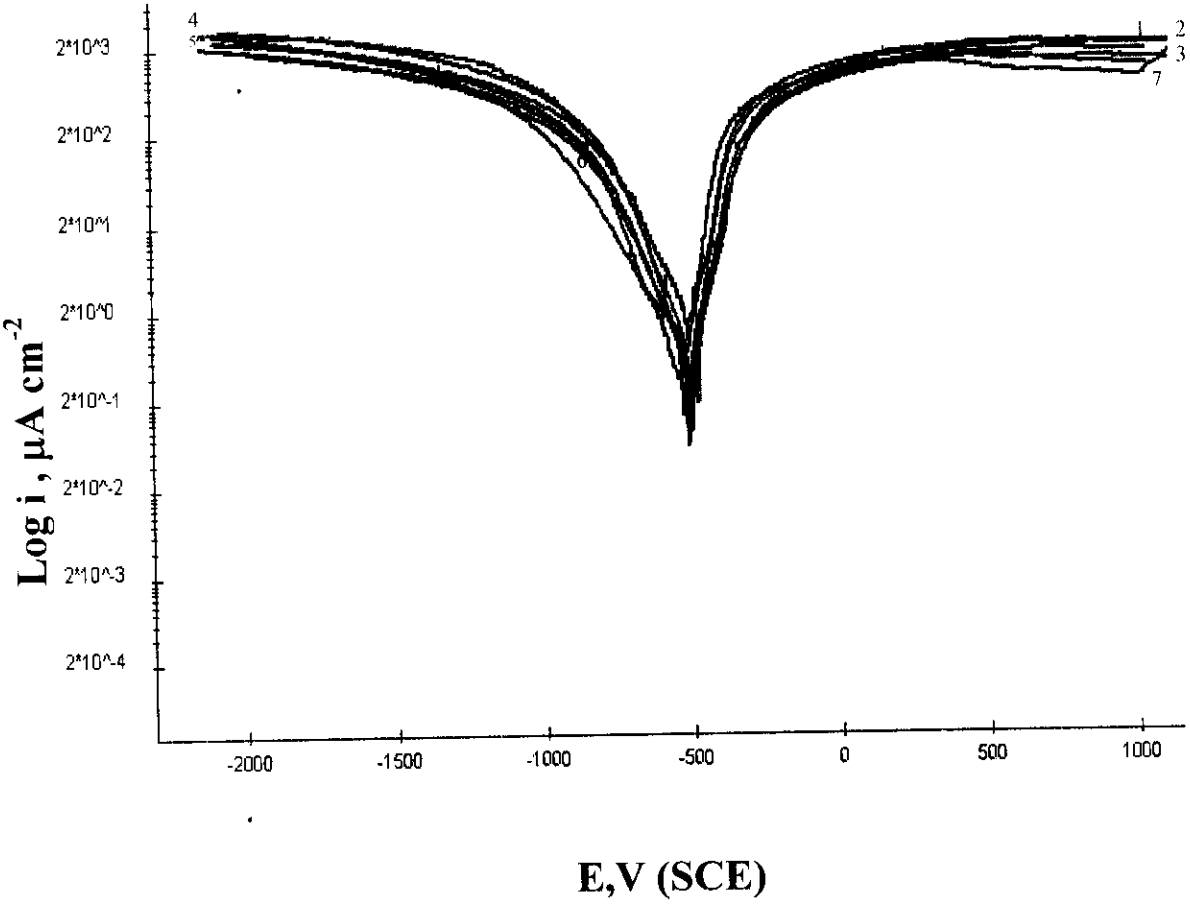

Fig.(3.46): Galvanostatic polarization curves for the dissolution of carbon steel in 2M HCl in absence and presence of different concentrations of compound (V) at 30°C. (1) 2 M HCl; (2) 2M HCl +1x10^{-6} M compound V (3) 2M HCl +1x10^{-5} M; (4) 2M HCl +5x10^{-5} M; (5) 2M HCl +1x10^{-4} M ;(6) 2M HCl +5x10^{-4} M;(7) 2M HCl +1x10^{-3} M

Table (3.8): Corrosion parameters obtained from anodic and cathodic polarization technique in 2M HCl containing different concentrations of compound I

Inhibitor concentration, M	I_{corr} (μAcm^{-2})	$-E_{corr}$ mV(SEC)	β_a mV dec^{-1}	β_c mV dec^{-1}	θ	%P
0.00	1.970	530	200	160	-	-
1x 10^{-}	0.878	508	202	197	0.554	55.43
1x 10^{-5}	0.8372	510	205	211	0.575	57.50
5x10^{-5}	0.8017	515	210	208	0.593	59.30
1x10^{-4}	0.7210	514	208	204	0.634	63.40
5X10^{-4}	0.6973	517	207	201	0.646	64.60
1X10^{-3}	0.5791	520	209	200	0.706	70.60

Table (3.9): Corrosion parameters obtained from anodic and cathodic polarization technique in 2M HCl containing different concentrations of compound II

Inhibitor concentration, M	I_{corr} (μAcm^{-2})	$-E_{corr}$ mV(SEC)	β_a mV dec^{-1}	β_c mV dec^{-1}	θ	%P
0.00	1.970	530	200	160	-	-
$1x\ 10^{-6}$	0.872	495	190	174	0.557	55.73
$1x\ 10^{-5}$	0.717	498	201	188	0.636	63.60
$5x10^{-5}$	0.699	502	198	178	0.645	64.51
$1x10^{-4}$	0.6567	505	203	189	0.666	66.66
$5X10^{-4}$	0.629	508	205	201	0.680	68.07
$1X10^{-3}$	0.4921	510	201	198	0.750	75.02

Table (3.10): Corrosion parameters obtained from anodic and cathodic polarization technique in 2M HCl containing different concentrations of compound III

Inhibitor concentration, M	I_{corr} (μAcm^{-2})	$-E_{corr}$ mV(SEC)	β_a mV dec^{-1}	β_c mV dec^{-1}	θ	%P
0.00	1.970	530	200	160	-	-
1x 10-6	0.844	510	188	197	0.571	57.15
1x 10-5	0.80	512	205	197	0.593	59.39
5x10-5	0.731	514	201	188	0.628	62.89
1x10-4	0.682	515	211	207	0.654	65.43
5X10-4	0.632	518	205	205	0.679	67.91
1X10-3	0.521	520	203	215	0.735	73.55

Table (3.11): Corrosion parameters obtained from anodic and cathodic polarization technique in 2M HCl containing different concentrations of compound IV

Inhibitor concentration, M	I_{corr} (μAcm^{-2})	$-E_{corr}$ mV(SEC)	β_a mV dec^{-1}	β_c mV dec^{-1}	θ	%P
0.00	1.970	530	200	160	-	-
$1x\ 10^{-6}$	1.07	511	210	203	0.456	45.68
$1x\ 10^{-5}$	1.031	517	205	200	0.476	47.66
$5x10^{-5}$	0.981	514	198	202	0.520	50.20
$1x10^{-4}$	0.942	518	204	199	0.521	52.18
$5X10^{-4}$	0.871	518	207	203	0.557	55.78
$1X10^{-3}$	0.782	519	211	220	0.603	60.30

Table (3.12): Corrosion parameters obtained from anodic and cathodic polarization technique in 2M HCl containing different concentrations of compound V

Inhibitor concentration, M	I_{corr} (μAcm^{-2})	$-E_{corr}$ mV(SEC)	β_a mV dec^{-1}	β_c mV dec^{-1}	θ	%P
0.00	1.970	530	200	160	-	-
$1x\ 10^{-6}$	0.882	503	202	194	0.552	55.22
$1x\ 10^{-5}$	0.833	506	201	200	0.577	57.71
$5x10^{-5}$	0.773	510	210	215	0.607	60.76
$1x10^{-4}$	0.711	512	207	211	0.639	63.90
$5X10^{-4}$	0.667	511	211	198	0.661	66.142
$1X10^{-3}$	0.610	513	210	205	0.690	69.03

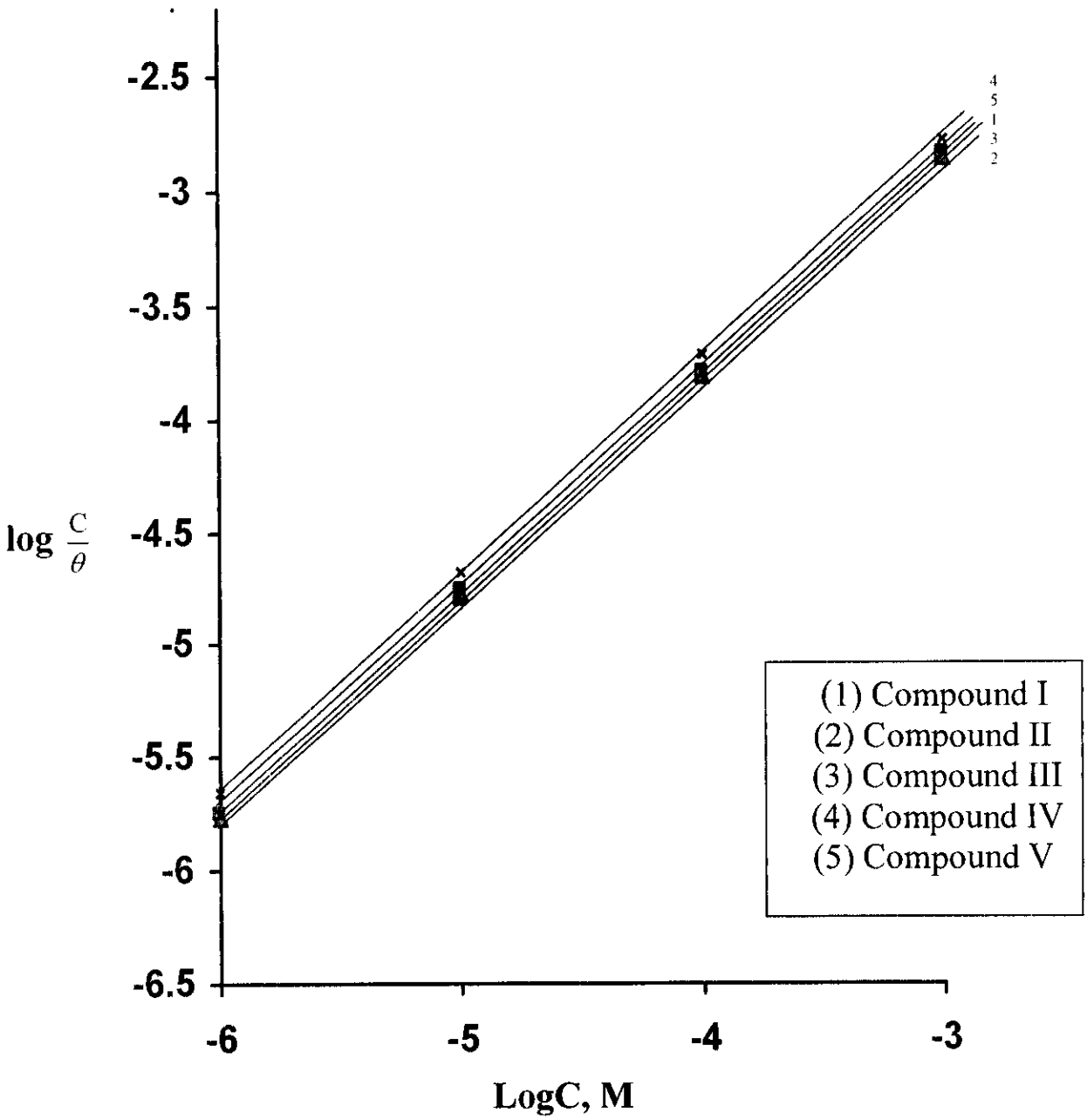

Fig.(3.47): Adsorption isotherm of azo dye compounds on C-steel surface in 2M HCl.

Section (C)

Initiation and Inhibition of Pitting Corrosion of Carbon Steel in Na_2CO_3 Solutions

Section (C)

Initiation and Inhibition of Pitting Corrosion of Carbon Steel in Na_2CO_3 Solutions

Pitting corrosion of carbon steel like other metals or alloys, occur when passivity breakdown takes place at local points on the surface exposing them to the corrosive environment and at those points the anodic dissolution proceeds whilst the most major part of the surface remains passive.

Two basic condition must be fulfilled for the initiation and propagation of pitting corrosion. Firstly, the major part is that the metal surface should be covered with an electronically conducting, passivating, inhibiting film at which the cathodic partial reaction takes place.

This film can be formed naturally, or be produced through alloying with an appropriate metal or by oxidizing agents with redox potentials equal to, or higher than the corresponding flade potential and / or by anodic protection. Secondly. The medium should contain an aggressive agent. Chloride ion the most dangerous pitting agent and for this reason pitting corrosion is sometimes referred to as "chloride corrosion". The other halogen ions Br^- and I^-, also cause pitting corrosion but to a less extent. Similarly under certain condition perchlorate[91] and sulphate [92] ions may cause localized corrosion.

In this part the technique of potentiodynamic anodic polarization is useful for studying the breakdown of passivity of a carbon steel anode in aqueous Na_2CO_3 solution containing Cl^- ions as pitting corrosion agent. The effect of some azo dye compounds as pitting corrosion inhibitors for carbon steel electrode is examined.

i) Initiation of pitting corrosion of carbon steel

The characteristic and theory of pitting corrosion was discussed by several authors[93-95]. The formation and development of this type of attack on the metal surface can occur only in solutions containing the aggressive ions such as Cl^-, Br^- and I^- ions. The pitting corrosion of certain metals or alloys occurs only with in a definite potential range lying in the passive region[93]. The critical potential at which pitting is initiated depends on a number of factors including the type and concentration of the attacking anion, type of metal used, presence and relative concentration of other anions and also on temperature[96].

The importance of the value of pitting potential is related both to an understanding of the pitting corrosion mechanism and to the prediction of the suitable method for inhibition of this type of attack[95].

Fig (3.48) represents the potentiodynamic anodic polarization curves of carbon steel electrode in 0.1M Na_2CO_3 solution in presence of increasing concentrations of NaCl at a scan rate of 1 $mV.sec^{-1}$. The slow scan rate permits more time for pitting initiation to occur at a less positive potential[97].

Inspection of the curve of Fig (3.48) reveals that:

i) There is no any active dissolution or oxidation peak observed during the anodic scan until at the beginning of oxygen evolution. This reflects the stability of the oxide film formed on the steel surface.

ii) Increasing the sodium chloride concentrations causes the current following a long the passive region to increase suddenly and markedly at some definite potentials denoting the destruction of the passivating oxide film and the initiation of visible pits. This is known pitting corrosion potential (E_{pitt}). The effect of increasing the chloride ions concentrations is the shift of the pitting potential into the active (negative) direction.

iii) The dependence of pitting corrosion potential, (E_{pitt}) of carbon steel electrode in 0.1M Na_2CO_3 solution on the a logarithm of the concentrations of chloride ion is shown in Fig (3.49). straight line relationship is obtained according to the following equation[98-99]:

$$E_{pitt} = a_1 - b_1 \log C_{Cl^-} \qquad (3.13)$$

where a_1 and b_1 are constants which depend on both the nature and type of aggressive anion and the electrode sample and C_{Cl^-} represents the chloride ion concentrations.

The differentiation between pit initiation and pit propagation is well explained by Aziz and Godard[100]. A pit can be started by artificial stimulation at an otherwise normal sites on the metal surface, yet continue to propagate if given the right environmental conditions. This concept has been widely used to explain pitting corrosion phenomena[101-103].

Hoars et al.[103] related pit initiation on a supposed oxide film, followed by its penetration through the film (without exchange) under the influence of an electrostatic field across the film/ solution interface. When the latter field reaches a certain critical value, corresponding to the pitting potential, pitting occurs, and the oxide film is presumably undetermined either by vacancy condensation at the metal interface, or it release cations rapidly at the electrolyte interface so that in either cases pitting proceeds. The induction period for pitting to occur is related to the time required for supposed penetration of the ions through the oxide film. Regarding this mechanism Leckie and Uhlig [104] argued that, if this is correct, either anion of large molecular size than the halogen ions e.g. SO^-_4, ClO^-_4, NO^-_3 and OH^-, which are practically having no pitting tendency, can also penetrate the passive oxide film causing the formation of pit.

The latter author[103] proposed another model based on the visible competitive adsorption of the aggressive ions with oxygen for adsorption sites on

the metal surface. This model is based on the assumption that adsorbed oxygen rather than metal oxide is the cause of passive film formation[105]. Oxygen has normally higher affinity than Cl^- ions for adsorption sites on the metal surface, but as the potential of the working electrode is shifted into the passive direction, higher Cl^- ions move into the double layer when the concentration of the latter reaches a certain definite value, corresponding to the pitting potential, it succeeds at favoured sites in destroying passivity by displacing adsorbed O_2 ions. The induction time for pitting is attributed here to the slow process of competitive adsorption. It is of interest to mention that similar view were also, reported by Kolotyrikin[106], Rosenfeld [107] and Schwenk et al.[108].

In constant to the model of competitive adsorption, Foroulis and Thubriker[109] based their argument on the findings that; the critical pitting potential of the polarized electrode depends on the thickness of oxide film at the metal surface. They concluded that, if competitive adsorption at the metal surface the controlling mechanism, then the thickness of any overlying oxide would have no influence on the critical potential at which the Cl^- ions displace the adsorbed oxygen on the metal bare. Foroulis[110] proposed a pit initial model for C-steel which involves field assisted adsorption of the chloride ions from the solution onto a hydrate C-steel oxide surface, followed by formation of a basic C-steel chloride salt on the surface. The latter is readly soluble and leads to the immediate separation of one or more adjacent cations from the oxide lattice.

In agreement with Foroulis proposal[110], Abd El-Haleem[111] assumed that the initiation of pitting on Zn-Ti-Cu alloy involves, as a rate controlling step, the adsorption of chloride ions on a layer of mixed oxides/hydroxides of Zn, Ti and/or Cu followed by the formation of the corresponding chloro-metal oxide or hydroxide complexes. The readly soluble of these complexes can go into solution, most probably the Zn complexes as soluble Zn^{2+}. These results in pit initiation with the continuous anodic dissolution of Zn^{2+} at the point of attack. This later

model was confirmed by the use of the electron microscope analyzer of performed pits.

ii) Effect of some azo dye compounds on the pitting corrosion of carbon steel under potentiodynamic anodic polarization.

Much more attention has been paid to the inhibition of uniform active than of localized metallic corrosion. In the first case " great number of different groups of inhibitors as well as the inhibiting mechanisms are known. However, less knowledge exists in the case of pitting corrosion inhibition of passive metal electrodes.

Two major effects seen to be possible for the inhibition of pitting corrosion. The first one is the competitive adsorption between the inhibitive and aggressive ions, the adsorption of the inhibitive ions predominate and the passive electrode will be protected. In this case the pitting potential is shifted into the anodic direction. This mechanism seems to be the effective way to avoid pitting corrosion.

A secondly way is given by the incorporation of the inhibitive molecules into the passive layer on the metal surface, forming an improved stability against the aggressive ions, further, once , pitting corrosion has been started the inhibitor can be adsorbed within the pits preventing metal dissolution.

Figures (3.49-3.53) represent the effect increasing concentrations of azo dye compounds I, II, III, IV and V, respectively, on the potentiodynamic anodic polarization curves of carbon steel electrode in 0.1M Na_2CO_3+ 0.1M NaCl at a scan rate of 1 mV/sec^{-1}.

Inspection of the curves of these figures reveals that the presence of increasing concentrations of these compounds cause a shift of the critical pitting potential into the noble positive direction. This indicates that increased resistance to pitting attack.

Figure (3.54) represents the relationship between pitting potential and the logarithmic of the molar concentrations of the added compounds. Straight lines were obtained and the following conclusion can be drawn:

i) An increase of inhibitor concentration causes the shift of the pitting potential into the more positive values in accordance with the following equation

$$E_{pitt} = a_2 + b_2 \log C_{add} \qquad (3.14)$$

where a_2 and b_2 are constants which depend on both nature of electrode and type of inhibitors used.

ii) At one and the same inhibitors concentrations the degree of resistance to pitting corrosion decreases in the following order

$$II > III > I > V > IV$$

This order is in a good agreement with the results obtained from weight loss and galvanostatic techniques.

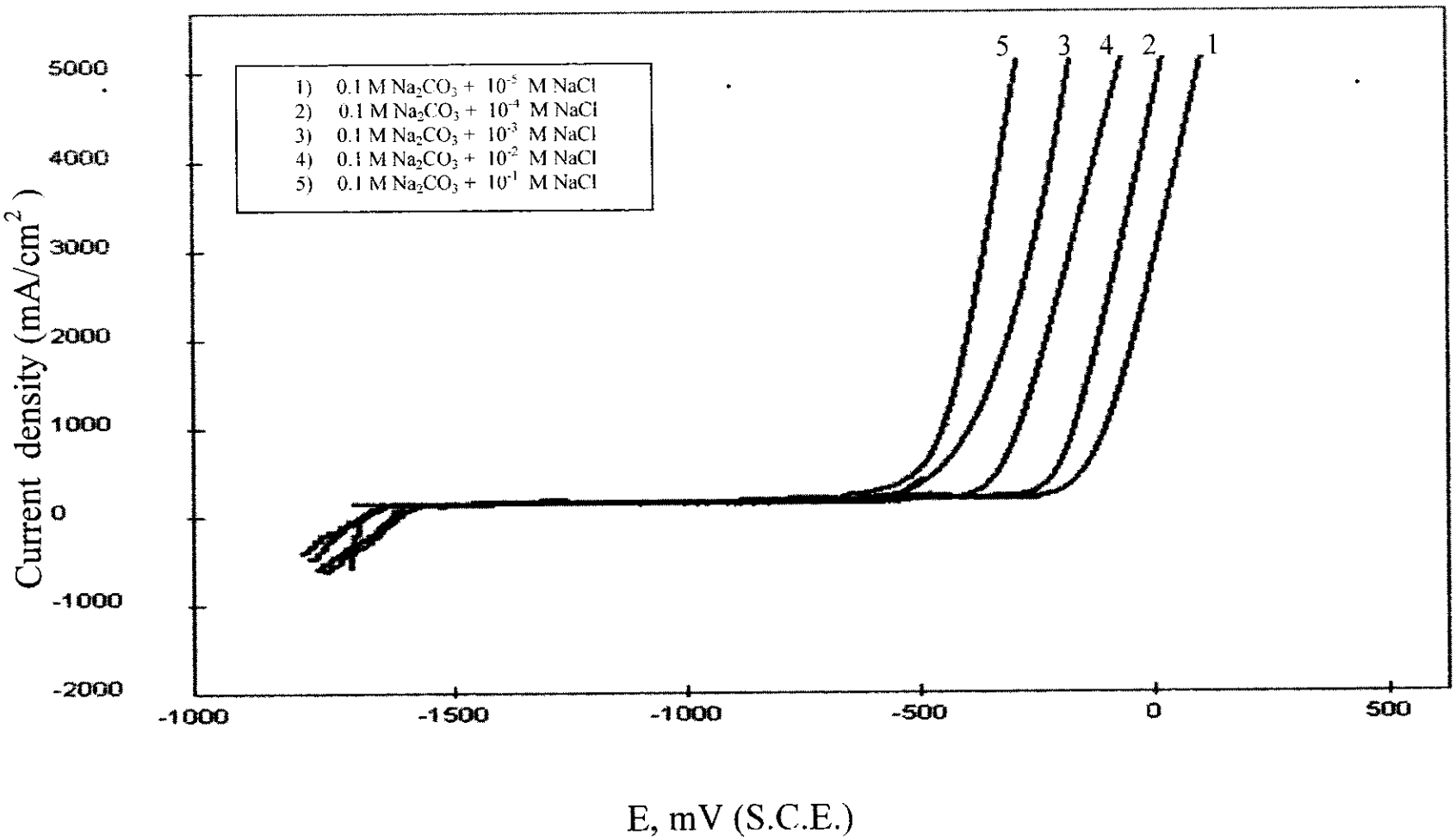

Fig. (3.48): Potentiodynamic anodic polarization curves of carbon steel in 0.1M Na_2CO_3 containing different concentrations of NaCl

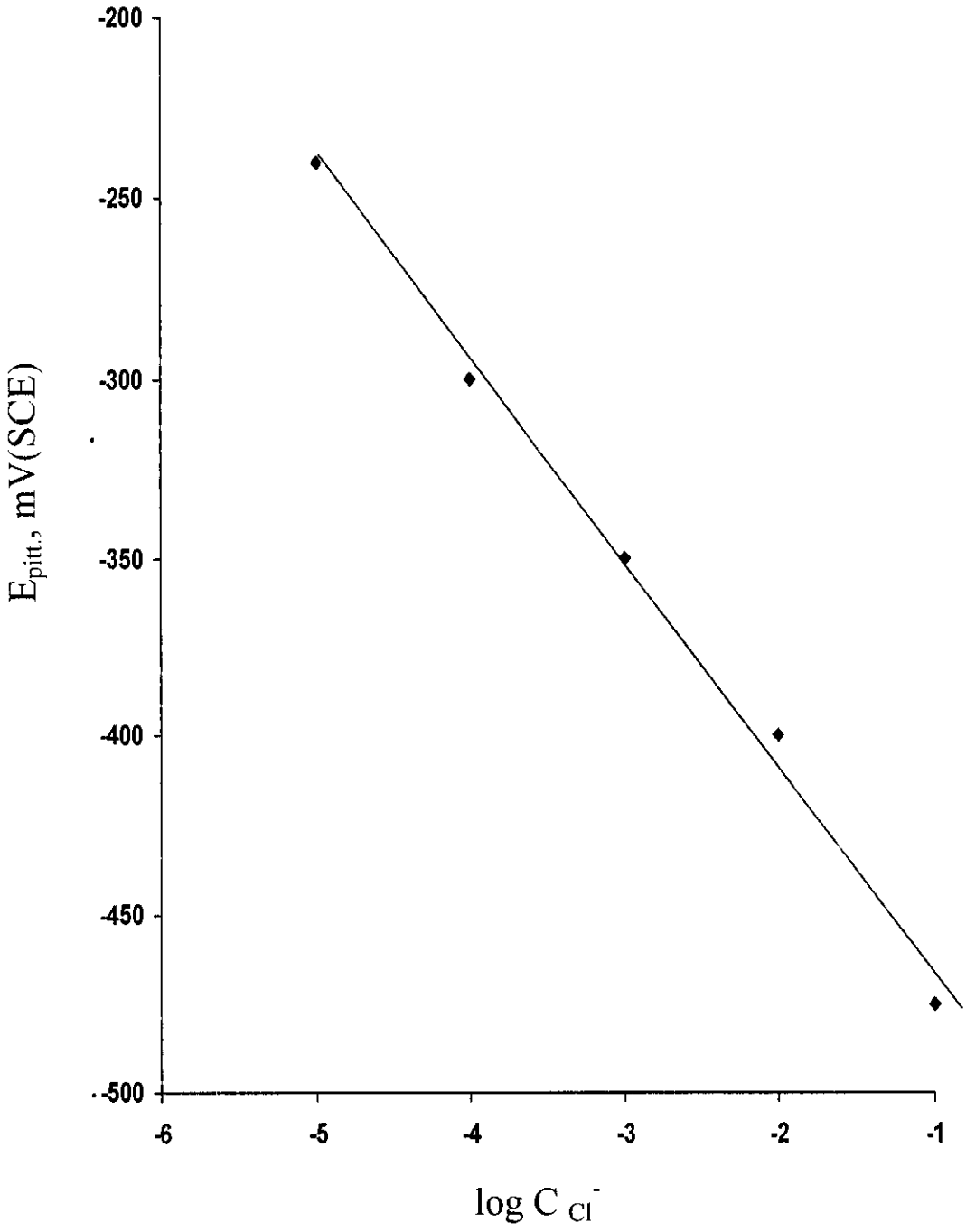

Fig.(3.49) : The relatinoship between pitting potential of C-steel and logarithm the concentration of NaCl

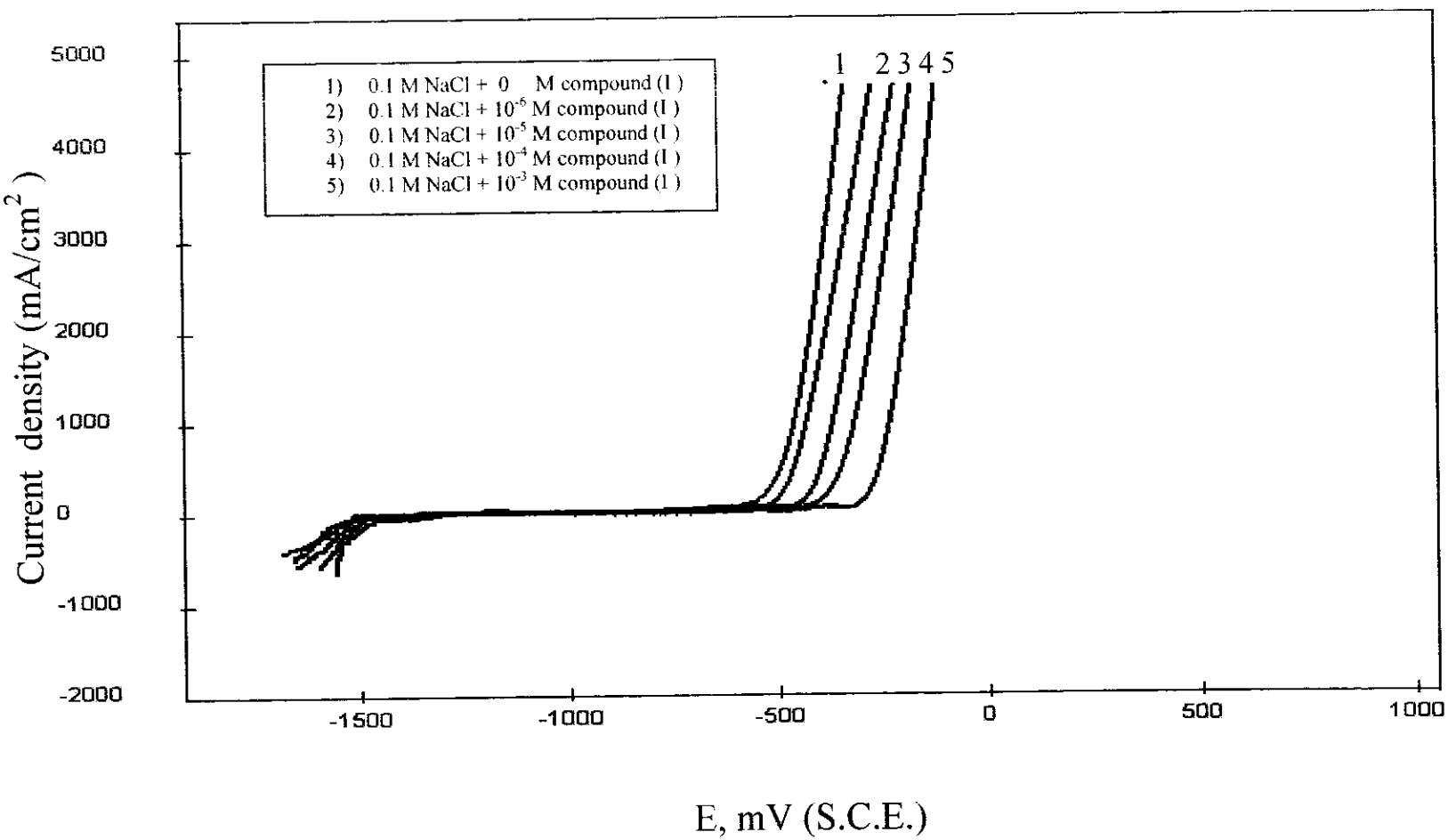

Fig. (3.50): Potentiodynamic anodic polarization curves of carbon steel in 0.1M Na_2CO_3 +0.1 M NaCl containing different concentrations of compound (I).

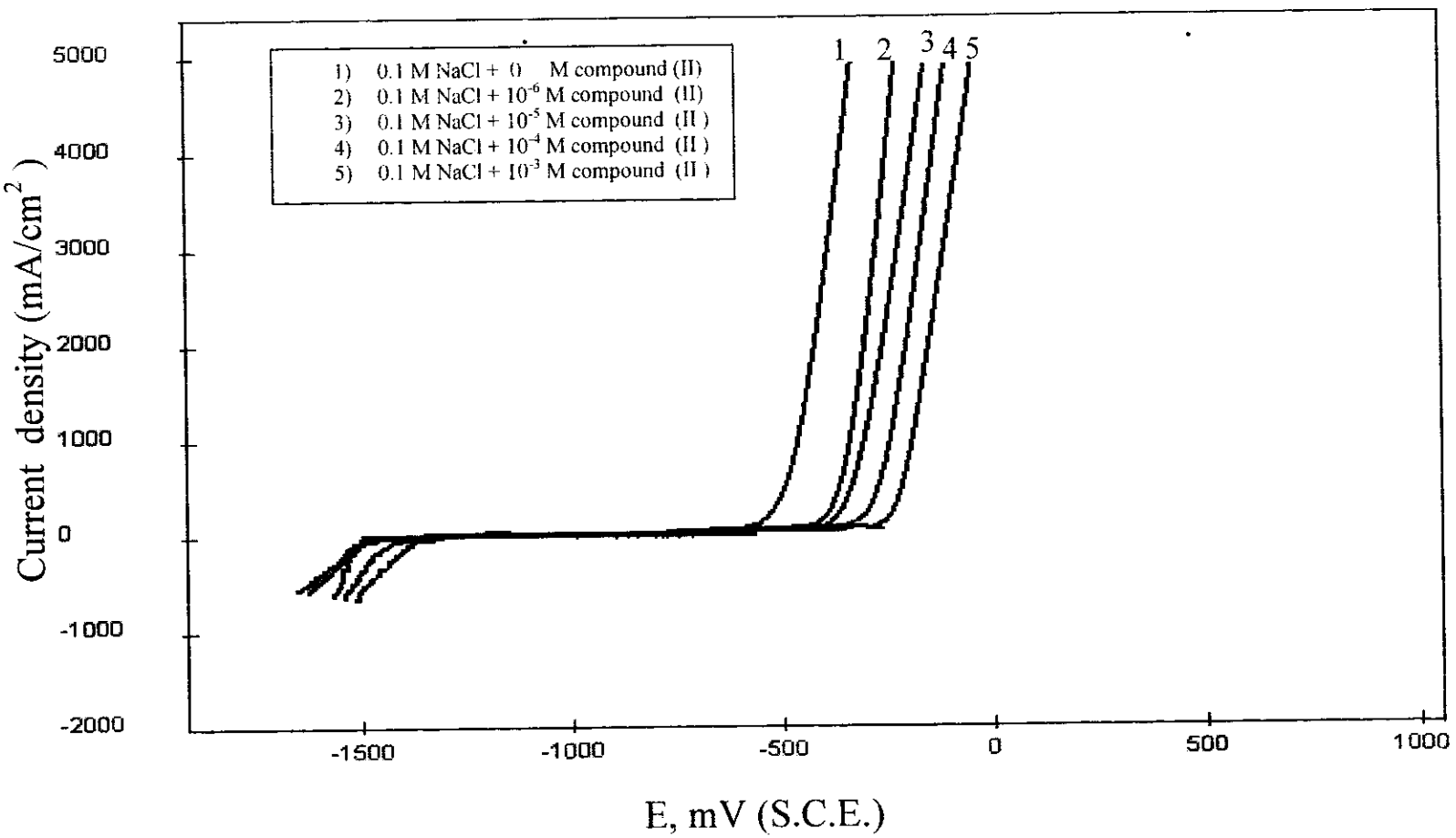

Fig. (3.51): Potentiodynamic anodic polarization curves of carbon steel in 0.1M Na_2CO_3 +0.1 M NaCl containing different concentrations of compound (II).

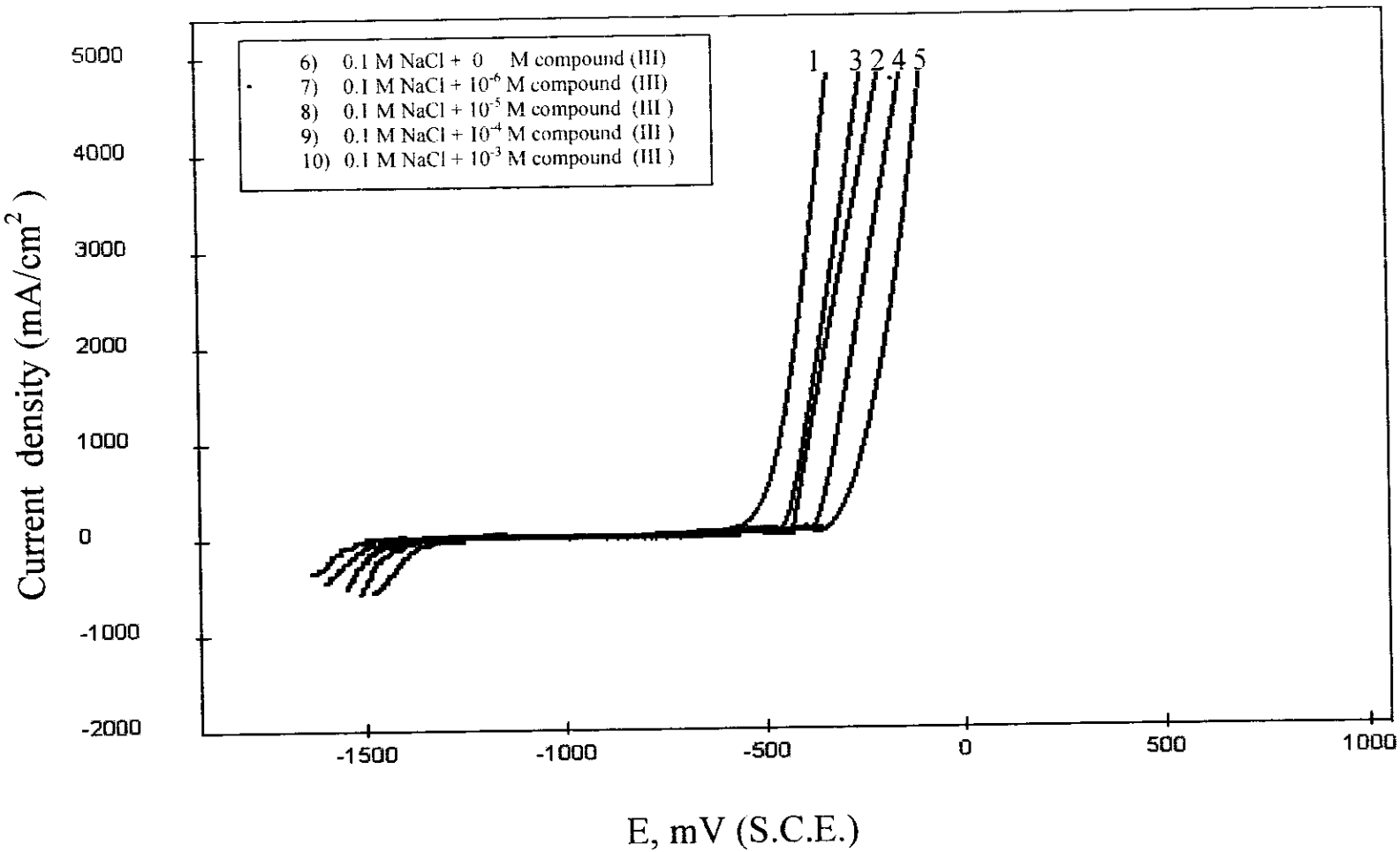

Fig. (3.52): Potentiodynamic anodic polarization curves of carbon steel in 0.1M Na_2CO_3 +0.1 M NaCl containing different concentrations of compound (III).

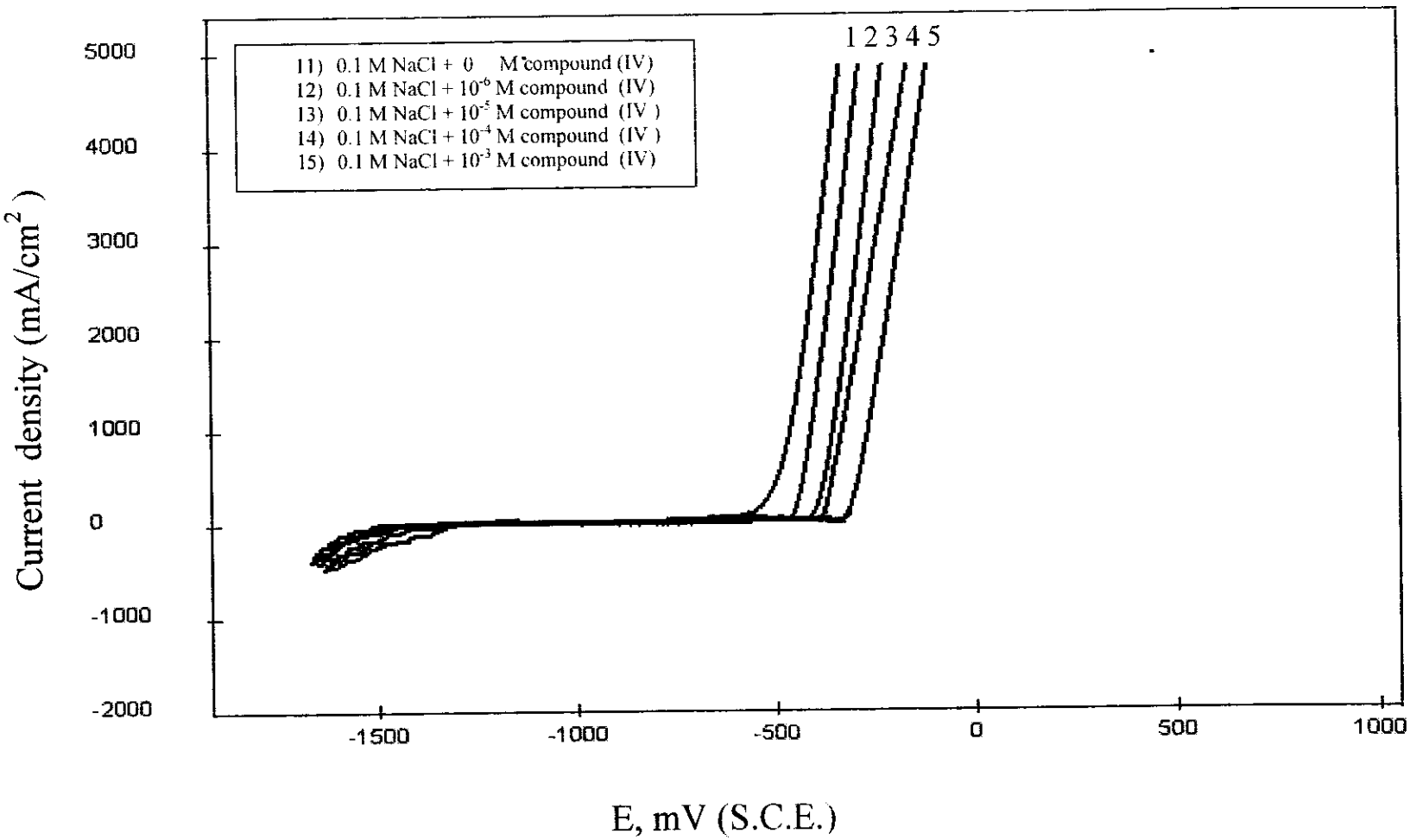

Fig. (3.53): Potentiodynamic anodic polarization curves of carbon steel in 0.1M Na_2CO_3 +0.1 M NaCl containing different concentrations of compound (IV).

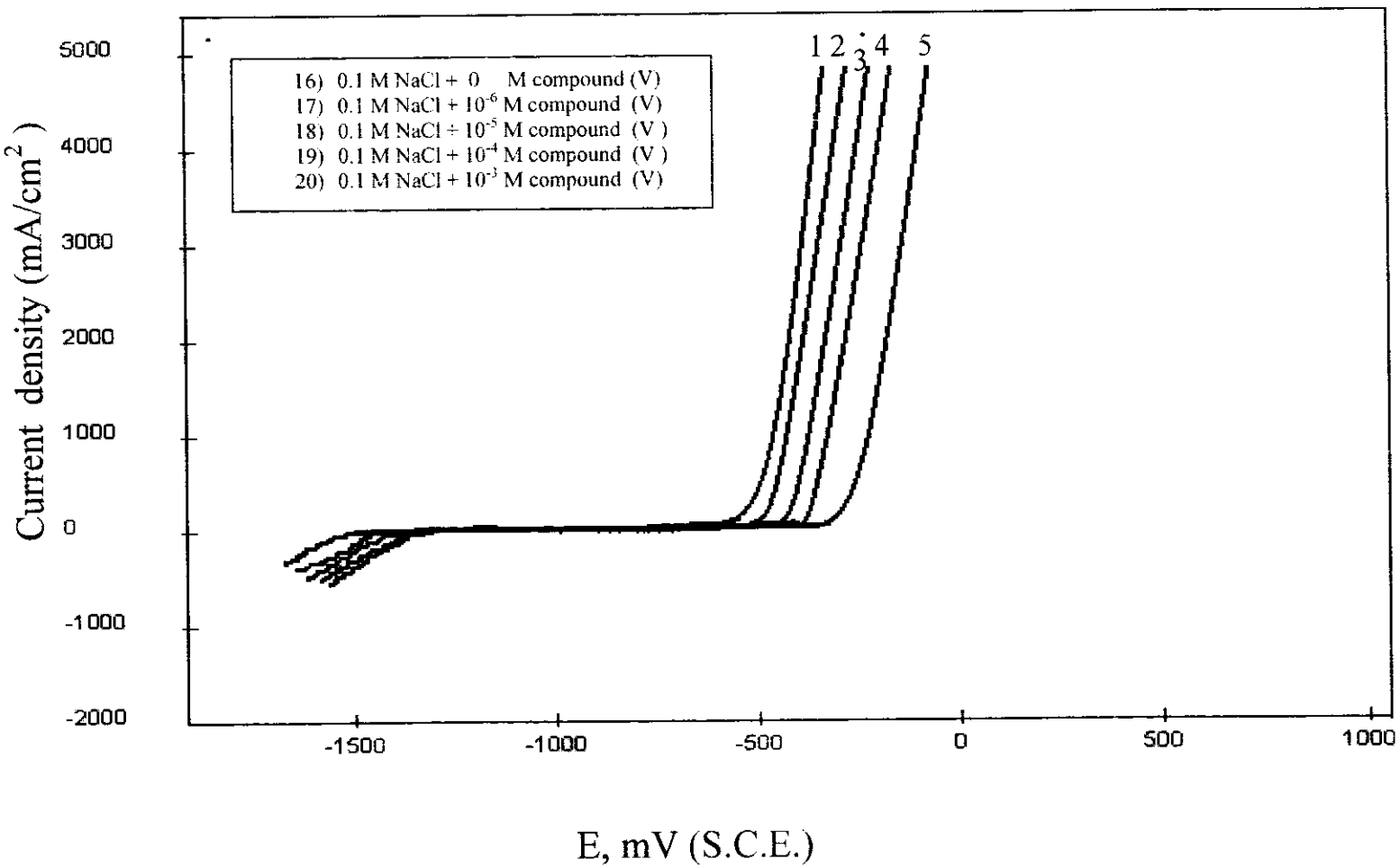

Fig. (3.54): Potentiodynamic anodic polarization curves of carbon steel in 0.1M Na_2CO_3 +0.1 M NaCl containing different concentrations of compound (V).

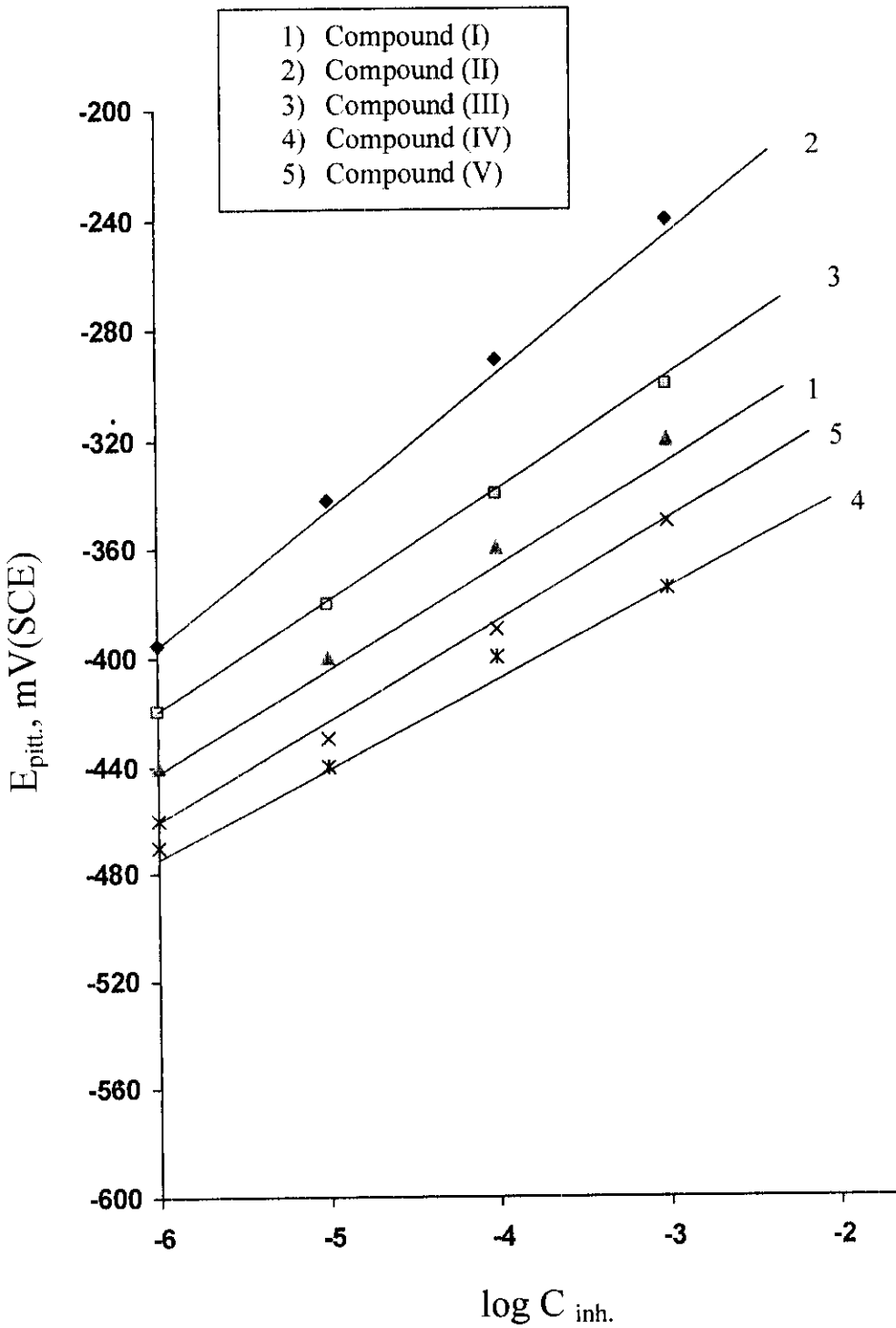

Fig.(3.55) : The relatinoship between pitting potential of C-steel and logarithm concentrations of the additives in presence of 0.1 M NaCl and 0.1 M Na_2CO_3